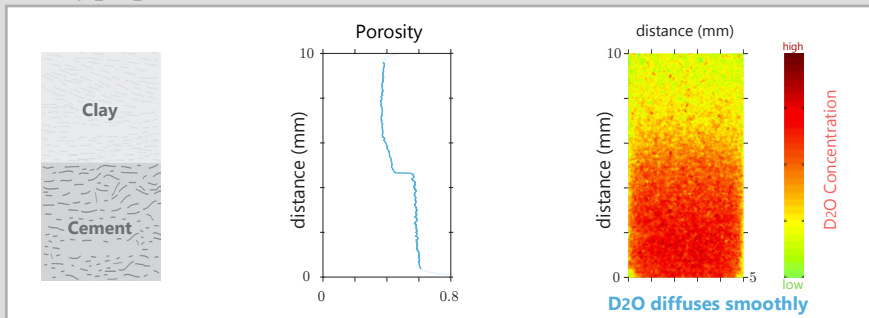
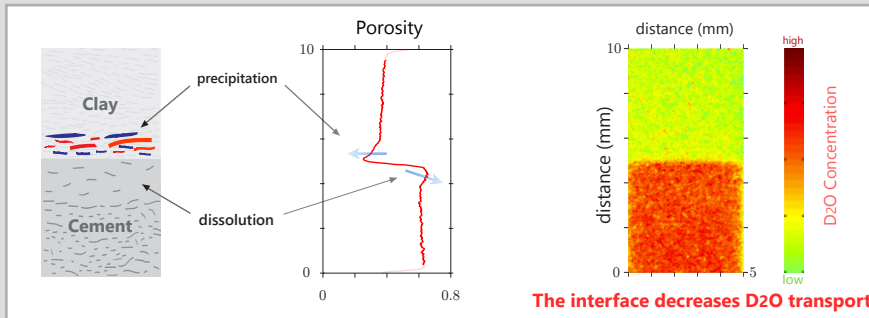


Freshly prepared interface



Interface after 10 months



Progress Report 2015

Laboratory for Waste Management :: Nuclear Energy and Safety Department

Cover

The geochemical contrast between cement and clay in underground disposal sites will provoke mineral dissolution and precipitation reactions at the interface (left). Neutron imaging experiments clearly show that such reactions lead to changes in porosity (middle) and changes in transport properties of the interfaces (right).

PAUL SCHERRER INSTITUT



Progress Report 2015

**Laboratory for Waste Management
Nuclear Energy and Safety Department**



See also our web-page
<http://www.psi.ch/les/>

Preface

The main task of the Laboratory for Waste Management (LES) is to carry out an R&D programme to strengthen the scientific basis for radioactive waste management.

The Laboratory serves an important national role by supporting the Swiss Federal Government and Nagra in their tasks to safely dispose of radioactive wastes from medical, industrial and research applications as well as from nuclear power plants. The activities are in fundamental repository geochemistry, chemistry and physics of radionuclides at geological interfaces and radionuclide transport and retardation in geological media and man-made repository barriers. The work performed is a balanced combination of experimental activities in dedicated laboratories for handling radioactive elements, field experiments and modelling. The work is directed towards repository projects and the results find their application in comprehensive performance assessments carried out by Nagra. In particular, a major priority for LES over the next decade or so will be to contribute to the Sachplan geologische Tiefenlagerung ("Sectoral Plan").

This report summarises the activities and results achieved in the reporting period. It is organised as an overview followed by individual reports on the five waste management group/sub-programme activities.

We gratefully acknowledge the help of the institute's management and of Nagra in our work.

Table of Contents

1	OVERVIEW	1
1.1	Introduction.....	1
1.2	General.....	1
1.3	Sectoral plan for deep geological disposal.....	3
1.4	Repository near field.....	3
1.4.1	Repository chemistry.....	3
1.4.2	Clay systems.....	3
1.4.3	Cement systems.....	4
1.4.4	Interfacial processes.....	5
1.5	Repository far field.....	6
1.6	Model development and code benchmarking.....	7
2	GEOCHEMICAL MODELLING	9
2.1	Overview.....	9
2.2	Database work.....	10
2.2.1	ThermAc project.....	10
2.2.2	THEREDA project.....	11
2.3	Consistent evaluation of acid base equilibria in NaCl rich aqueous solutions at high temperatures.....	11
2.4	Thermodynamic model for illite/smectite layers.....	12
2.5	FIRST-Nuclides project.....	13
2.5.1	Introduction.....	13
2.5.2	X-ray spectroscopy.....	13
2.5.3	Leaching experiments.....	14
2.5.4	Thermodynamic calculations.....	15
2.6	GEMS and its applications.....	16
2.6.1	Introduction.....	16
2.6.2	Ongoing work.....	16
2.7	Solid solution – Aqueous solution systems.....	17
2.8	Water rock interactions in Icelandic hydrothermal systems.....	22
2.9	References.....	22
3	TRANSPORT MECHANISMS	25
3.1	Overview.....	25
3.2	Sectoral plan for deep geological disposal.....	26
3.2.1	DR-A field experiment in the Mont Terri Underground Rock Laboratory.....	26
3.2.2	DR-B field experiment in the Mont Terri Underground Rock Laboratory.....	27
3.2.3	Influence of Fe redox sorption behavior on montmorillonite surfaces on the Ni(II) migration.....	28
3.2.4	Experimental observation of the evolution of porosity at cement-clay interfaces and the subsequent effect on transport parameters.....	29
3.2.5	Assessment of water content in Opalinus Clay samples using ultrasound technique.....	30
3.3	Fundamental understanding of transport and sorption mechanisms: Multi-scale molecular modelling of ion sorption by C-S-H phases.....	30
3.4	Benchmarking and validation of coupled codes.....	31

3.4.1	Experimental benchmarks for the verification and validation of reactive transport codes: a multi-scale investigation	31
3.4.2	Lattice Boltzmann pore-level modelling of dissolution-precipitation processes (epitaxial growth and rim formation mechanism)	32
3.4.3	OpenGeoSys-GEM: benchmarking and applications	33
3.5	Advances in computational methods for geochemical and reactive transport modelling	34
3.6	References	35
4	CLAY SORPTION MECHANISMS.....	37
4.1	Introduction	37
4.2	Mechanistic sorption studies	37
4.2.1	Sorption of Cs ^I , Ni ^{II} , Eu ^{III} and Th ^{IV} on montmorillonite, native and altered MX-80 bentonite at 25 °C and 90 °C	37
4.2.2	Zn-Na ion equilibrium on illite	38
4.2.3	Sorption of uranyl on montmorillonite under reducing condition	40
4.2.4	Influence of ferrous iron on the retention of Np and Tc on montmorillonite	41
4.3	XAS related activities	42
4.3.1	EXAFS investigations of structural Fe in clay minerals	42
4.3.2	Molecular modelling of structural iron in clay minerals	43
4.4	References	44
5	CEMENT SYSTEMS	45
5.1	Overview	45
5.2	Activities in support of the Sectoral Plan: Report on the evolution of heterogeneities in the cementitious near field	45
5.3	Speciation and fate of organic compounds in the cementitious near field	45
5.3.1	¹⁴ C project	45
5.3.1.1	Installation of the new GC-MS and development of analytical methods	46
5.3.1.2	Identification and quantification of organics released during iron corrosion	46
5.3.1.3	Coupling separation techniques with accelerator mass spectrometry (AMS) for compound-specific carbon-14 analysis	46
5.3.1.4	Development of a reactor for the corrosion experiment with activated steel	48
5.3.2	Chemical stability of organic compounds under hyper-alkaline conditions	49
5.3.3	Sorption/diffusion of LMW organic compounds	49
5.4	Retention of selenium by cementitious materials under reducing conditions	50
5.5	References	53
6	COLLOID CHEMISTRY	55
6.1	Overview	55
6.2	Activities in the CFM project	55
6.3	References	56
7	DIFFUSION PROCESSES	57
7.1	Overview	57
7.2	Transport phenomena in compacted clay systems (TRAPHICCS)	57
7.3	Porosity changes in porous media	58
7.4	Transport of small organic molecules in dense clay systems	59
7.5	Anion exclusion phenomena in low porosity clay rocks (ANPOR)	59
7.6	Water properties in confinement	60

7.7	References.....	61
8	PUBLICATIONS.....	63
8.1	Peer reviewed journals.....	63
8.2	Conferences/workshops/presentations.....	64
8.3	Invited talks.....	67
8.4	Teaching.....	67
8.5	Other.....	67

1 OVERVIEW

S.V. Churakov

1.1 Introduction

The progress made in the Laboratory for Waste Management (LES) over the period from January to December 2015 is summarized in the first part of the report. The detailed description of main activities carried out in the individual groups is then provided in chapters 2 to 7. These are either predominantly "experimental" or predominantly "modelling" in their nature. However, most of the projects are multidisciplinary and require strong interactions between groups and individual group members from both experimental and modelling sides.

1.2 General

In January 2015 the Federal Department of Energy (BFE) has announced the siting regions proposed by Nagra for a deeper investigation in the Stage 3 of the Sectoral Plan for Deep Geological Disposal (SGT). The documentation submitted by Nagra in support of the site selection process is currently under revision by the regulatory bodies. According to the updated planning the government decision on Stage 2 SGT and the formal launch of Stage 3 is expected before the end of 2018.

In the past years, the work conducted at LES has been focused on development of numerous databases and scientific reports required in Stage 2 of the SGT for the Provisional Safety Analyses (PSAs). In the beginning of 2015 careful and detailed evaluation of the LES research portfolio took place. The main objective of this evaluation was the assessment of the current state of research in the Swiss program for geological waste disposal, identification of expertise and knowledge needed for Stage 3 and the following General License Application (RBG). The identified topics were discussed with Nagra. Particular attention was paid to the long term personnel planning and knowhow transfer towards RBG and beyond. Accordingly, the geochemistry of *in situ* conditions, the long term evolution of the multi-barrier systems, and radionuclides retention will remain to be the core activities in the LES research portfolio. These include theoretical and experimental investigations of coupled reactive transport phenomena, sorption/retention of radionuclides in clay systems and cement (e.g. support of the sorption models, sorption/competition) and transport/release of dose determining nuclides (e.g. C-14, anions).

As part of a general effort to diversify the funding of projects at LES, a significant progress has been made in attracting non-Nagra funding for PhD and post-doctoral projects. Particularly successful was LES

participation in the EURATOM HORIZON 2020 program and funding by the Swiss National Science Foundation (SNF):

Two LES-PhD projects were approved within the "Cement-based materials, properties, evolution, barrier functions (CEBAMA)", EURATOM (H2020-NFRP-2014/2015, <http://www.cebama.eu/>) research program. The projects located at LES will focus on the reactivity of the cementitious barriers in the repository near field and the retention of doses determining nuclides in the cement matrix.

Further, LES represents Switzerland in the Horizon2020 collaborative project "Sustainable network for independent technical expertise (SITEX-II, 2015-2017, www.sitexproject.eu). The overall objective of this project is to ensure a sustainable capability of developing and coordinating joint and harmonized activities related to the independent technical expertise in the field of safe geological disposal of radioactive waste.

In collaboration with ETH Zürich, LES participates in the SNF Sinergia project "COTHERM: Combined hydrological, geochemical and geophysical modelling of geothermal systems." A one year extension of the project was supported by SNF. Within this project a postdoc fellow hosted at LES will perform reactive transport simulation of alternation processes in the Icelandic geothermal systems. This will allow testing the performance of modelling concepts and thermodynamic data used in the simulation of geological disposal against other natural systems.

A new PhD project "Thermodynamic and spectroscopic studies of Fe and S speciation in cement" was approved by SNF. In this project the influence of Fe and S on the stability of cement phases in cement will be investigated.

A new collaborative PhD project "Sorption of thallium to illite and birnessite and its impact on thallium solubility in soils" was approved by SNF (main project applicant: Andreas Voegelin, EAWAG). The PhD student will be employed by EAWAG and conduct sorption experiments at LES in close collaboration with the clay sorption group. The investigation will allow testing the applicability of the sorption model for radionuclides developed at LES to simulate the uptake of other environmentally relevant elements like thallium.

The collaboration within the 7th EU Framework Program: "Carbon-14 Source Term" (CAST) is ongoing.

The main multi- and bi-lateral co-operations with external institutions and universities are summarized in Table 1.1.

Table 1.1: National and international co-operations.

Co-operations
Nagra Major financial contribution Various technical working groups
Multinational 7 th EU FP: CAST Mont Terri Project (Diffusion Retardation, Clay Cement Interaction) Grimsel Test Site (Colloid Formation Migration) HORIZON 2020: CEBAMA, SITEX-II
Universities Bern, Switzerland (mineralogy, petrography, water chemistry, C-14 AMS) EPFL, Switzerland, UCB, Dijon, France (cement systems, molecular modelling) Tübingen, Germany (geosphere transport) ETH, Zürich, Switzerland (GEMS) University of Helsinki, Finland (GEMS)
Research Centres CEA*, France (near- and far-field) CIEMAT, Spain (colloids) EMPA*, Switzerland (cement) IRE, HZDR*, Germany (XAS, TRLFS) INE, KIT*, Germany (near- and far-field; TRLFS) SCK/CEN, Belgium (clay and cement systems) UFZ*, Germany (reactive transport) BRGM, France (Sorption) *formal co-operation agreements

Ongoing PhD and postdoc projects hosted at LES are listed below:

Y. Chen (PhD student): "Retardation of low-molecular weight organic compounds in clays". Start date: March 2013. (Funding: Nagra/PSI).

A. Kéri (PhD student): "Shedding light on metal adsorption processes on clay minerals inferred from atomistic simulations and X-ray Absorption Spectroscopy." Start date: January 2015. (Funding: SNF)

J. Poonosamy (PhD student): "Experimental benchmarks for verification and validation of reactive transport codes." Start date: October 2012. (Funding: Nagra/PSI).

A. Shafizadeh (PhD student): "Porosity and structural changes at clay-cement interfaces and their relations to transport properties." Start date: February 2012. (Funding: Nagra/PSI CROSS proposal in collaboration with the Neutron Activation and Imaging Group (NUM)).

C. Wigger (PhD student): "Anion accessibility in low porosity argillaceous rocks (ANPOR)" Start date: February 2014. (Funding: NWMO, Canada).

Dr. B. Cvetković (postdoc): "Development of C-14 AMS-based analytical methods for the identification and quantification of C-14 labeled dissolved and volatile organic compounds." Start date: November 2013. (Funding: Swissnuclear).

Dr. L. Pegado (Guest scientist): "A thermodynamic model for C-S-H/C-A-S-H from a bottom up approach". This is a joint project between University of Bourgogne (Dijon), LES/PSI and EPFL. Dr. Pegado works at LES approximately one working day per week. (Funding: NANOCHEM). The project is finalized by the end of 2015.

Dr. A. Leal has finalized the one year postdoc project on "Development of robust and efficient computational methods for geochemical modeling and application of finite element methods for reactive transport simulations." Within this project the performance of the OpenGeoSys-GEMS coupling could be improved significantly. Dr. Leal continues the development of reactive transport codes in the group of Prof. Saar at the ETH Zürich. Further collaboration between the group of Prof. Saar at the ETH Zürich and LES/PSI on the benchmarking of reactive transport codes is ongoing.

Guest scientist Dr. H. Rojo-Sanz has completed the project "The fate of selenium and technetium in a cementitious repository near-field under reducing conditions." Funding from November 2012 to August 2014 was provided by the German Ministry for the Education and Research (BMBF) in the framework of Verbundprojekt "IMMORAD": Grundlegende Untersuchungen zur Immobilisierung langlebiger Radionuklide durch die Wechselwirkung mit endlager-relevanten Sekundärphasen.

Dr. B. Thien has completed the four years postdoctoral project on "Combined hydrological, geochemical and geophysical modelling of geothermal systems." He will continue his research on the characterization and the modelling of geothermal alteration in Icelandic basalts at the ETH Zürich. To continue the existing collaboration Dr. Thien continues working at LES approximately 1 day per week till the middle of 2016.

Several personnel changes took place in the reporting year. PD Dr. Degueldre has retired. Over several decades PD Dr. Degueldre had been coordinating various activities related to colloidal migration. PD Dr. Th. Gimmi has successfully habilitated at the University of Bern. Prof. Dr. S.V. Churakov has taken the chair of Mineralogy at the Institute of Geological

Sciences in Bern (a joint appointment between PSI and the University of Bern).

1.3 Sectoral plan for deep geological disposal

After the submission of the documentation for the Stage 2 of the SGT, major activities at LES are focused on Stage 3 and the general license application of the SGT. These include experimental studies aimed at filling gaps in the sorption and thermodynamics databases, further development of the bottom up approach for a consistent evaluation of parameters in SDB for host rocks and confining units, support of databases for mobility of cations and anions in host rocks, further evaluation of temperature effects on sorption and transport of radionuclides and model based description of in situ geochemical conditions in the repository near field. Several Nagra technical reports on these topics are currently in preparation.

Preliminary kinetic and mass balance calculations were performed to reveal chemical processes and transport phenomena which can potentially occur due to heterogeneous material (waste) distributions in the low- and intermediate- level waste (L/ILW) repository. The resin-containing bitumized waste package, and a cemented waste package and resin-containing waste embedded in polystyrene have been selected as representatives of important waste forms. The temporal evolution of the waste matrix in these packages was described on the basis of important chemical reactions: i) metal corrosion, ii) degradation of organics and iii) dissolution of silicate aggregates. The aforementioned reactions are considered to govern the alteration of the waste matrix inside the waste packages. This work will continue in the coming years in order to include the latest waste inventory data, to integrate kinetics laws into reactive transport models and their dependence on pH. This is necessary for an accurate evaluation of the mineral reactions, corrosion reactions and degradation reactions of organic matter (gas production rates) within the existing thermodynamic model for reference concrete.

1.4 Repository near field

1.4.1 Repository chemistry

In October 2015 LES has become a partner in the thermodynamic reference database project (THEREDA). The scope of this project is to establish a comprehensive and internally consistent thermodynamic database for the geochemical modelling of processes occurring in the near- and far-field of the different host rock formations considered for potential geological disposal of radioactive waste in Germany. The project is coordinated and carried out by leading

German research centers for radioactive waste disposal (GRS Braunschweig, KIT-INE Karlsruhe, HZDR-IRE Dresden-Rossendorf, and TU-BAF Freiberg) and financed by four German Federal Ministries. Within this project LES evaluates relevant thermodynamic data for cementitious systems. Participating in the THEREDA project LES benefits from the full access to the thermodynamic database, which can also be used for specific problems in the Swiss waste disposal program.

In the current design of the multi-barrier system for the repository near field clay and cement material come into direct contact. This results in dissolution and re-precipitation of mineral phases. Accurate description of these processes requires consistent thermodynamic data for all relevant phases in the system. Accordingly, a solid-solution based model for montmorillonite has been developed recently. This model takes into account dissolution, precipitation, cation exchange and redox equilibria. Since the preferred host rock in Switzerland contains considerable quantities of illite-smectite mixed layers the development of a corresponding model for illite has been initiated. Currently, the reference stoichiometry of illite/smectite layers, consistent with the former model for montmorillonite has been set up based on available X-ray diffraction data, wet chemistry and data from thermogravimetric analysis. Calibration of the thermodynamic properties of end members is ongoing.

During 2011-2014 LES participated in the FP-7 EU project FIRST-Nuclides. The final report on experimental and modelling activities has been completed in 2015.

Activity coefficients of ionic species in the Nagra-PSI database are calculated on the basis of the specific ion interaction theory (SIT). This approach is robust and allows accurate prediction of the activity data in a wide range of ionic concentrations and temperatures. However, the available data are limited to few simple ion pairs like NaCl. The missing data are obtained based on the co-called isoelectric reaction equilibrium approach. In this approach the enthalpy of the isoelectric reaction is assumed to be constant. Applying three-parameter approximation for temperature and medium effects on the protonation reactions the SIT interaction parameters for carbonate, sulphates, phosphates, acetates, oxalates, citrates, and few other organic acids are being determined.

1.4.2 Clay systems

The development of a thermodynamic sorption database (TD-SDB) for clay minerals based on the 2SPNE SC/CE (e.g. estimation of model parameters site types, site capacities, selectivity coefficients, surface

complexation constants) is ongoing. The aim is to formulate a unified approach to the calculations of sorption values for the safety analysis under relevant geochemical conditions taking into account the effects of sorption competition phenomena and possible temporal variation of the porewater chemistry. Reports on these topics are in preparation and it is foreseen that they will be finalised in 2016.

According to the current multi-barrier concept for geological waste disposal, the vitrified high level waste and spent fuel has to be contained by the steel canister for at least 10000 years after the emplacement. During this period the bentonite buffer and host rock in the direct vicinity of the disposal casks will experience an elevated temperature pulse which may modify the sorption properties of the barriers. It is therefore essential to understand the effect of temperature on the clay rocks and their sorption capacity. Samples of thermally treated bentonite (up to 140 °C for 2 years) have become available from the "Alternative buffer material (ABM)" experiment at the Aspö URL. Sorption experiments with Cs(I), Ni(II), Eu(III) and Th(IV) were performed at 25 °C and 90 °C using the reference montmorillonite (Milos) and thermally treated bentonite from the ABM experiment in order to make a direct comparison of the sorption behavior of the above-mentioned radionuclides in original and altered bentonite materials. The main conclusion from this study is that a 2 years heat treatment up to 140 °C does not affect the sorption properties of MX-80 towards Cs(I), Ni(II), Eu(III) and Th(IV). The uptake of these nuclides is controlled by the sorption complexation onto clay edge sites which is almost unaffected by temperature.

The selectivity coefficients for the cation exchange reactions in the 2SPNE SC/CE sorption model are generally extracted from measurements of sorption edges at low pH for a trace radionuclide concentration. It therefore remains open if the results of such studies are also applicable to the high radionuclide concentrations or in highly compacted systems (e.g. in situ conditions in the repository). The exchange equilibrium between Zn^{2+} and Na^+ was conducted on illite du Puy (IdP) at Zn loadings covering 10 to 90 % of the total cation exchange capacity (CEC). The experiments show that within the range of Zn loading the selectivity coefficients remain constant.

The retardation of redox sensitive actinides and fission products such as U, Np, Tc depends strongly on their oxidation state. In the most oxidized form (i.e. $U(VI)O_2^{2+}$, $Np(V)O_2^+$, $Tc(VII)O_4^-$) these radionuclides are highly mobile whereas in the reduced state (e.g. (IV)) their transport is believed to be very slow. This assumption has been confirmed experimentally for

Th(IV) only, whereas other tetravalent nuclides (U, Np, Tc) are considered as the chemical analogs of Th(IV). To merge the gap in the available experimental data, a series of experiments on redox-controlled adsorption of uranium on montmorillonite (STx) were conducted in an electrochemical cell. First, the oxidized UO_2^{2+} was pre-equilibrated with STx under anoxic conditions (no imposed E_h). After three days the electrochemical potential was set to -170 mV. Reduction of U(VI) to U(IV) was monitored by EXAFS, which confirmed the change in the uranium coordination shell indicative for the U(VI) to U(IV) transition. The experimental data confirmed the increase in U retardation as the reduction proceeded.

The corrosion of steel disposal casks in the repository for high level radioactive waste will release large quantities of Fe(II) into the bentonite buffer. Ferrous iron bound to oxide/clay minerals was found to be much more reactive with respect to reduction reactions of inorganic and organic compounds than dissolved aqueous complexes. Not only the kinetics of the corresponding reactions is faster but also the redox potential of the clay/oxide associated Fe(II)/Fe(III) redox couple is lower than that of aqueous iron. Depending on the Fe sorption mechanism, its reactivity can change by orders of magnitude. Accordingly, the influence of Fe(II) adsorbed by clay minerals on the reduction of Np(V) and Tc(VII) is investigated within a collaborative project between LES, ROBL/HZDR, INE/KIT and BRGM.

A sorption model for the oxidative uptake of iron by montmorillonite has been implemented in the reactive transport code MCOTAC and applied to estimate the sorption competition effect of the Fe(II)/Fe(III) redox couple on transport and retardation of divalent radionuclides. A case study on Ni(II) transport revealed a slight reduction of Ni(II) retardation when oxidative adsorption uptake of Fe(III) is included. It should be noted, however, that in the current formulation of the 2SPNE CE/SC sorption model, Fe(II) and Fe(III) are considered to adsorb on the same sorption sites. The validity of this assumption has to be confirmed by spectroscopic studies. It also remains open whether Fe(III) may compete with the trivalent radionuclides.

1.4.3 Cement systems

Thermodynamic equilibria calculations predict that ^{14}C containing low molecular weight (LMW) organic molecules released during the corrosion of activated steel are not chemically stable under the hyper-alkaline reducing conditions of a cement-based repository (WIELAND & HUMMEL 2015). However, complete thermodynamic equilibrium is rarely

achieved in the C-H-O system at moderate temperatures and it is still unclear what kind of organic compounds will predominate in the repository, and if the thermodynamic equilibrium is kinetically hindered. The chemical stability of acetic acid under hyper-alkaline anoxic conditions is currently being studied. The experimental results obtained in 2015 indicate that the decomposition of LMW molecules into CH_4 and CO_2 predicted by thermodynamic equilibrium calculations is kinetically hindered. The experiment will be repeated in the presence of iron and at elevated temperature.

^{14}C containing LMW organic molecules may further interact with cementitious materials thus being retarded in the near field. In the past years sorption and diffusion studies with LMW organics, in particular methanol, ethanol, formaldehyde, acetaldehyde, acetic and formic acids, were carried out. The studies show that most of the LMW organics are only weakly and largely reversibly bound to HCP and cement phases. Formic acid is so far an exception which shows a partially irreversible uptake.

Next to ^{14}C , ^{79}Se (half-life $3.27 \cdot 10^5$ years) is the second most important dose-determining radionuclide in an L/ILW repository. The selenium speciation and sorption behavior in cement depend on the redox condition. Under oxidizing conditions SeO_4^{2-} and SeO_3^{2-} are the dominant species while in alkaline, reducing conditions, $\text{Se}(0)$, HSe^- and poly-selenide species prevail. Robust sorption data and, in particular, a sufficiently detailed mechanistic understanding of Se(-II) retention in a cementitious environment are lacking. Accordingly, the Se(-II) uptake by various cement phases (C-S-H phases, AFm phases, AFt) was investigated in the framework of the German collaborative project IMMORAD. In the case of the AFm phases, the R_d values for Se strongly depend on the interlayer distance (d-spacing) and the type of anion originally present in the interlayer. These observations suggest that interlayer sorption could be important for the SeO_3^{2-} and HSe^- uptake by AFm phases. The sorption isotherm measurements clearly confirm the observations made earlier in kinetic tests that the uptake of both SeO_3^{2-} and HSe^- by AFm-OH- CO_3 is stronger than uptake by AFm- CO_3 , thus further supporting the idea that the anion present in the AFm structure (and thus the interlayer distance) has a strong effect on the uptake.

Amorphous Calcium Silicate Hydrates (C-S-H) are the main binding phases in cement paste. These phases can incorporate considerable amounts of alkali ions and thus control the chemical equilibria in cement paste. The accurate thermodynamic model for these phases is indispensable for the robust reactive transport simulations of in situ conditions in the

repository near field. Stepwise parametrization of the sub-lattice solid solution model for the CASHNK system ($\text{CaO-Al}_2\text{O}_3\text{-SiO}_2\text{-H}_2\text{O-Na}_2\text{O-K}_2\text{O}$) has been continued. Currently, the model describes thermodynamic relationships in the C-A-S-H system (Al containing C-S-H). A remarkable feature of the current model is the ability to predict the mean silicate chain in close agreement with the spectroscopic data.

In collaboration with the group of Dr. Labbez at the University of Bourgogne Franche-Comté, Dijon, France, a thermodynamic modelling approach of ion adsorption on a C-S-H/C-A-S-H particle using an extended grand canonical simulation technique is further developed. To improve the description of ion-surface interaction mean interaction potentials were obtained by combining ab initio and classical molecular dynamics simulations. The accuracy of these effective interaction potentials was tested on available experimental data for aqueous solutions.

1.4.4 Interfacial processes

^{14}C can be carried by LMW organic compounds. Due to poor knowledge of ^{14}C speciation, current performance assessment studies treat ^{14}C as a non sorbing tracer. Accordingly, ^{14}C provides the major contribution to the dose released from an L/ILW repository. The major source of ^{14}C in the L/ILW repository is the corrosion of activated steel under reducing conditions. A number of activities are ongoing whose aim is to quantify the processes relevant to release, speciation and potential transport mechanisms of ^{14}C in the cementitious near field. These activities include various batch-type experiments with irradiated and non-irradiated steel, the development of measurement protocols for compound specific ^{14}C quantification and ^{14}C transport experiments.

The activity of ^{14}C released in the corrosion experiments with activated steel is very low. Therefore, the compound-specific detection of ^{14}C requires sophisticated analytical equipment. To this aim IC-MS and GC-MS system were installed in the Hot Laboratory and coupled to the oxidation reactor, which enables to collect compound specific fractions for further determination of ^{14}C using accelerator mass spectrometry (AMS). The corresponding analytical methods previously developed in collaboration with the Institute for Chemistry and Bioanalytics at the University of Applied Sciences Northwestern Switzerland (ICB/FHNW) were adapted and optimized for the equipment newly installed at PSI. In 2015, extensive tests and control measurements have been performed to optimize the equipment for actual measurements of the active samples. These include reproducibility tests with the improved analytical

setup at PSI against the results obtained previously at ICB/FHNW and literature data published by other research groups.

Cement and clay come into contact at the boundaries of the repository. These materials will react by changing the mineralogical composition and porosity of the engineered barriers at the interface. These changes can have both favorable and unfavorable effects on the performance of the barriers which have to be quantified. Within the PhD project "Evolution of cement-clay interfaces" (A. Shafizadeh) reduction of transport through the reacted cement clay interface could be clearly demonstrated measuring D_2O transport in situ at the ICON neutron facility at PSI. In this in situ transport study several cement clay interfaces were reacting in a dedicated cell designed to be transparent for neutrons. The neutron scattering contrast between hydrogen and deuterium was used to identify the diffusion of deuterium through the sample. The measured D_2O profile reacted for about one year demonstrates the presence of a thin zone at the cement clay interface with strongly reduced diffusivity. The data were found to be consistent with the conventional diffusion experiments and the radiographic measurements of water content.

Dissolution-precipitation processes taking place at strong geochemical gradients modify the transport properties of the media in a complex nonlinear way. It is very difficult to describe these phenomena in macroscopic simulations without fitting to the experimental data because the pore scale phenomena are not resolved at this scale. In the PhD project of Jenna Poonoosamy an experimental setup has been developed to simulate precipitation in the granular porous media and their effect on transport. The results of the simulations were applied to calibrate porosity-permeability relationships in the reactive transport code (OpenGeoSys-GEM) used for the simulations of the repository near field.

To further improve the model-based description of precipitation and dissolution of minerals in porous media and their effect on the transport properties of the system, an initial development of a pore scale transport model on the basis of the Lattice Boltzmann approach has started. The overall aim is the upscaling of the atomistic information on the crystal growth and the fluid transport at pore scale to the continuum scale in order to be able to provide transport parameters for the macroscopic transport simulations. As a first step, dissolution and precipitation reactions investigated in the lab scale reactive transport experiment have been modelled and the epitaxial growth of barite on celestite crystals has been simulated in realistic geometries directly obtained from the experimental samples. This level of description allows the direct

measurement of the effect of geochemical reactions on the effective diffusivity and permeability of the domain of interest.

1.5 Repository far field

Diffusion studies of strongly sorbing tracers initiated within the European project CatClay have been continued with the aim of testing the internal consistency of sorption data and diffusion data for illite and testing the blind prediction of the surface diffusion model. In-diffusion experiments with $^{65}Zn^{2+}$ tracer in compacted illite support the idea that the diffusive behaviour of transition metal cations can be described most effectively based on the generalised surface diffusion concept. In this model the ion adsorbed on the surface of minerals are considered as mobile and thus contribute to the diffusive flux. Chemically different surface species may exhibit different surface mobilities and the assessment of cation diffusion in compacted swelling clays cannot be understood without a thorough knowledge of the chemical type of these interactions on the surface. The model was further applied to predict diffusion of Eu(III) in illite at low pH conditions, at which the sorption is dominated by cation exchange. The blind predictions of the model were found to be in good agreement with the experiment.

Anionic species are repelled from the surface of clay minerals due to the negative electrostatic charge of the clay mineral platelets. Therefore, total porosity accessible to the anions is a fraction of the total porosity. The exclusion depends on the ionic strength. At higher ionic strength positive ions effectively screen the electrostatic potential of the surface whereas at low ionic strength the screening is low. The effect of ionic strength on anion accessible porosity is investigated in the framework of a PhD project (C. Wigger) funded by the NWMO (Canada). The total ion porosity is obtained by through diffusion experiments for different ionic strengths maintained by 1:1 and 2:1 salts.

Current performance assessment studies assume that ^{14}C carrying molecules do not sorb in the far field. If however a weak retardation can be robustly demonstrated, this would lead to a significant reduction of the dose measured at the surface. Accordingly, possible retardation of organic molecules by host rocks (e.g. Opalinus Clay) is investigated within a PhD project (Y. Chen) supported by Nagra. The retardation of organic molecules produced due to anaerobic corrosion of steel is investigated in infiltration experiments through compacted illite and kaolinite as well as Opalinus Clay. In 2015, the focus was on the behaviour of stereoisomers (D- and L-lactate enantiomers) in illite

and on the transport behaviour of these and several other organic molecules in Opalinus Clay. It could be clearly shown that D- and L-lactate have a different retention behaviour in illite and Opalinus Clay. The results suggest that the hydroxy group in the α position is involved in the sorption reaction. First results on Opalinus Clay also indicate a clear retention of α -hydroxycarboxylic acids.

Several experimental activities are devoted to the upscaling of laboratory data and the validation of the models at field scale. The DR-A field experiment at the Mont Terri Underground Rock Laboratory aims at investigating the effects of chemical perturbations on transport of sorbing and non-sorbing tracers. The field part of the experiment has been completed and LES is currently coordinating the modelling activity of the experimental data between several groups applying different modelling concepts and codes. The goal of this joint effort is to cross-benchmark different codes/models and to identify the most robust ones. DR-B is a long term experiment aimed at long term in situ monitoring of the anion transport in Opalinus Clay. The design of the experiment has been aligned according to the scoping calculation for iodine break through curves. Accordingly, the injection borehole and the two observation boreholes were installed.

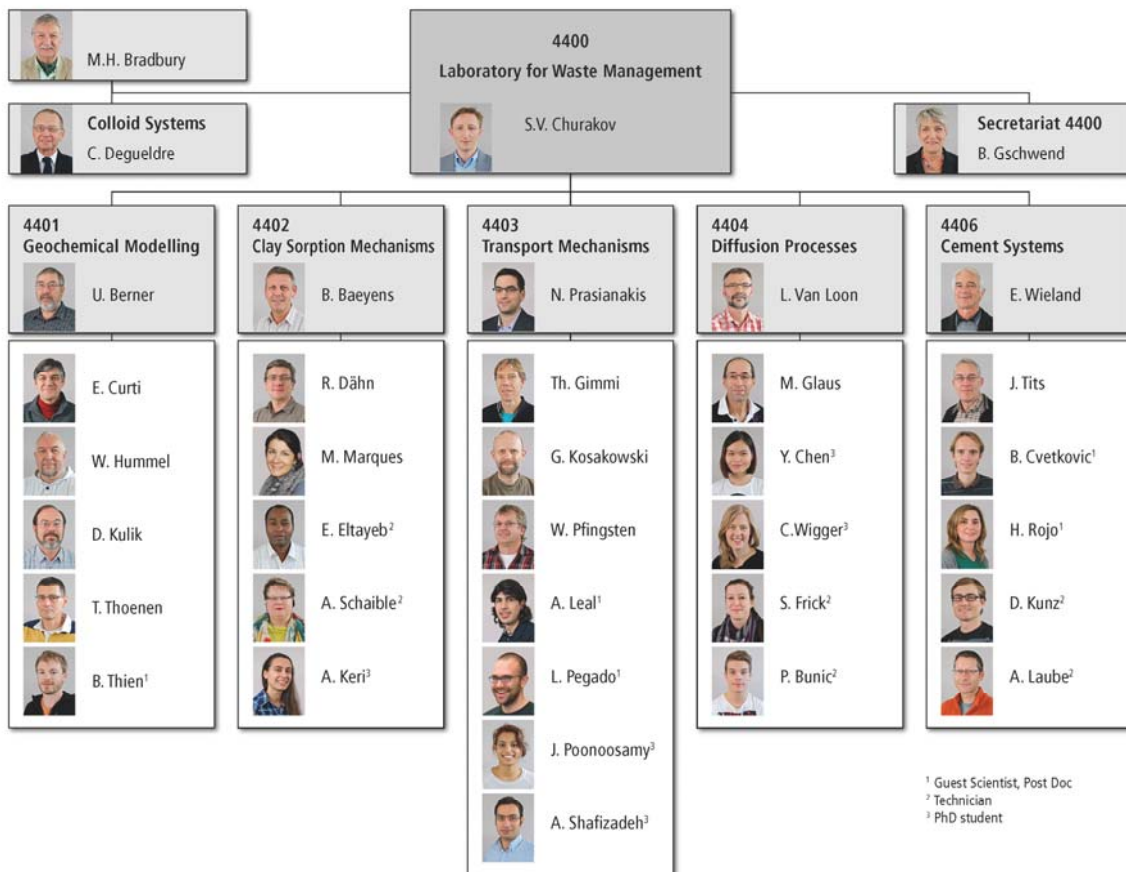
Over several decades LES has participated in the international program on colloid elicited radionuclide transport at the Grimsel Test Site. Within these project activities a significant progress has been made in understanding the generation and mobility of colloids at different conditions. The data and models obtained are advanced and mature for the needs of the RBG. Final sampling and colloid analysis was completed in spring 2015.

1.6 Model development and code benchmarking

The GEM Software is the basic tool used at LES for the thermodynamic modelling, thermodynamic data management and geochemical evaluation of experimental data. The software is actively developed in order to provide access to the state of the art thermodynamic models and algorithms. A substantial part of this development is conducted through external collaboration. Such collaboration also ensures that the software is benchmarked and tested on a wide range of applications. Within the postdoc project of Dr. Leal, in 2015 a new hybrid algorithm for the equilibrium calculation has been developed and made available for the reactive transport simulations. The algorithm unites the advantages of the classical Gibbs Free Energy Minimization technique for the phase selection and the numerical robustness of the Law of Mass Action (LMA) approach. With this algorithm the stability of coupling between OpenGeoSys-GEM and convergence speed up could be achieved.

A reactive transport experiment designed within the PhD project of J. Poonosamy to evaluate porosity-permeability changes triggered by dissolution precipitation processes was accepted for the publication in the book of OpenGeoSys numerical benchmarks. Currently, an international group of three teams apply four different codes to conduct the simulation of the experimental data. Reference calculations include:

1. Flow and advective-dispersive/diffusive transport in a 2D setup
2. Same as in (1) but including effects of liquid density on the transient flow field
3. Flow, transport and kinetically controlled chemical reactions that change porosity and permeability
4. The same as (3), but including effects of liquid density on the transient flow fields.



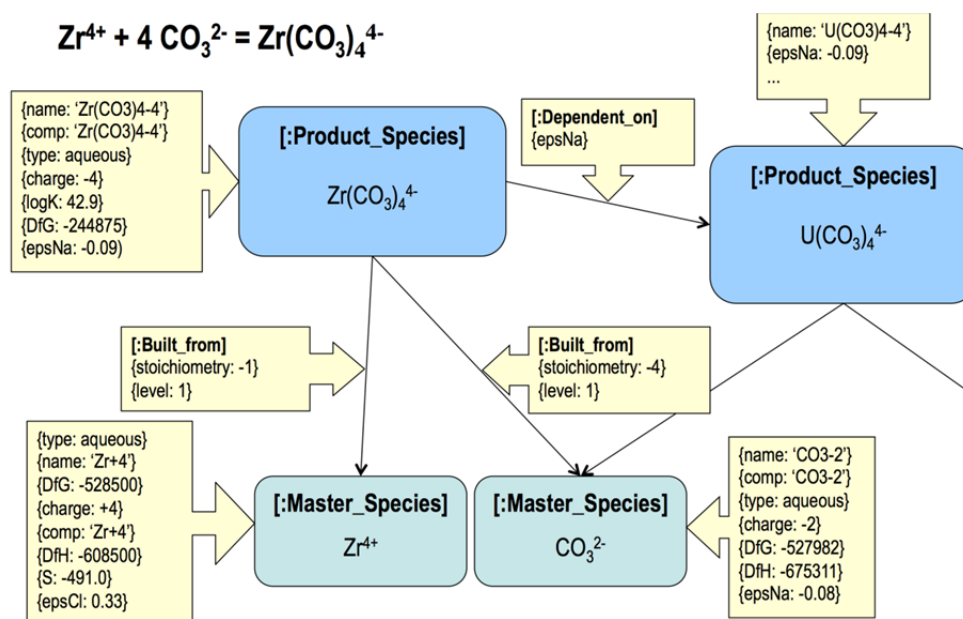


Fig. 2.2: Representation of thermodynamic data in a labeled property graph database. Data as key-value-pairs (yellow arrow boxes) are associated with nodes (rounded rectangles) and directed connectors between nodes. The formation reaction of $\text{Zr}(\text{CO}_3)_4^{4-}$ is represented by the nodes for the product species and the two reactant species Zr^{4+} and CO_3^{2-} and the connectors $[:\text{Built_from}]$ pointing from the product to the reactants. The connector $[:\text{Dependent_on}]$ signifies that the SIT-coefficient $\varepsilon(\text{Zr}(\text{CO}_3)_4^{4-}, \text{Na}^+)$, epsNa , was assumed to be identical with $\varepsilon(\text{U}(\text{CO}_3)_4^{4-}, \text{Na}^+)$. In this example, the nodes are labeled with $[:\text{Master_Species}]$ or $[:\text{Product_Species}]$, and the connectors with $[:\text{Built_from}]$ or $[:\text{Dependent_on}]$.

2.2 Database work

2.2.1 ThermAc project

ThermAc is a collaborative project (Verbundprojekt) concerned with the "Investigation of thermodynamics and speciation of actinides at elevated temperatures in combination with estimation methods, spectroscopic and quantum chemical methods". It is financed by the German Federal Ministry of Education and Research and involves KIT-INE Karlsruhe (with GRS, Braunschweig; Amphos²¹, Barcelona; and LES as subcontractors), HZDR-IRE, Dresden-Rossendorf; FZJ Jülich; Universität Heidelberg; and TU München (duration: 01.03.2015-28.02.2018). The planned contributions by LES are (1) the systematic evaluation and application of isocoulombic reaction equilibria for the extrapolation of equilibrium constants to higher temperatures and (2) the combination of separate (already existing) codes developed by or in collaboration with LES — PMATCHC and the GEM subpackages GEMSFITS, GEM-Selektor and GEMS3K — into an integrated software package for managing, estimating, fitting, and calculating thermodynamic data as a function of temperature and pressure. The database management software PMATCHC will be the central supplier of thermodynamic data to GEMSFITS, developed by D. Miron (ETHZ) for the fitting and optimization of internally

consistent thermodynamic parameters against experimental data (<http://gems.web.psi.ch/-GEMSFITS>), to GEM-Selektor, our geochemical modelling package for the calculation of complex geochemical equilibria at P and T, based on Gibbs free energy minimization, (<http://gems.web.psi.ch>), and to GEMS3K, the numerical kernel of GEM-Selektor. The central role envisaged for PMATCHC requires a major overhaul and we started with the replacement of its outdated database structure. We decided to base the revised version, PMATCHC++, on the labelled property graph database model. A graph database uses graph structures for queries, where data are associated with nodes and edges (also called connectors or relationships) between nodes. Such a graph structure is ideally suited for storing thermodynamic data of chemical reactions. Chemical species and phases can be represented by nodes, and the reactions between them by connectors, which point from products to the related reactants (see Fig. 2.1). Data are stored as key-value-pairs on nodes and connectors (see Fig. 2.2). Properties of chemical species (name, composition, charge, $\Delta_f G^\circ$, $\Delta_f H^\circ$, S° , etc.) are associated with the corresponding nodes, reaction properties (e.g. $\log K^\circ$, $\Delta_r H^\circ$, etc.) with the nodes of the corresponding product species, and stoichiometric coefficients with the connectors relating product species with reactants. Another type of connector can be used to indicate dependencies of

thermodynamic data, e.g., the specific ion interaction theory (SIT) coefficient $\varepsilon(\text{Zr}(\text{CO}_3)_4^{4-}, \text{Na}^+)$ was assumed to be identical with $\varepsilon(\text{U}(\text{CO}_3)_4^{4-}, \text{Na}^+)$. Thus the connector pointing from $\text{Zr}(\text{CO}_3)_4^{4-}$ to $\text{U}(\text{CO}_3)_4^{4-}$ is associated with this information (see Fig. 2.2). In a similar way, different literature references can be represented as nodes with connectors pointing from species nodes to the corresponding reference nodes. Last but not least, an important advantage of the graph database model is that charge patterns of reactions can be easily queried and found, which facilitates the formulation of isocoulombic reactions, the cornerstone of the isocoulombic method for extrapolating equilibrium constants at reference conditions to higher temperatures.

2.2.2 THEREDA project

On 1.10.2015 LES has become a partner of the thermodynamic reference database (THEREDA) project which is organized and carried out by leading research institutions in the field of radioactive and chemotoxic waste disposal in Germany (GRS Braunschweig, KIT-INE Karlsruhe, HZDR-IRE Dresden-Rossendorf, and TU-BAF Freiberg) and financed by four German Federal Ministries or Offices. THEREDA was started in 2006 with the main objective to establish a comprehensive and internally consistent thermodynamic database for the geochemical modelling of processes occurring in the near- and far-field of the different hostrock formations under discussion in Germany for the long-term underground storage of radioactive waste. In the framework of THEREDA, LES evaluates and updates the thermodynamic data related to cementitious systems.

2.3 Consistent evaluation of acid base equilibria in NaCl rich aqueous solutions at high temperatures

Protonation constants reported for carbonates in NaCl aqueous solutions to 5 m and temperatures to 250°C (PATTERSON et al. 1984) triggered a first attempt to evaluate electrolyte and temperature effects concomitantly using the SIT. If the carbonate protonation constants are combined with the dissociation constant of water, measured under the same conditions (BUSEY & MESMER 1978), and the activity of water in aqueous NaCl electrolyte solution as a function of temperature is considered (PITZER et al. 1984), the results become very simple (Fig. 2.3). The temperature variation of the so called isoelectric equilibrium (Eq. 2.1):



can be described by van't Hoff's approach, i.e. by a constant reaction enthalpy only, and the SIT interaction parameter becomes independent of temperature:

$$\begin{aligned} \log_{10}K(I_m, T) - 2 \cdot D(I_m, T) + \log a(\text{H}_2\text{O}) &= A + C / T - \Delta\varepsilon \cdot I_m \\ &= \log_{10}K^\circ + \Delta_r H^\circ / (R \cdot \ln(10)) \cdot (1/T^\circ - 1/T) - \Delta\varepsilon I_m \end{aligned} \quad (2.2)$$

with $\log_{10}K^\circ = 3.75 \pm 0.17$, $\Delta_r H^\circ = -43.7 \pm 1.2 \text{ kJ} \cdot \text{mol}^{-1}$, and $\Delta\varepsilon = -0.075 \pm 0.010$

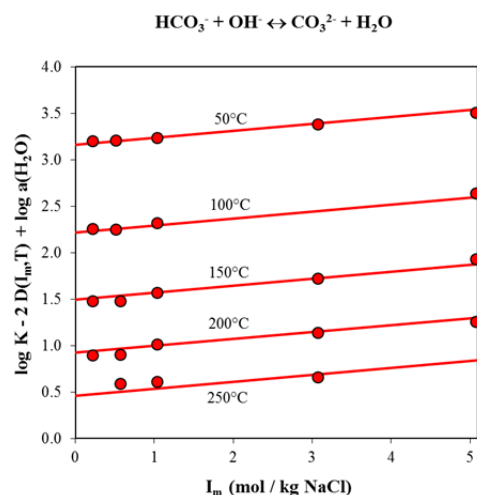


Fig. 2.3: First protonation constant of carbonate in NaCl medium at various temperatures. The values are presented as isoelectric equilibrium constants. The experimental data are shown as symbols. The solid lines are calculated by a 3-parameter expression (see text).

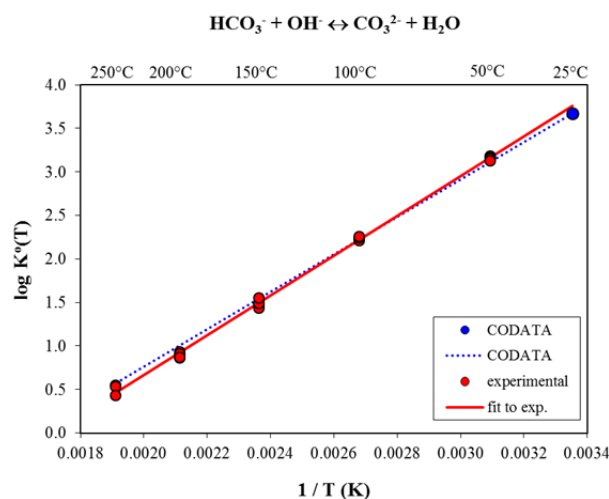


Fig. 2.4: Carbonate protonation versus reciprocal temperature at various NaCl concentrations. The isoelectric equilibrium exhibits linear van't Hoff behaviour. The dotted line is calculated using $\log_{10}K^\circ$ and $\Delta_r H^\circ$ values recommended by CODATA (COX et al. 1989).

Plotting the experimental data versus the reciprocal temperature (Fig. 2.4) reveals that the isoelectric equilibrium (Eq. 2.1) exhibits a linear van't Hoff behaviour up to 250°C. This three-parameter set is easily accounted for in chemical thermodynamic databases for environmental modelling and it ensures some robustness with respect to systemic errors in the original experimental data. As a first step in exploring the range of applicability of this approach, $\log_{10}K^\circ = 3.67 \pm 0.07$ and $\Delta_r H^\circ = -41.1 \pm 0.3 \text{ kJ} \cdot \text{mol}^{-1}$, recommended by CODATA (COX et al. 1989) have been used to predict the temperature dependence of the protonation reaction. The first protonation of carbonate (Fig. 2.4) is predicted with sufficient accuracy within the entire range of experimental data.

The consequences of the three-parameter approximation describing temperature and medium effects of protonation reactions are two-fold. (1) Only the dissociation of water has to be described by complex temperature and ionic strength expressions. This poses no principal difficulty as the dissociation of water has been carefully determined in different media up to 300°C. (2) Besides carbonate, other acid base equilibria, e.g. sulphate, phosphate, acetate, oxalate, citrate, and other organic acids can be modelled to high temperatures by constant reaction enthalpies and temperature-independent SIT interaction parameters when combined with the dissociation of water.

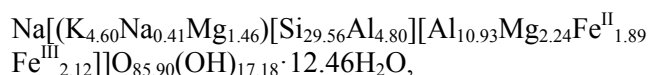
2.4 Thermodynamic model for illite/smectite layers

Clay rocks are presently considered to be the host rock of choice for the disposal of radioactive wastes in the Swiss radioactive waste management programme. When considering the retention of hazardous elements (radionuclides, heavy metals) in deep geological repositories, constituents of clay host rocks (e.g. illites, montmorillonites, mixed layers) have excellent properties. In general, these clay host components show very favourable sorption properties, ion exchange characteristics and act as efficient barriers against the out-diffusion of hazardous elements.

A large amount of ion exchange- and sorption properties of clay minerals and corresponding model approaches are available. In these models the underlying solid clay phase itself is often not considered to have (geo)-chemical properties as this is usually the case for system determining phases. Instead, it is assumed to be chemically inert. We do not believe that this view of clay phases being an inert carrier of properties should be pursued into the future, given that our understanding of geochemical processes continues to improve. We rather believe, and have ample evidence, that clay phases undergo

geochemical reactions and interact with the associated geochemical system.

In an earlier report we developed, calibrated and successfully applied a thermodynamic model for montmorillonite phases in modelling the temporal evolution of deep underground barrier materials (BERNER et al. 2013). Work has now begun to develop a similar model for illite/smectite layers (BERNER 2015), which often is a more abundant constituent/fraction of clay rocks than montmorillonite alone. This illite/smectite layers are an important phase in dealing with reactive transport processes. A key difference compared to montmorillonite is given by the fact that most part of the interlayer is occupied by potassium, which in general prevents illite/smectite layers from swelling due to uptake of water in the interlayer. The first part of the work aims at setting up the stoichiometry of illite/smectite layers, consistent with the former model for montmorillonite and consistent with available analytical data. From available experimental data we derived a stoichiometric composition for the illite/smectite phase:



This rather complex stoichiometric composition is fully consistent with:

- Assumptions concerning the mixing of illite- and montmorillonite-type TOT layers (see Fig. 2.5) including chemically bound interlayer water consistent with weight loss when heating to 1000 °C,
- An exact 2:1 TOT layer composition,
- Assumptions on the distribution between the substituting ions Fe(II) and Fe(III) based on the former montmorillonite model,
- XRD and Rietveld analyses and assumptions on impurities in the illite/smectite layers,
- Elemental analyses of the solid phase,
- Measurements of the cation exchange capacity (CEC),
- Exact charge neutralisation of structural charges with exchangeable and non-exchangeable counterions,
- Absolutely precise electro-neutrality calculated over the entire solid phase (a requirement of databases and codes).

The thermodynamic calibration of the illite/smectite solid against measured solution compositions under the assumption of equilibrium will then be the second part of the study (work in progress).

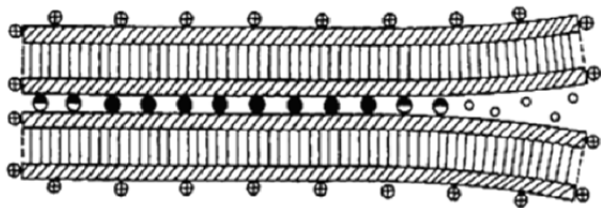


Fig. 2.5: Simple sketch of two interconnected TOT layers used in the present model. The centre part (~ 80 %) of the two layers is interconnected by K^+ (filled symbols, illite section); the edge part(s) (~ 20 %) are interconnected by exchangeable cations (mainly Na^+) associated with water (empty symbols, smectite section). Half-filled symbols may indicate non-exchangeable counter ions different from K^+ in the interlayer of the smectite part. The options of representing illite/smectite layers as alternating illite- and smectite layers or even as a mechanical mixture of illite and montmorillonite are not followed in this work for operational reasons.

Extensive solution data from conditioning processes are available. Similar to the montmorillonite model a solid solution approach will be set up to account for the well-known ion exchange properties of the illite/smectite phase.

2.5 FIRST-Nuclides project

2.5.1 Introduction

The European collaborative project "FIRST-Nuclides" aimed at understanding and quantifying the early release of radionuclides from spent nuclear fuel (SNF) subject to aqueous corrosion in a geological repository (the so-called Instant Release Fraction, shortly IRF). Although the project was officially terminated on Dec. 31, 2014, the evaluation and interpretation of the data was finalized during the year 2015. The present contribution only reports on the final results obtained at PSI from the above mentioned project. All other results are documented in previous LES progress reports (2013, 2014).

Previous studies have shown that the release of radionuclides from SNF under geologic disposal conditions is controlled by two mechanisms: (a) the rapid release of soluble fission products, mainly long-lived radioisotopes of Cs, I, Cl as well as ^{14}C , and (b) the slow release of actinides and fission products due to the dissolution of the UO_2 matrix. In the long-term safety assessment terminology, the rapid release is often referred to as IRF and is thought to include the release of soluble nuclides from the fuel/cladding gap (first days/weeks) and the release of soluble nuclides segregated at fuel grain boundaries accessible to water

(weeks/months). The IRF is a critical parameter in safety assessment, but this parameter is frequently affected by large uncertainties due to the scarcity of reliable experimental data, particularly for high burn-up fuel. A main objective of FIRST-Nuclides was to reduce such uncertainties by providing new IRF data for high burn-up UO_2 and MOX fuel irradiated in different pressurized water reactors (PWR) or boiling water reactors (BWR) in Europe.

PSI contributed with: (a) Leaching experiments on high-burnup SNF from the Gösgen and Leibstadt nuclear power plants, using a 19 mM NaCl - 1 mM $NaHCO_3$ (pH ~ 7.4) leaching solution; (b) Characterization of the chemical state (oxidation state, coordination environment) of selenium in pristine (non-leached) SNF. The main purpose of task (a) was to provide new IRF data on SNF from Swiss nuclear power plants, with particular focus on high burn-up UO_2 fuels and MOX fuel. The data were integrated in a database encompassing all IRF data from other project partners and will help defining nuclide-specific IRF parameters for safety assessment calculations. For task (b), the goal was to provide a mechanistic explanation for the unexpectedly low release of Se (IRF < 0.22 %) measured in both, earlier (JOHNSON et al. 2012) and current experiments through X-ray spectroscopy studies.

2.5.2 X-ray spectroscopy

The main objective of the spectroscopic measurements was to determine primary oxidation state and atomic-scale coordination of Se in selected non-leached UO_2 SNF samples, in order to understand the non-appearance of Se release in aqueous leaching experiments. X-ray spectroscopy data previously obtained on micro-samples of UO_2 SNF from the Leibstadt and Oskarshamn-III reactors (see LES progress reports 2013, 2014) suggested that Se probably occurs as Se(-II) substituent in oxygen sites of the UO_2 lattice, however, the evidence was not conclusive. During this year, we were able to measure the Se K-edge XANES spectrum of an uranium selenide (Use) sample available from another project at PSI. The XRD characterization (Fig. 2.6) showed that, in spite of the long storage time (11 years), no Se oxidation occurred. Only a minor quantity of another U selenide compound (U_3Se_4) formed during this time. Therefore, the sample could be used as a Se(-II) reference for comparison with the Se K-edge XANES of the SNF samples. The comparison of the absorption spectra (Fig. 2.7) shows a good match between SNF and "Use" XANES spectra, thus providing evidence that Se in the SNF samples is directly bound to U atoms as selenide. This conclusion is strengthened by the even better agreement with the theoretical XANES spectrum of Use (Fig. 2.8) obtained using the

FDMNES software (JOLY, 2001). The calculation was performed on small spherical clusters (3 Å radius) of the cubic UO_2 structure around a central Se absorber replacing an oxygen atom, assuming an amplitude reduction factor (S_{O_2}) of 1.0, Green formalism (multiple scattering) on a muffin-tin potential and self-consistent potentials.

The results of the spectroscopic investigations are thoroughly documented in two publications (CURTI et al. 2014, CURTI et al. 2015).

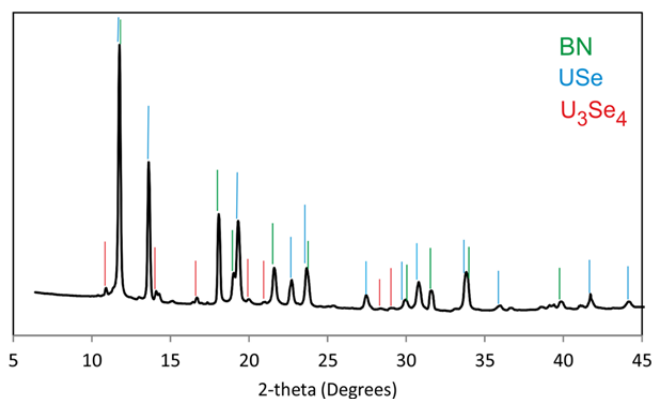


Fig. 2.6: XRD pattern with assigned reflections obtained from the "USe" reference sample. Boron nitride (BN) was present as diluting substance for the XANES acquisition in transmission mode.

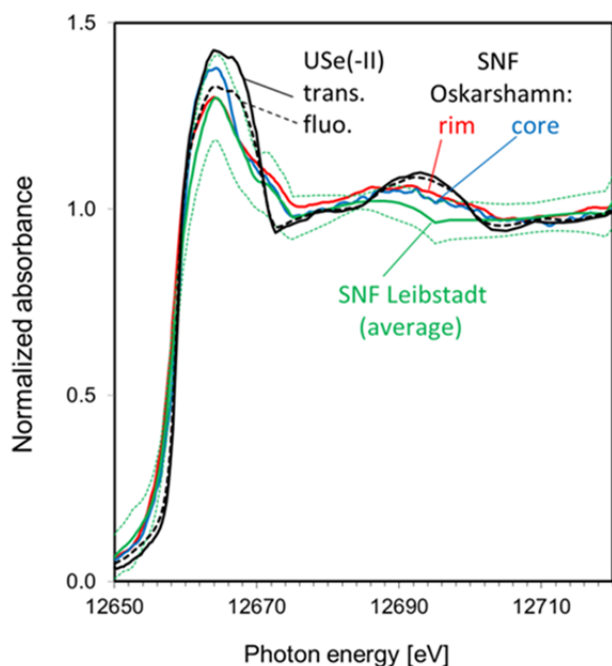


Fig. 2.7: Superposition of experimental XANES spectra obtained on USe(-II) in transmission (trans.) and fluorescence (fluo.) with the averaged spectra of SNF samples. The dotted green lines delimit the envelope of all data from Leibstadt fuel. The "rim" and "core" curves refer to samples obtained from the center and periphery of the same pellet of Oskarshamn-III fuel.

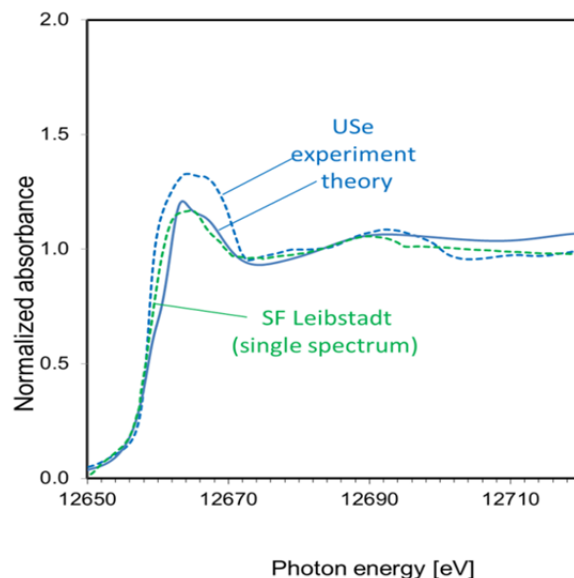


Fig. 2.8: Superposition of theoretical and experimental spectrum for USe (top) compared to a typical single spectrum collected on Leibstadt SNF.

2.5.3 Leaching experiments

^{129}I and ^{137}Cs release data were obtained up to a leaching time of 182 days on UO_2 SNF samples from the Leibstadt (BWR) and from the Gösgen (PWR) nuclear power plants. During reactor operation the fuel rods achieved average burn-ups of 57.5 and 56.6 $\text{GWd}\cdot(\text{t iHM})^{-1}$, respectively. A MOX fuel rod from Gösgen with 63.0 $\text{GWd}\cdot(\text{t iHM})^{-1}$ was also included in the series of leach experiments. Based on the experience made during analogous earlier experiments (JOHNSON et al. 2012) UO_2 fuel rod specimens of 20 mm length were prepared for the BWR and PWR samples, whereas a 10 mm length was judged sufficient for the MOX samples and an UO_2 sample dedicated to the determination of the fuel burn-up. Some experiments were carried out with intact pellet segments, whereas other leach tests were performed with fuel fragments separated from the cladding.

The samples were introduced in glass columns (total volume approx. 250 mL) which were filled with 30 mL of leaching solution (19 mM NaCl + 1 mM NaHCO_3 solution, pH ~ 7.4). After 7 days ("pre-leaching"), the entire solution volume was sampled for analysis through a sealed outlet cock with an integrated glass filter preventing clogging by solid particles. The columns were then immediately refilled with 115 mL of fresh solution and 15 mL aliquots were subsequently taken sequentially after total leaching times of 28, 56 and 182 days (no refill). The equipment is shown in Fig. 2.9.

Fig. 2.10 shows the experimental results in terms of "Fraction of Inventory in the Aqueous Phase" (FIAP) as a function of leaching time for ^{137}Cs and ^{129}I , calculated from measurements of the radionuclide activity in the probed leaching solutions (gamma-spectrometry) after normalization to a model reference inventory. As expected, the FIAP-values roughly correlate with the fission gas release (FGR) measured from puncture tests. Consistent with earlier tests described in JOHNSON et al. (2012), release of both ^{137}Cs and ^{129}I is larger from the Gösgen samples (particularly from MOX fuel) than from Leibstadt samples. The most important insight is that FIAP values of both ^{137}Cs and ^{129}I are 2-3 times higher for the intact cladded UO_2 Gösgen pellet than for fragmented fuel, in spite of the much higher surface area of the latter (see insert in Fig. 2.9). From this observation, one deduces that the IRF contribution from the fuel/cladding gap must be much larger than the contribution from fissures and grain boundaries inside the UO_2 matrix for Gösgen samples.



Fig. 2.9: Experimental setup of the spent fuel leaching experiments at PSI. The insert shows spent fuel fragments separated from the cladding.

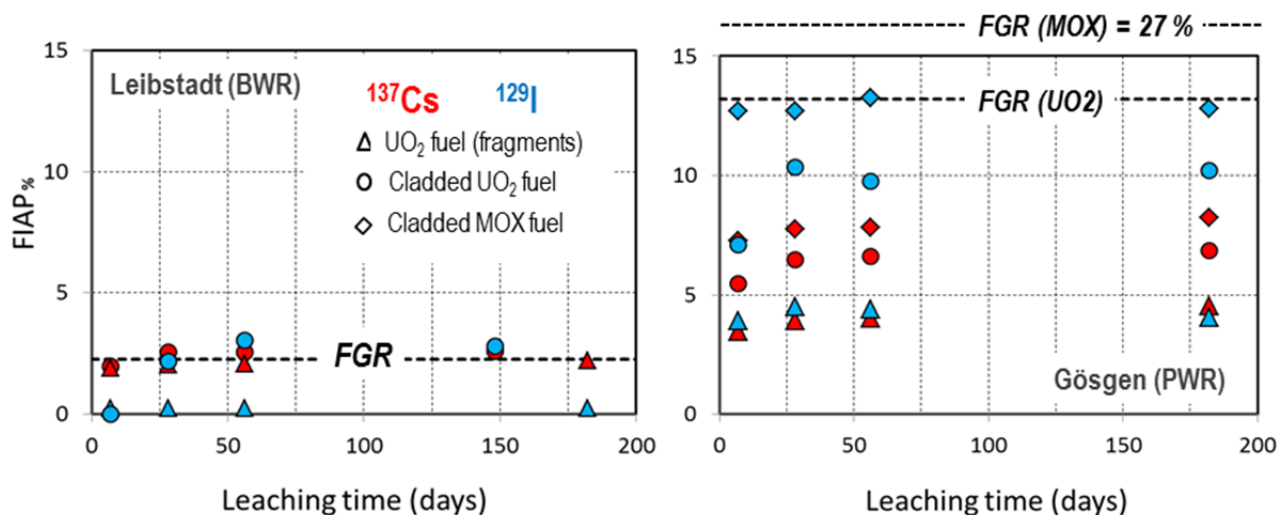


Fig. 2.10: Experimental results of SNF leaching tests carried out at the hot laboratory of PSI (FGR: Fission Gas Release).

2.5.4 Thermodynamic calculations

Simple thermodynamic calculations were carried out to determine the stability of Se redox species in SNF under reactor operation and dry storage conditions. The results of these calculations are reported in a classical Ellingham diagram (Fig. 2.11). Such diagrams are routinely used to evaluate the chemical state of fission products in SNF. This is done by comparing the oxygen potential ($\Delta G_{\text{O}_2} = RT \ln p_{\text{O}_2}$) of a given fission product (FP) at a given temperature with the oxygen potential of the fuel. At any given temperature, fission products with an equilibrium oxygen potential for a specific oxidation-reduction reaction exceeding that of the fuel should be stable in the reduced form (e.g. metallic state). Conversely, if

the oxygen potential of the fuel exceeds that of the fission product oxidation-reduction equilibrium, the latter should be stable in the oxidized form.

The determination of the fuel oxygen potential, even for pure UO_2 fuel, is not a trivial task as it depends on UO_2 hyper-stoichiometry, the concentration of FPs and actinides in the UO_2 lattice and on the ability of incompatible FP to buffer the oxygen potential in a complex way. CORDFUNKE & KONINGS (1988) were able to restrain this parameter for light water reactor (LWR) fuels to a range between -550 and 450 kJ/mol, which we used for the comparison with the oxygen potential calculations of Se species. In order to evaluate the stability of Se oxidation states (-II, 0, IV, VI) in spent UO_2 fuel, the following equilibria have

been assessed, using the data compiled in OLIN et al. (2005):

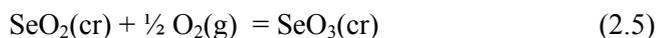
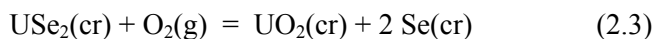


Fig. 2.11 shows the stability limits for pairs of the pure selenium phases according to reactions I-III, compared to the range of oxygen potentials for LWR UO_2 fuels estimated by CORDFUNKE & KONINGS (1988). The results indicate that at typical operation temperatures of 1500 K in the center of the fuel pellet, $\alpha\text{-USe}_2$ would be the stable phase. As the SNF cools down ($T < 700$ K) metallic Se becomes more stable. Thus, during reactor operation formation of selenide is favoured, whereas under storage conditions there is a tendency for conversion to metallic Se. Whether such a conversion can take place or not will largely depend on kinetic factors. If Se fission products are first stored as dispersed selenide ions in the UO_2 matrix, as indicated by our spectroscopic results, a subsequent transformation to a segregated discrete $\text{Se}(0)$ phase would require high ionic mobility. However, reaction and diffusion rates rapidly decrease as the fuel cools below 1000 K (CORDFUNKE & KONINGS 1988), thus limiting migration and oxidation of $\text{Se}(\text{-II})$ to $\text{Se}(0)$. According to Fig. 2.11, easily soluble oxidized forms like $\text{Se}(\text{IV})$ and $\text{Se}(\text{VI})$ should not be stable under any conditions.

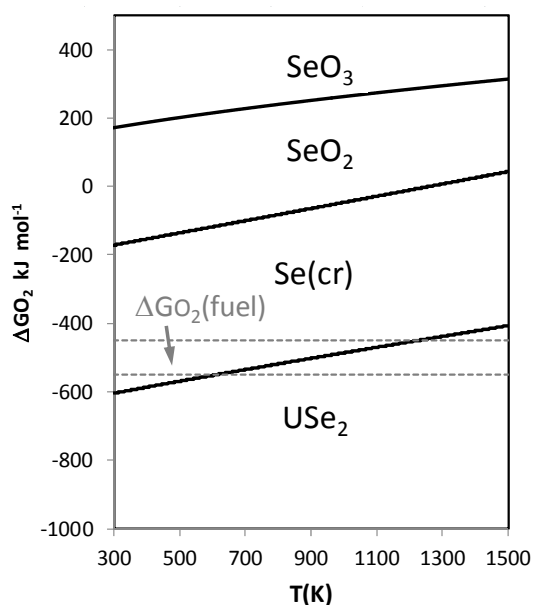


Fig. 2.11: Ellingham diagram showing the stability regions of the indicated selenium phases, compared with the range of oxygen potentials for LWR UO_2 fuels.

2.6 GEMS and its applications

2.6.1 Introduction

The widely used GEM Software (GEMS) code packages (<http://gems.web.psi.ch>) have been developed since 2000 in LES by a non-committal team led by Dr. Dmitrii Kulik. GEMS-compatible chemical thermodynamic databases include the PSI-Nagra Chemical Thermodynamic Database 12/07 (www.psi.ch/les/database) for applications related to geological radioactive waste disposal. The imported SUPCRT98 database is provided to support hydrothermal geochemistry applications. Third-party databases for hydrated cement systems (www.empa.ch/cemdata) and for nuclear materials (www.psi.ch/heracles/gems-specific-heracles-database) are available as well.

2.6.2 Ongoing work

GEMSFITS code is a tool for optimization of multiple input parameters of chemical thermodynamic models (MIRON et al. 2015). In the reporting period, the code was improved to version 1.1 and heavily used in on-going research projects (see below).

TSolMod library (WAGNER et al. 2012). Extensions made in 2015 were aimed at improving multi-site models of mixing in sublattice solid solutions by adding reciprocal non-ideality terms, as well as adding Calphad-type interaction parameters. These extensions are used in parameterization of CASHNK solid solution models (see below).

NextGEMS prototypes. In the reporting period, the development of GEMS was strongly advanced by participation of Dr. Allan Leal (postdoc, now at ETHZ IG GEG) in connecting GEMS with his Reaktoro framework for modelling chemically reactive systems (www.reaktoro.org). The Reaktoro library contains several efficient and robust numerical methods for chemical equilibrium and kinetics calculations created by A. Leal in strong collaboration with LES (see also section 3). As a result, the GEMS4R prototype solver of chemical equilibria (<https://bitbucket.org/gems4/gems4r>) coupled with the Reaktoro framework (Fig. 2.12) is now under testing. All alternative GEM algorithms use the same classes for the calculation of activities of components in phases and/or kinetic rates, while using the same interface to upper-level codes as the previous GEMS3K kernel. The GEMS4R code has the potential to come into the mainstream of GEMS development.

This work was motivated by our needs for improving the robustness and speed of reactive transport modelling, and by the observations that no single GEM algorithm is best for all types of chemical systems.

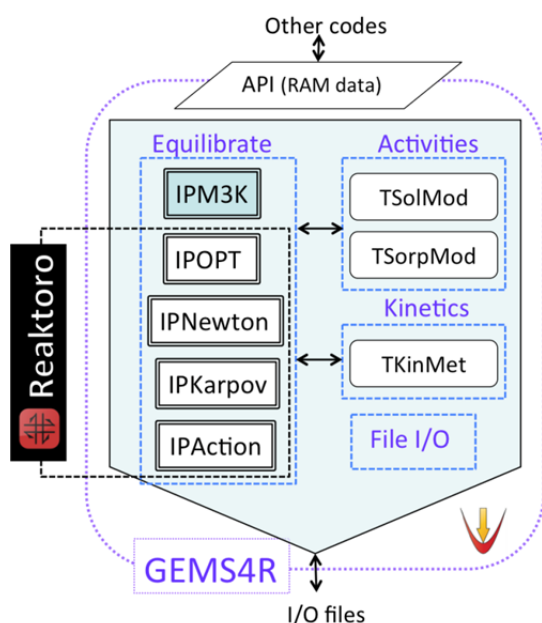


Fig. 2.12: General structure of the GEMS4R kernel prototype. IPNewton, IPKarpov and IPAction are new GEM algorithms implemented in the Reaktoro framework by A. Leal during his work at LES PSI. IPM3K is the default GEM algorithm (KULIK et al. 2013).

One of the new algorithms (IPAction) is especially promising because it combines the advantageous features of both LMA and GEM approaches and, thus, can be considered as a "Revised LMA" (LEAL et al. 2015, in submission). Having the option of using different algorithms is beneficial because switching to another algorithm can often solve the equilibrium state if the previously chosen GEM algorithm failed to converge.

Utilizing LMA-style thermodynamic databases in GEM calculations. There are several databases (Phreeqc.dat, Phrqpitz.dat, EQ3/6.dat, PSINagra.dat) used with popular LMA codes such as PHREEQC (<http://www.hydrochemistry.eu>) or VMINTEQ (<http://vminteq.lwr.kth.se>). Such databases were built upon a pre-selection of *master components* (usually aqueous ions, organic and surface ligands), in terms of which the bulk system composition must be defined. *Master chemical species* correspond to master components and directly come with their amounts into the mass balance. Other, *product chemical species* (i.e. aqueous complexes, gases, minerals, surface complexes) are then defined through their reactions of formation from master species. Product species are taken into the mass balance via *LMA equations* for those reactions with equilibrium constants ($\log_{10}K$) that are kept in the database. The *speciation*, i.e. mole amounts of all species in equilibrium, is computed by simultaneously solving mass-balance equations with LMA equations (REED 1982).

Unfortunately, LMA-style databases cannot be directly used in GEM equilibrium calculations that require standard chemical potentials (Gibbs energy per mole) G° for all components in all phases. In general, converting an LMA-style database into a form usable in GEM requires a non-trivial procedure of merging it with the SUPCRT98 or similar database to retrieve standard thermodynamic properties of master species and propagate them to that of product species, as done for the GEMS version of the Nagra-PSI database in THOENEN & KULIK (2003). However, in some cases such procedures are difficult, especially when some master species are surface sites or metastable organic ligands whose standard thermodynamic properties are not available.

Yet, there is a motivation to enable GEM methods, such as IPNewton (LEAL et al. 2015) or IPAction (LEAL et al. 2015, in submission), to take advantage of the available LMA-style thermodynamic databases, and thus re-use thousands of existing modelling cases. To make this possible, we developed a simple alternative method for conversion of LMA- into GEM-style databases, in which the conditional G°_{cond} values of all species are calculated solely from $\log_{10}K$ values for product species (LEAL et al. 2015, in prep.). We have shown (by benchmarking PHREEQC, Reaktoro and GEMS4R calculations) that the new database conversion method, implemented in the Reaktoro framework, www.reaktoro.org, successfully produces GEM-calculated equilibrium speciation largely equivalent to LMA-calculated speciations.

2.7 Solid solution – Aqueous solution systems

In the LES progressC-S-H report 2014, we described the CASHNK multi-site solid solution model based on the defect-tobermorite structure. By permutation of all assumed substitution moieties in three structural sites (sublattices), the model generates a multitude of end members (45 in total), most of which do not exist in pure state. Some substitutions on sites may be related to excess energies and, thus, need non-ideal interaction parameters. The feasibility of such a complex solid solution model was shown for the C-S-H sub-system by scoping calculations with the GEM-Selektor code.

In 2015, we parametrized the CASHNK model using the GEMSFITS v.1.1 code (MIRON et al. 2015) with the following strategy:

1. Start with the C-S-H sub-system (initial G° of 8 end members) with zero interaction parameters; proceed with fitting G° values of end members against the C-S-H solubility and mean chain length (MCL) data, then fine-tune the model by optimizing the on-site interaction parameters.

- Extend the C-S-H sub-system to C-S-H-K by adding 4 potassium-containing end members; fit G° values of these end members to available solubility data, then fine-tune interaction parameters, if necessary.
- Apply the same procedure as at step 2 to derive the C-S-H-N sub-system with the addition of 4 sodium-containing end members. Keep all parameters optimized at steps 1 to 3 fixed in subsequent parameterization steps.
- Step back to the C-S-H sub-system and extend it to C-A-S-H system by adding 19 Al-containing end members; adjust G° values of 19 end members to solubility data, then fine-tune the interaction parameters; check against the available MCL data, solubility and aluminium speciation data in GEM-Selektor trial calculations.

All parameters fitted at one stage are fixed in the subsequent parameterization stages. To date, stage (1) is completed, and stages (2) to (4) are in the preparation. In the following, we report the results from stage (1), where we used the following experimental C-S-H solubility datasets: Ch04D: "Curve C^w" or double decomposition data (CHEN et al. 2004); ELH: C-S-H co-precipitation data (L'HOPITAL et al. 2014); Haas: Data from (HAAS & NONAT 2015; HAAS 2012). The trends in all three datasets are very similar, common for the solubility of C-S-H obtained by co-precipitation synthesis methods. Based on this, the Ch04D, ELH and Haas datasets were combined into one dataset. Of 62 samples in total, 2 were excluded as outliers. Parameter optimization was performed using the least-square objective function that included several parts as described in (MIRON et al. 2015).

At step 1 of fitting, we used the global genetic evolutionary algorithm GN_ESCH. The freely adjustable parameters were the G°_{298} values of all 8 C-S-H end members (all interaction parameters W in the Berman model were set to zero). In the results (not shown), the fit for Ca_{AQ} was good, for Si_{AQ} reasonable (too high at target $\text{Ca}/\text{Si} > 0.9$); and the fit for MCL was bad at $0.75 < \text{Ca}/\text{Si} < 1.3$. Conversely, to improve the MCL fit, i.e. the structural consistency of the sublattice solid solution model of C-S-H, the objective function must include the MCL data with a weight comparable to that for the solubility data. However, the ^{29}Si MAS NMR data from which the MCL data were derived are scarce and not available for all samples in all datasets. Fortunately, the available MCL data plot very well into the same trend as function of Ca/Si ratio in C-S-H for all three co-precipitation datasets (Fig. 2.13). Keeping in mind that the MCL data result from deconvolution of NMR peaks and, thus, are not very precise, we have

regressed the data Ch04D and ELH (using the SigmaPlot 11 software) with an exponential decay function

$$MCL = (0.391 \pm 0.083) \exp \frac{(2.302 \pm 0.267)}{C/S - (0.195 \pm 0.035)} \quad (2.6)$$

where C/S stands for the Ca/Si ratio in C-S-H. With this equation, the MCL values were restored for all data points in all three experimental datasets, and then used in the objective function as MCL pseudo-data.

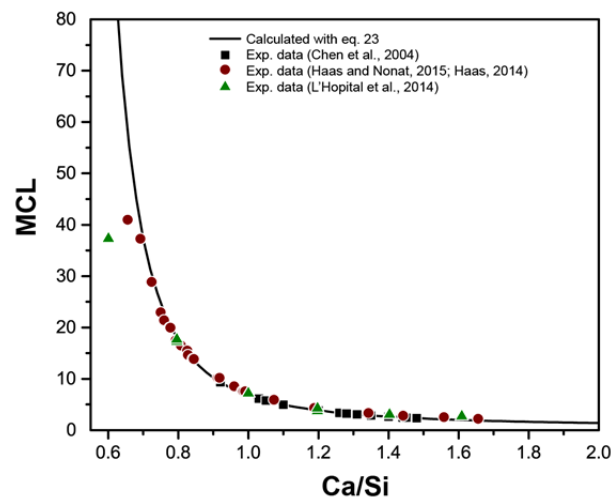


Fig. 2.13: MCL data plotted against Ca/Si ratio in C-S-H. MCL-fit is the curve of eq (2.6). Scattered symbols denote the experimental data sets.

At step 2, to improve the fit for MCL, the fitting task was run with the objective function that included the MCL data, using the same global algorithm and settings as in step 1. The results revealed a perfect fit for the MCL data, but a bad fit for both Ca and Si solubility data (not shown). Clearly, the solid solution model without the excess Gibbs energy terms could not fit well the solubility and the MCL trend at the same time. To prepare an initial dataset for local fitting runs (step 3) with the G_{ex} interaction parameters, the fitted G° values from steps 1 and 2 were compared, and their averages were taken as initial values, with the bounds UB (upper bound) and LB (lower bound) taken slightly greater than half-differences.

At step 3, the initial values for G°_{298} of the end members were taken from fitted values from step 2, bracketed with ± 10 kJ/mol. The weight for the MCL part of the objective function was decreased slightly. The model was fitted at this stage with the local optimization algorithm LN_BOBYQA using the Berman model for excess Gibbs energy of mixing. Two substituting moieties per structural site in the C-S-H model (cross-site interaction parameters are not permitted) lead to six interaction parameters of the asymmetric model or three interaction parameters of the symmetric model.

Table 2.1: Symmetric site interaction parameters (Berman model).

Sublattice (sites)	Site index	Interaction parameter	Substituting moieties (codes)
IC (interlayer cations)	0	$W_{\text{HC},0}$	$(\text{H}_3\text{O})_2^{2+} - \text{H}_2\text{OCa}^{2+}$ (H – C)
BT (bridging tetrahedra)	1	$W_{\text{Sv},1}$	$\text{SiO}_2 - \text{Va}$ (S – v)
CU (CH units)	2	$W_{\text{Cv},2}$	$\text{Ca}(\text{OH})_2 - \text{Va}$ (C – v)

Note: end-members are coded by combining one moiety per sublattice (T stands for the Tobermorite unit, common for all end members), e.g. THSv end-member formula is $\{(\text{H}_3\text{O})_2^{2+}\}:\{\text{SiO}_2\}:\{\text{Va}\}:\text{Ca}_2\text{Si}_2\text{O}_5(\text{OH})_4$.

Table 2.2: Initial and fitted parameters of the C-S-H multi-site solid solution model (in kJ/mol).

Parameter, end member	Initial estimate	Fitted I value	Fitted I – Initial	Fitted II value	Confidence interval 95%	Fitted II – Fitted I
G_{298}° TCSC	-6205.14	-6225.45	-20.31	-6225.68	1.807	-0.23
G_{298}° TCSv	-5308.13	-5328.42	-20.29	-5327.71	1.207	0.71
G_{298}° TCvC	-5354.53	-5336.29	18.24	-5335.98	7.234	0.31
G_{298}° TCvv	-4457.51	-4456.72	0.79	-4456.67	0.598	0.05
G_{298}° THSC	-6014.85	-6042.95	-28.1	-6042.74	0.314	0.21
G_{298}° THSv	-5117.84	-5124.53	-6.69	-5124.59	0.273	-0.06
G_{298}° THvC	-5164.24	-5155.60	8.64	-5155.01	1.021	0.59
G_{298}° THvv	-4267.22	-4264.86	2.36	-4265.12	0.237	-0.26
$W_{\text{HC},0}$	0	-2.29	-2.29	-3.27	0.888	-0.98
$W_{\text{Sv},1}$	0	-10.77	-10.77	-10.78	0.328	-0.01
$W_{\text{Cv},2}$	0	-19.28	-19.28	-19.56	0.633	-0.28

For abbreviations of end member names, see Table 2.1.

Comparison of fits with the symmetric and asymmetric Berman model showed that they are of good overall quality, although the symmetric model yields a slightly worse fit of MCL data but a better fit for dissolved CaAQ concentrations. This fact allows considering the symmetric non-ideality with binary interactions, Table 2.1, as the basis for further extension of the C-S-H model because of a smaller number of fitting parameters.

Parameters fitted for the symmetric case (Table 2.2, Fitted I values) were used in GEM-Selektor for forward process calculations to test the quality and performance of the parameterized C-S-H model. The results are shown in Fig. 2.14.

Evidently, the fits to both solubility and MCL data are good. From Table 2.2, it can be seen that the

initial estimates of thermodynamic properties of end-members (and initial zero interaction parameters), in fact, have much smaller uncertainties (20 - 30 kJ/mol or less) than the uncertainty of 50 kJ/mol used in global fitting. In Fig. 2.14B one can see peaks at mole fractions of the THSC (fully polymerized) and THvv (dimeric) end members around Ca/Si = 0.96 of about equal height; the MCL is close to 5 in accord with the assumed ordered T5C end member of the earlier C-S-H3T model of C-S-H solid-solution (Kulik 2011, Table 3).

Our structurally consistent model somewhat over-predicts the experimental data for dissolved Si at Ca/Si > 1.1, similar to earlier C-S-H solubility models (KULIK 2011, LOTHENBACH & NONAT 2015). Inspection of aqueous speciation of silicon at bulk

Ca/Si > 1.6 (calculated with GEM-Selektor) reveals that the predominant species at these conditions is the CaSiO₃(aq) complex (96% of dissolved Si and 0.12% of dissolved Ca).

Note that in the GEMS database, CaSiO₂(OH)₂(aq) is represented as CaSiO₃(aq) under the assumption that $K = 1$ for the reaction CaSiO₂(OH)₂(aq) = CaSiO₃(aq) + H₂O.

Selection of data for this complex in the PSI-Nagra database 12/07 (HUMMEL 2014, THOENEN et al. 2014) was based on a single set of potentiometric titrations of Si(OH)₄(aq) in the presence of Ca²⁺ and Mg²⁺ in 1 M NaClO₄ up to pH 9 (SANTSCHI & SCHINDLER 1974). In this work, in order to avoid the formation of polymeric silicate species and the precipitation of amorphous silica, the total ligand concentration was less than 2.3·10⁻³ M. Based on chemical arguments, interpretation of the experimental data could be done in terms of two equilibria:



with the values $\log_{10}K^0(\text{Eq. 2.7}) = (1.2 \pm 0.1)$ and $\log_{10}K^0(\text{eq. 2.8}) = (4.6 \pm 0.2)$. Note that the underlying experimental data were obtained at pH < 9, although only in the pH region between 11.5 and 12.5 relevant for solubility of Ca-rich C-S-H, the CaSiO₃(aq) (CaSiO₂(OH)₂(aq)) complex becomes really predominant. Therefore, the uncertainty of $\log_{10}K^0(\text{eq. 2.8})$ must be much greater than ± 0.2 and can only be reduced when new experimental data for Ca-Si complexation at pH between 9 and 13 become available. So far, the C-S-H solubility is the only kind of such data.

We performed an indirect test of the hypothesis that $\log_{10}K^0(\text{eq. 2.8}) = 4.6$ is too strong using our C-S-H aqueous – solid solution model against the C-S-H solubility data. It yielded that in this system (with stable C-S-H and portlandite phases), the total dissolved molality Si_{AQ} is about 2.5 times higher than typical experimental values of about 1·10⁻⁵ m. To fix this by adjusting the stability of CaSiO₃(aq) complex, its initial $G_{298}^0 = -1517.557$ kJ/mol was changed to $G_{298}^0 = -1514.703$ kJ/mol by adding 2.854 kJ/mol or 0.5 log₁₀K units, and the speciation calculation was repeated. The Si_{AQ} was less than 1·10⁻⁵ m, although the CaSiO₃(aq) complex was still predominant with 88%. The impact of such correction on the C-S-H solubility diagram is shown in Fig. 2.14D. We also tried the adjustment of G_{298}^0 of CaHSiO₃⁺ by 0.5 log₁₀K units, but this had no visible effect on the solubility diagram of C-S-H (Fig. 2.14B) because this complex remains insignificant at pH above 9.7.

At step 4, we undertook one more fitting exercise with GEMSFITS to see how the adjustment of the stability of the CaSiO₃(aq) complex can improve the overall fit of the C-S-H solid solution model against the solubility data. To evaluate the parameter confidence intervals, Monte Carlo (MC) sampling was performed in 300 trials. The initial $G_{298}^0 = -1517.557$ kJ/mol of CaSiO₃(aq) was adjusted (by 1.5 to 3.0 kJ/mol) in a series of calculations. We found that the optimal fit can be achieved at $G_{298}^0 = -1515.845$ kJ/mol (1.713 kJ/mol more positive, or 0.3 pK units). Results are given in Fig. 2.15 and Table 2.2 "Fitted II" values; adjustments were minor (<1 kJ/mol).

This worked example of simultaneous fitting of 11 parameters of the C-S-H sub-model of the sublattice CASHNK model clearly demonstrates the efficiency of the GEMSFITS code in obtaining internally consistent thermodynamic datasets by using various kinds of experimental and spectroscopic data. The above description covers only the first part of the multi-stage fitting process (KULIK, MIRON & LOTHENBACH 2016, in preparation).

In addition, these fitting results show that the stability constant of the CaSiO₃(aq) (CaSiO₂(OH)₂(aq)) aqueous complex as given in the PSI-Nagra 12/07 database is about 0.3 to 0.5 pK units too stable. Reconsideration of experimental data (SANTSCHI & SCHINDLER 1974) shows that at pH < 9 the neutral species, CaSiO₃(aq), is minor and its stability as determined in eq. (2.8) is quite uncertain (B. Lothenbach, pers. comm.). It seems that C-S-H solubility data at Ca/Si > 1 may be the only source to constrain the stability of this species (to make it 0.3 – 0.4 pK units less stable, to $\log_{10}K^0 = 4.3 \pm 0.4$ in eq. 2.8) in fitting the aqueous solid-solution model of C-S-H to the solubility data.

For the C-S-H-K and C-S-H-N solid solution models, reasonable fits of the solubility data were also obtained, but the calculated MCL values were higher than those determined for alkali C-S-H. A similar observation has been made for the C-A-S-H sub-system, namely that no good consistency of the solid solution model to structural data can be achieved if such data were not involved in the parameterization. Unfortunately, a large part of experimental solubility data where dissolved Al concentrations fall at or below detection limits must be discarded because of poor quality and/or dependence on reaction time in the experiments. Better fits were only obtained at relatively high Ca/Si ratios. Work on this topic is still in progress.

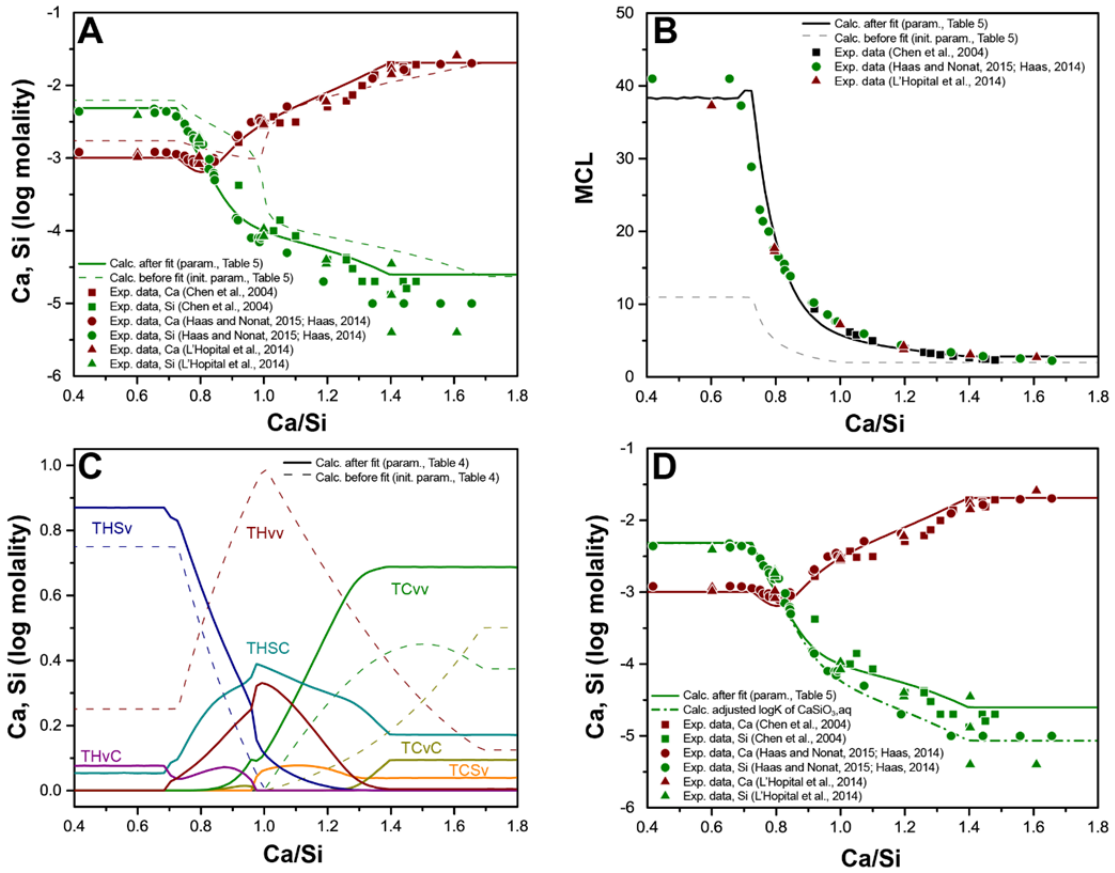


Fig. 2.14: GEM-Selektor process diagrams for the parameterized C-S-H model: A: solubility, B: MCL data, C: end-member mole fractions. Dotted curves correspond to the initial parameter values from Table 2.2; solid curves result from using the fitted I parameter values. Panel D compares the same calculation with fitted parameters as in (A) (solid curves) and that with G°_{298} of the $\text{CaSiO}_3(\text{aq})$ aqueous complex corrected by +2.854 kJ/mol or 0.5 logK units less stable (dotted curves). Scattered symbols correspond to the same composite dataset of 60 co-precipitation samples that has been used in fitting exercises, including the MCL pseudo-data.

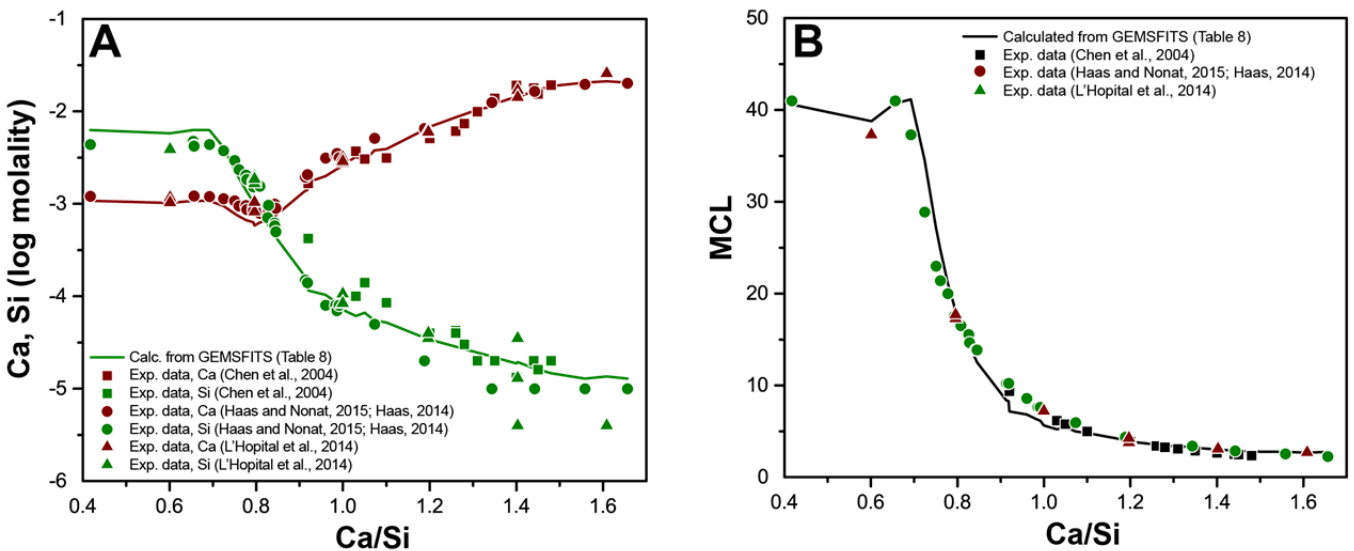


Fig. 2.15: GEMSFITS plots for the re-parameterized C-S-H model (Table 2.2, "Fitted II" columns): A: Ca and Si solubility (in log molal units), B: MCL. Curves connect optimized model-calculated values, scattered symbols represent experimental data.

2.8 Water rock interactions in Icelandic hydrothermal systems

Sinergia project COTHERM - COmbined hydrological, geochemical and geophysical modelling of geoTHERMal systems (T. Driesner, ETHZ, coordinator), Sub-project 2, "Geochemical reactive transport modelling of fluid-rock interaction" (D. Kulik, G. Kosakowski, B. Thien, co-PIs). The main goal of SP2 is to explore how the consideration of mineral dissolution/precipitation kinetics improves the understanding and prediction of the geochemical evolution of a geothermal system over realistic time scales, based on reactive mass transport simulations of the fluid - basaltic rock interaction along realistic P-T-flow paths in the up- and down-flow parts, and constraints available from field-derived data. Such simulations of natural systems help to validate the models and concepts used in reactive transport simulations. For the work progress, see below and publications by SCOTT et al. (2015), and THIEN et al. (2015). Since 01.09.2015, SNF has approved the extension of COTHERM-2 for 12 months.

Two main kinds of rock formations are found in fossil Icelandic hydrothermal systems: volcanoclastites (tiny fragments of glassy basalt with high porosity and permeability) and lavafloes (compact basalt with low porosity and permeability). Volcanoclastites had been completely altered within a few hours to a few years, whereas lavafloes are practically not altered except in vesicles and in rims of a few cm thickness around certain fractures (THIEN et al. 2015). We investigated the formation conditions of the alteration rim in the lavafloes with the help of field data and geochemical reactive transport simulations.

First results indicate that the presence of the observed alteration rims implies the presence of significant amounts of volcanic gases (CO_2 and H_2S) in the circulating fluid. There is clear evidence that the specific surface area of primary minerals is the most important parameter driving the alteration. The effect of the kinetics of secondary mineral precipitation (i.e. rate constant and specific surface area) has been found also to be important; there is a coupling between dissolution kinetics of primary minerals and precipitation kinetics of secondary minerals.



Fig. 2.16: An alteration rim in a fractured zone (yellow and light grey colors) in a lavaflow formation. The rest of the rock is practically not altered.

2.9 References

- BERNER U. (2015)
Thermodynamic model for illite/smectite mixed layers
Part 1: stoichiometric considerations. PSI Technical Report TM-44-15-02, Villigen, Switzerland.
- BERNER U., KOSAKOWSKI G., KULIK D.A. (2013)
Geochemical impact of a low-pH cement liner on the near field of a repository for spent fuel and high-level radioactive waste. *Phys. Chem. Earth* 64, 46-56.
- BUSEY R.H., MESMER R.E. (1978)
Thermodynamic quantities for the ionization of water in NaCl media to 300C. *J. Chem. Eng. Data* 23, 175-176.
- CORDFUNKE E.H.P., KONINGS R.J.M (1988)
Chemical interactions in water cooled nuclear fuel – a thermochemical approach. *J. Nucl. Mat.* 152, 301-309.
- COX J.D., WAGMAN D.D., MEDVEDEV V.A. (1989)
CODATA Key Values for Thermodynamics. Hemisphere, New York.
- CURTI E., FROIDEVAL-ZUMBIEHL A., GUENTHER-LEOPOLD I., MARTIN M., BULLEMER A., LINDER H.P., BORCA C.N., GROLIMUND D. (2014)
Selenium redox speciation and coordination in high-burnup UO_2 fuel: Consequences for the release of Se-79 in a deep underground repository. *J. Nucl. Mat.* 453, 98-106.

- CURTI E., PURANEN A., GROLIMUND D., JÄDERNAS D., SHEPTYAKOV D., MESBAH A. (2015)
Characterization of selenium in UO₂ spent nuclear fuel by micro X-ray absorption spectroscopy and its thermodynamic stability. *Env. Sci-Processes & Impacts* 17, 1760-1768.
- HILLERT M. (1998)
Phase equilibria, phase diagrams and phase transformations: Their thermodynamic basis. Cambridge Univ. Press, Cambridge.
- JOHNSON L., GÜNTHER-LEOPOLD I., KOBLER WALDIS J.B, LINDER H.P., LOW J., CUI D., EKEROTH E., SPAHIU, K., EVINS L.Z. (2012)
Rapid aqueous release of fission products from high burn-up LWR fuel: Experimental results and correlations with fission gas release. *J. Nucl. Mat.* 420, 54-62.
- JOLY Y. (2001)
X-ray absorption near-edge structure calculations beyond the muffin-tin approximation. *Phys. Rev. B* 63, 125120.1-10.
- KULIK D.A., WAGNER T., DMYTRIEVA S.V., KOSAKOWSKI G., CHUDNENKO K.V., BERNER U. (2013)
GEM-Selektor geochemical modeling package: Revised algorithm and GEMS3K numerical kernel for coupled simulation codes. *Comput. Geosci.* 17, 1-24.
- LEAL A.M.M., KULIK D.A. (2015)
Using equilibrium constants of reactions in Gibbs energy minimization algorithms. In preparation.
- LEAL A.M.M., KULIK D.A., KOSAKOWSKI G. (2015)
Computational methods for reactive transport modeling: A Gibbs energy minimization approach for multiphase equilibrium calculations. *Adv. Water Res.* (accepted).
- MIRON G.D., KULIK D.A., DMYTRIEVA S.V., WAGNER T. (2015)
GEMSFITS: Code package for optimization of geochemical model parameters and inverse modeling. *Appl. Geochem.* 55, 28-45.
- OLIN Å., NOLANG B., OHMAN L.O., OSADCHII E., ROSEN E. (2005)
In: F.J. Mompean, J. Perrone, M. Illemassene (eds.), *Chemical Thermodynamics of Selenium*. Chemical Thermodynamics 7, OECD, Nuclear Energy Agency, Elsevier, Amsterdam, 851 p.
- PATTERSON C.S., BUSEY R.H., MESMER R.E. (1984)
Second ionization of carbonic acid in NaCl media to 250°C. *J. Sol. Chem.* 13, 647-661.
- PITZER K.S., PEIPER J.C., BUSEY R.H. (1984)
Thermodynamic properties of aqueous sodium chloride solutions. *J. Phys. Chem. Ref Data* 13, 1-102.
- REED M.H. (1982)
Calculation of multicomponent chemical equilibria and reaction processes in systems involving minerals, gases and aqueous phase. *Geochim. Cosmochim. Acta* 46, 513-528.
- SCOTT S., DRIESNER T., WEIS P. (2015)
Geologic controls on supercritical geothermal resources above magmatic intrusions. *Nature Communications* 6, 1-6.
- THIEN B.M.J., KOSAKOWSKI G., KULIK D.A. (2015)
Differential alteration of basaltic lava flows and hyaloclastites in Icelandic hydrothermal systems. *Geothermal Energy* 3, 1-32.
- THOENEN T., KULIK D.A. (2003)
Nagra/PSI Chemical Thermodynamic Data Base 01/01 for the GEM-Selektor (V.2-PSI) Geochemical Modeling Code: Release 28-02-03. PSI Technical Report TM-44-03-04, Villigen, Switzerland.
- WAGNER T., KULIK D.A., HINGERL F.F., DMYTRIEVA S.V. (2012)
GEM-Selektor geochemical modeling package: TSolMod library and data interface for multicomponent phase models. *Can. Miner.* 50, 1173-1195.

3 TRANSPORT MECHANISMS

N.I. Prasianakis, S.V. Churakov, Th. Gimmi, A. Jakob, G. Kosakowski, W. Pflingsten, L. Pegado (guest scientist), A. Leal (post doc), J. Poonoosamy (PhD), A. Shafizadeh (PhD student), A.M. Lopez (exchange PhD student), S. Kimura (exchange PhD student), S. Meng (master student)

3.1 Overview

In December 2014, Nagra has proposed siting regions for the further investigation in Stage 3 of the Swiss Sectoral Plan for Geological Waste Disposal. Accordingly, the research activities in the group were shifted towards preparation to the future needs of the Sectoral Plan. Compared to the previous years the focus has moved towards studies of complex, reality-near geochemical systems and material fluxes between buffer materials which lead to changes in transport properties and in in-situ conditions in the repository near field.

To test the models in the field, group members coordinate the modelling activities of the DR-A experiment in the Underground Rock Laboratory at Mont Terri. The experiment investigates the effects of chemical perturbations in the porewater on the transport of ions in Opalinus Clay. Within the modelling exercise, several international groups apply different models available in Flotran, MCOTAC, PHREEQC, MIN3P and CrunchFlow-MC transport codes. Furthermore, members of the group participate actively in the setup and design of the DR-B field experiment. The purpose of this experiment is to perform long term (>10 years) monitoring of tracer transport in Opalinus Clay on a field scale.

Mineralogical and porosity changes at the cement-clay interface and their subsequent effect on transport parameters were further investigated on a micrometer scale within the CROSS financed, interdepartmental (NUM-NES) PhD project partially supported by Nagra and PSI-Director's reserve (project title: "Evolution of cement-clay interfaces", Amir Shafizadeh). Dynamic neutron imaging showed a reduction of flux across the interface, which is consistent with the water content measurements and prediction of reactive transport modelling (SHAFIZADEH et al. 2015). Moreover, the time series of water content profiles allowed the estimation of the reaction front propagation rate.

To evaluate the effect of sorption competition on the transport of radionuclides, the influence of Fe redox sensitive sorption on Ni(II) migration in bentonite was investigated using the 2SPNE CE/SC sorption model in the multispecies transport code MCOTAC. In this case, sorption competition phenomena have a weak influence on the retardation of bivalent radionuclides in bentonite.

The uptake of ions by C-S-H phases was investigated by multi-scale molecular simulations. The aim was to refine a thermodynamic model for ion sorption at the level of a single C-S-H/C-A-S-H particle. The results of the simulations provide input and support for the macroscopic phenomenological thermodynamic models. In addition, the mechanism and thermodynamics of Al incorporation in C-S-H phases has been further investigated by ab initio molecular dynamics simulations with explicit solvent.

The benchmarking and verification of reactive transport coupled codes is an on-going activity in the Transport Mechanisms Group. The co-operation with the Center for Environmental Research, UFZ Leipzig in the area of reactive transport (OpenGeosys-GEM) was strengthened and focused in benchmarking and code testing. Within the PhD project "Experimental benchmark for the verification and validation of reactive transport codes" (PhD student Jenna Poonoosamy, supported by Nagra), reactive transport experiments in granular porous media have been conducted, analyzed and modelled using the OpenGeoSys-GEM coupled code. Results of the experiment have been documented and published in the book of OpenGeoSys benchmarks (KOLDITZ et al. 2016). Post-mortem analysis of the samples allowed the in-depth investigation of dissolution-precipitation mechanisms at the pore scale (POONOOSAMY et al. 2015b). This information is used as an input for both microscopic pore-level modelling and macroscopic transport models.

To obtain a more fundamental description of precipitation and dissolution of minerals in porous media and their effect on transport properties of the system, an initial development of a pore scale transport model on the basis of the lattice Boltzmann approach has started. The overarching scope is on one hand the upscaling of atomistic information regarding crystal growth, and on the other hand the subsequent upscaling of fluid transport from pore scale to the continuum scale in order to provide transport parameters for the macroscopic transport simulations. As a first step, dissolution and precipitation reactions investigated on a lab scale reactive transport experiment have been modelled and the epitaxial growth of barite on celestite crystals has been simulated in realistic geometries, directly obtained from the experimental samples. This level of

description allows the direct measurement of the effect of geochemical reactions on the effective diffusivity and permeability of the domain of interest, thus improving the modelling and predictive capability.

Within the postdoc project of Dr. A. Leal (joint project with the thermodynamics group), the numerical stability and efficiency of the GEMS algorithm used for reactive transport simulations has been improved significantly. A hybrid algorithm which combines the numerical efficiency of the LMA solver with the flexibility of the traditional Gibbs energy minimization method for multiphase equilibrium calculations has been implemented and benchmarked (LEAL et al. 2015).

Finally, two exchange PhD students from A Coruña University (A. Mon, Spain) and from Tokyo Institute of Technology (S. Kimura, Japan) conducted part of their research studies at LES. In the first project, the influence of a temperature pulse on the evolution of mineralogy and porosity in the near-field of a high-level radioactive waste repository was studied. In the second project, the water content of Mont-Terri Opalinus clay samples has been quantified using ultrasound technique.

3.2 Sectoral plan for deep geological disposal

3.2.1 DR-A field experiment in the Mont Terri Underground Rock Laboratory

The DR-A field experiment in the Mont Terri Underground Rock Laboratory aims at investigating the effects of an increase of the ionic strength of the solution on the transport of sorbing and non-sorbing tracers. An increase of the ionic strength provokes changes in the cation populations on the different sorption sites (notably on exchange sites) and possibly increases the accessibility of the pore space to anions. Several groups with different modelling concepts are currently modelling the data. Numerical codes such as Phreeqc and CrunchFlow-MC follow a multi-porosity approach, where the pore space is split in two regions that are in chemical equilibrium. The solution composition in the first region (denoted as "external") is unaffected by surface charges and thus can become equal to that stipulated at an external boundary. The second region (called "internal") has increased cation concentrations and decreased anion concentrations compared to the external pore water. The equilibrium between the two regions is calculated from the Poisson-Boltzmann equation or from the Donnan equation based on a mean electric potential in the internal region. An alternative, kinetic way to simulate a Donnan distribution was developed using the code Flotran. It is based on the diffusion potential that

arises when different ions diffuse with individual diffusion coefficients and which leads to electromigration terms that increase or counteract molecular diffusion. The diffusion potential becomes a Donnan potential if charged-immobile species are present. This approach is computationally more efficient, it can be applied to Phreeqc or CrunchFlow-MC as an alternative method and offers additional simulation possibilities compared to the solution of the Poisson-Boltzmann or the Donnan equations. For example, the final ion distribution between the Donnan space and an external solution can be calculated through a diffusive process that depends on the individual species diffusion coefficients. A careful verification for single salt electrolytes was performed to test whether the results of the new approach match those of direct Donnan calculations. It turned out that the Flotran simulations were identical to the direct Donnan calculations for symmetric electrolytes (e.g., NaCl), but differed for asymmetric electrolytes (e.g., CaCl₂, see Fig. 3.1). The same was observed for Phreeqc and CrunchFlow-MC when implementing the new approach. It has been finally shown that the incorrect results were related to the numerical implementation of the calculation of the electromigration terms, in all the aforementioned codes. A modification of these numerical implementations led in the end to correct results (see Fig. 3.1). The simulations for the DR-A field experiment will be recalculated with the corrected Flotran version.

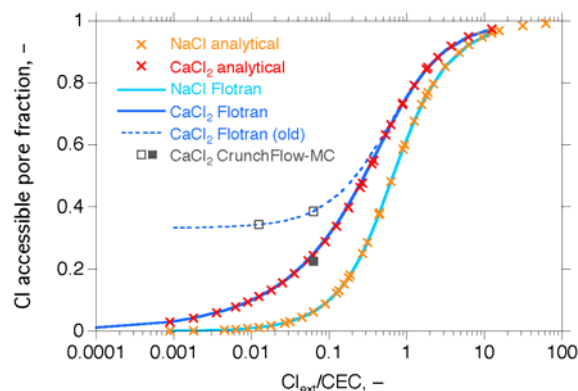


Fig. 3.1: Numerical Donnan simulations with Flotran based on the newly developed approach (solid lines) compared to the analytical solution for Donnan equilibrium for single salts (crosses). Shown are the calculated Cl accessible pore fractions as a function of the external Cl concentration normalized with the cation exchange capacity of the clay, for a NaCl electrolyte and for a CaCl₂ electrolyte. Results obtained with the old Flotran version, demonstrating an incorrect asymptotic behaviour (dashed line) as well as results obtained by CrunchFlow-MC via electromigration terms (open squares) and via the multi-porosity approach (solid square) are shown for comparison.

The ionic strength of the pore water solution applied as chemical perturbation in the DR-A experiment is as high as $I=1.16$ M. Davies or similar ionic strength corrections are not valid for such conditions. In order to estimate the effects of ionic strength correction and sorption competition, the data from the DR-A experiment were modelled using the in-house transport code MCOTAC (PFINGSTEN 1996, 2002) which consistently uses the charge balanced 2SPNE CE/SC sorption model for ion sorption on clay minerals (PFINGSTEN et al. 2011) and the SIT ionic strength correction. Initial modelling included simple tracer modelling (HTO, Cl, Br), for which the injection loop concentrations and final bore core profiles are available. At a later stage, more complex models have been set up to model the ionic strength perturbation where the water composition has been changed to a 1.16 M Na-K-Cl solution. First calculations for HTO loop concentration and HTO profiles are shown in Fig. 3.2.

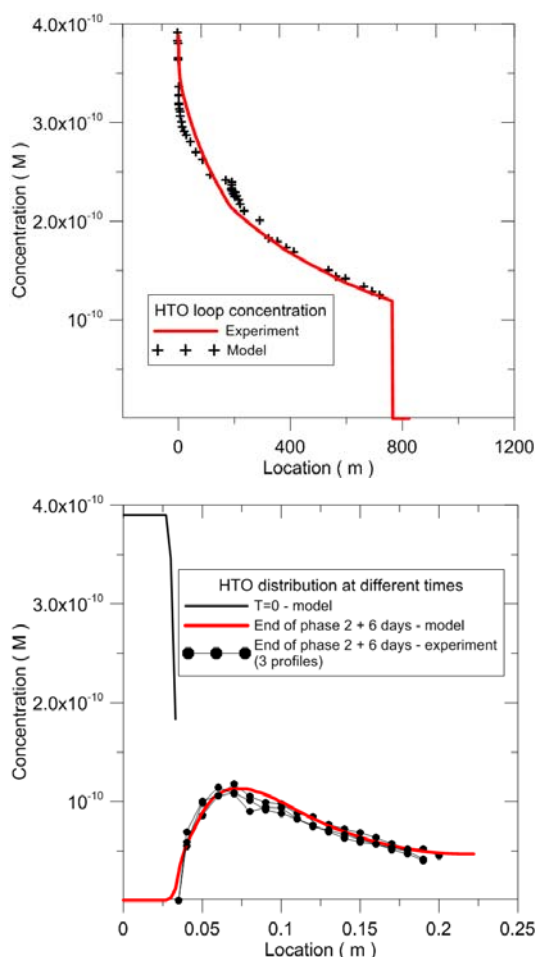


Fig. 3.2: DR-A HTO modelling and experimental results for tritium profiles measured after overcoring of the injection interval, and related HTO loop concentration (top).

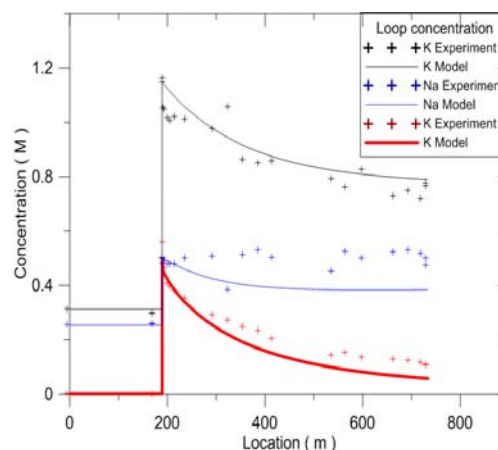


Fig. 3.3: Loop concentration for Cl, Na, K measured during DR-A experiment and related MCOTAC modelling results using SIT ionic strength correction for both experimental periods: early, low ionic strength phase ($I=0.5$ M), and later, high ionic strength phase ($I=1.2$ M).

Loop concentrations for Na, K, and Cl, which were used to modify the ionic strength (ionic strength perturbation) and their evolution in time are plotted in Fig. 3.3. After the perturbation phase, the loop concentrations are dependent on the diffusion of ions through the surrounding rock. The modelling challenge lies in the calculation of an appropriate data set for which all measured ion concentrations, including those of Mg, Ca, Br, I, Cs, SO₄, Sr, can be reproduced by a single model run with reasonable agreement.

3.2.2 DR-B field experiment in the Mont Terri Underground Rock Laboratory

The DR-B experiment is planned as a long-term, low-maintenance diffusion experiment that allows testing new monitoring equipment such as a novel mobile X-ray fluorescence probe. It is currently supported by Nagra and by NWMO (the Canadian Nuclear Waste Management Organization). The development of the mobile X-ray fluorescence probe was commissioned by Nagra and Areva Mining to a specialized team. The probe (50 mm diameter) is optimized for well-localized downhole measurements of elemental distributions at trace concentrations in small diameter monitoring boreholes. This required the development of a bottom plate for a guide hole and an actuator, which allow precisely setting the axial and angular position of the probe window. The probe can be advanced stepwise along the observation borehole, about 10 m below the tunnel floor, and can be pointed to the desired direction. A special carbon lining of the monitoring boreholes was commissioned in order to minimize the disturbance of the signals. Various chemical elements can be measured by the probe. For instance, I, Se, Cs or U can be detected down to

concentrations in the order of a few ppm's in Opalinus Clay.

The basic installations were set up in the Mont Terri Underground Rock Laboratory in May 2015. A packed-off interval of 0.6 m diameter and 1 m length was equipped with a cage and filled with sand and artificial pore solution. Two observation boreholes within a distance of 1.2 m from the central test interval were also drilled and equipped with bottom plates and linings. They serve to guide the newly developed mobile X-ray fluorescence probe that will be used for determining local tracer ion concentrations. Additional observation drill holes, closer to the test interval, are planned. To start the experiment, the artificial pore solution will be exchanged by a NaI solution. Fig. 3.4 shows simulated iodide breakthrough curves for different distances of the observation borehole for an initial source concentration of 2 M NaI. Note that in these scoping calculations charge coupling during transport was neglected. The simulations were performed using COMSOL Multiphysics.

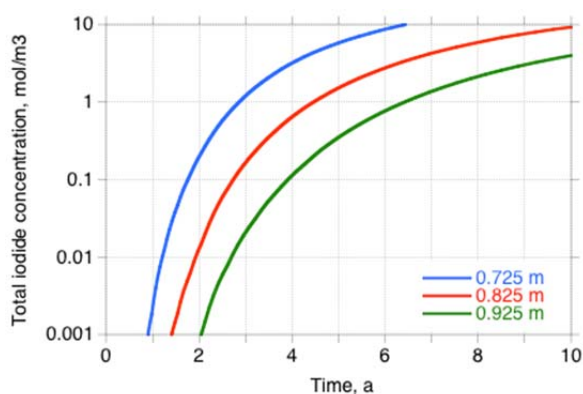


Fig. 3.4: Simulated breakthrough curves for iodide at distances of 0.725 m, 0.825 m, and 0.925 m from the central test interval that contained initially a 2 M NaI solution.

3.2.3 Influence of Fe redox sorption behavior on montmorillonite surfaces on the Ni(II) migration

Recent investigations of Fe(II)-(III) sorption behavior on bentonite showed that the oxidation of Fe(II) into Fe(III) on the surface of montmorillonite could lead to increased Fe uptake. This effect has been confirmed by Moessbauer spectroscopy recently in SOLTERMANN et al. (2014). In order to examine the influence of these processes on sorption competition reactions of divalent cations during diffusion through clay/bentonite samples, Ni(II) diffusion has been modelled. The redox sensitive Fe uptake on bentonite has been described on the basis of the 2SPNE CE/SC sorption model in Table 3.1 (SOLTERMANN et al. 2014).

Table 3.1: Surface complexation reactions for Fe(II) and Fe(III) on bentonite as defined in SOLTERMANN et al. (2014).

Surface complexation reaction	Log K
$\equiv\text{S}^{\text{SOH}} + \text{Fe}^{2+} \leftrightarrow \equiv\text{S}^{\text{SOFe}^+} + \text{H}^+$	1.9 ± 0.3
$\equiv\text{S}^{\text{WOH}} + \text{Fe}^{2+} \leftrightarrow \equiv\text{S}^{\text{WOFe}^+} + \text{H}^+$	-1.7 ± 0.3
$\equiv\text{S}^{\text{SOH}} + \text{Fe}^{2+} \leftrightarrow \equiv\text{S}^{\text{SOFe}^{2+}} + \text{H}^+ + \text{e}^-$	-1.4 ± 0.3
$\equiv\text{S}^{\text{WOH}} + \text{Fe}^{2+} \leftrightarrow \equiv\text{S}^{\text{WOFe}^{2+}} + \text{H}^+ + \text{e}^-$	-3.8 ± 0.3

The straightforward implementation of the additional redox surface reactions within MCOTAC coupled to the 2SPNE CE/SC sorption model has been applied in the case of Ni(II) diffusion through bentonite with a) Fe(II) sorption competition only, and b) with Fe(II) and Fe(III) sorption competition. In the system setup, Ni(II) diffuses at a constant concentration level at $x = 0$ m (boundary) into a bentonite sample with initially zero Ni(II) concentration. As can be seen in the calculated Ni(II) breakthrough curves at a distance of 4 mm (Fig. 3.5), the additional Fe(III) surface reactions yield a slightly less retarded Ni(II) breakthrough compared to the case of Ni(II) sorption competition with Fe(II) only. It should be noted that the formulation which has been used, in the 2SPNE CE/SC sorption model, implies that Fe(III) occupies the same sites as Fe(II), which yet has to be confirmed. The accuracy of this assumption can be the subject of further spectroscopic investigations. Nevertheless, as has been shown here, additional surface (redox) reactions may slightly reduce divalent radionuclide retardation in bentonite.

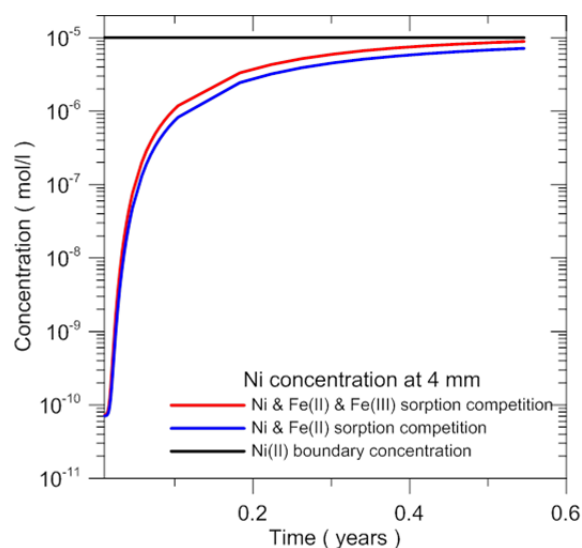


Fig. 3.5: Ni(II) diffusion through bentonite using MCOTAC. Bentonite breakthrough curves for two different setups: a) Ni(II)-Fe(II) sorption competition, and b) Ni(II)-Fe(II)-Fe(III) sorption competition.

3.2.4 Experimental observation of the evolution of porosity at cement-clay interfaces and the subsequent effect on transport parameters

The PhD project "Evolution of cement-clay interfaces" (A. Shafizadeh) continued in 2015. The last stage of the project involved the in-situ observation of porosity alteration at cement-clay interfaces using high resolution neutron imaging. Moreover, the feedback on solute transport across the interface was quantified. Measurements of the water content across the interface of the sample at the ICON facility revealed slight reduction of porosity on the clay side followed by an increase in the porosity on the cement side (Fig. 3.6, middle) with increasing reaction time. The effect of these structural transformations at the interface on the transport parameters were studied further by dynamic neutron imaging (Fig. 3.6, right). Results from dynamic neutron imaging showed a reduction of flux across the interface but not complete clogging, which is consistent with the water content measurements and numerical models (SHAFIZADEH et

al. 2015). In addition, time series of water content profiles across the evolving interface, over a period of 2 years, showed the porosity increase/reduction at the interface, and at the same time allowed to estimate how fast the reactive front is advancing in the cement domain. Fig. 3.7 shows the time series measurements, with a closer look at the interface for the cement side (right). Fig. 3.8 depicts the reactive front position within the cement at different reaction times. The latter was modeled using the equation for the diffusion length $L = \sqrt{D_a t}$, which allows the propagation rate of the reaction front on the cement side of the interface to be estimated.

Finally, using the same methodology and in collaboration with the diffusion group (L. Van Loon) the precipitation of $\text{BaSO}_4/\text{SrSO}_4$ in clay systems and its feedback on transport parameters was explored. These experiments are one of the main topics of the exchange PhD student Y. Fukatsu from Tokyo Institute of Technology.

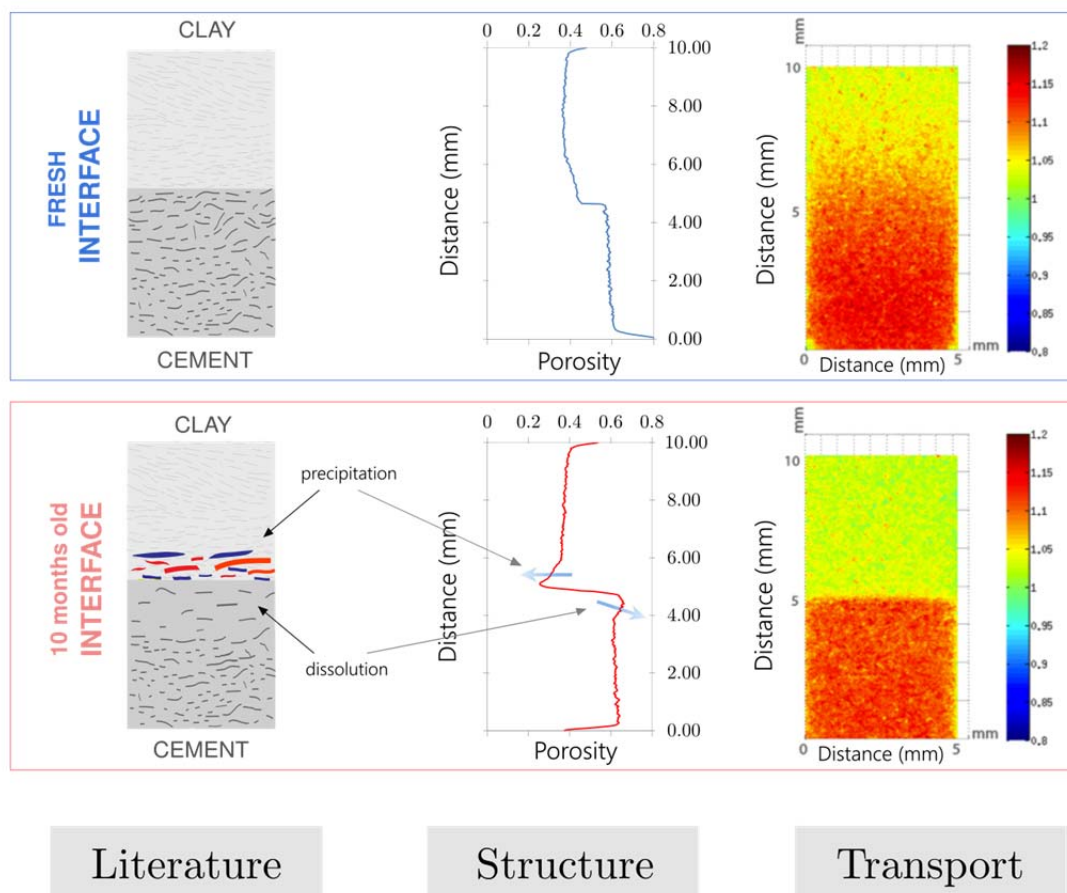


Fig. 3.6: Left: Schematic presentation of the cement-clay interactions. Middle: Selected water content (porosity) profiles. Right: Transmission image of D_2O advancement (normalised to a reference time) across an aged interface (top row) and a fresh one (bottom row) measured using a neutron beam. Higher values (in red) indicate higher relative D_2O concentration. The D_2O was introduced to the cement part of the sample.

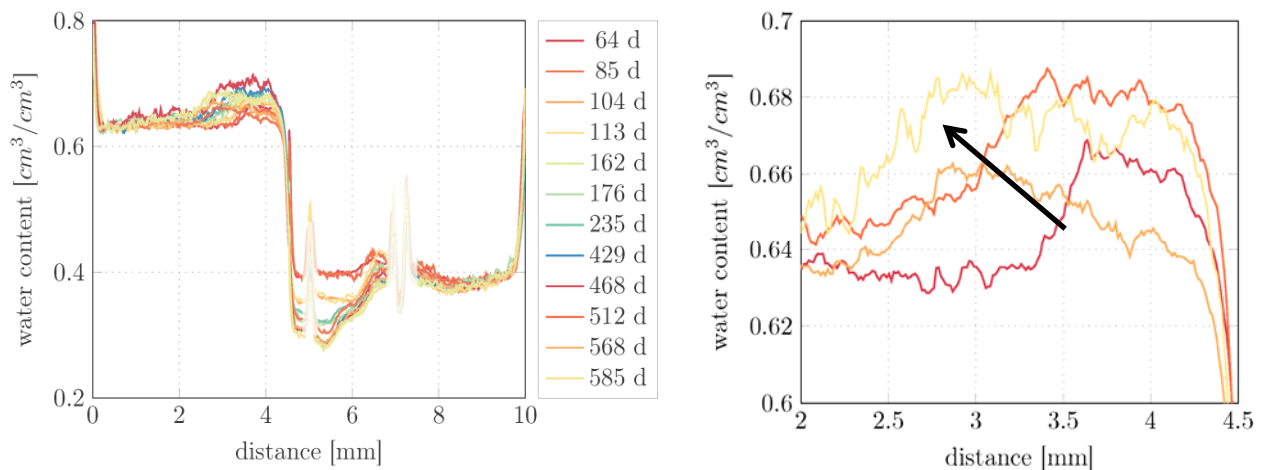


Fig. 3.7: Left: Time series of water content measurements (64-585 days) obtained via neutron radiography at the ICON facility at PSI. Right: A zoomed view over the interface with the arrow indicating the propagation of the reactive front.

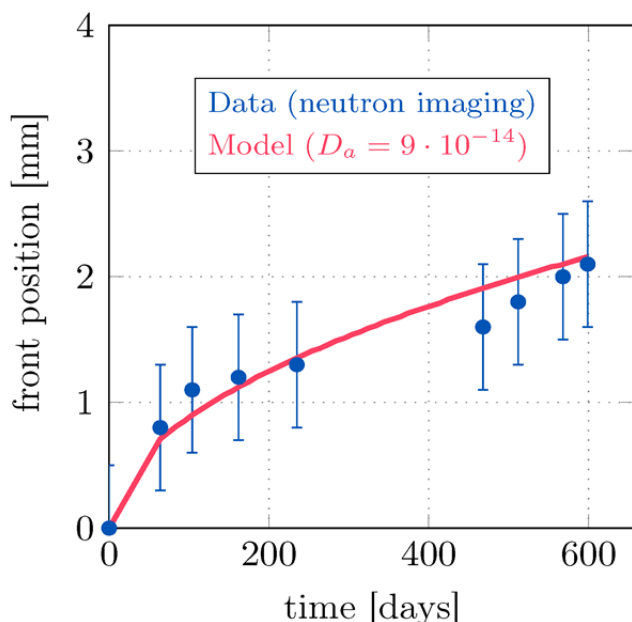


Fig. 3.8: Advancement of the reaction front on the cement side of the interface.

3.2.5 Assessment of water content in Opalinus Clay samples using ultrasound technique

S. Kimura, an exchange PhD student from the department of Nuclear Engineering (Prof. H. Kikura) of Tokyo Institute of Technology, conducted part of his research at LES for four months. Through this collaboration the potential of non-destructive ultrasound methods in the measurement of water content of Opalinus Clay samples was assessed. Fresh and old Opalinus Clay samples from Mont-Terri have been trimmed in appropriate dimensions for the measurements. The saturation level directly affects the propagation of speed of sound in a measurable way. The precision of these measurements strongly depends on the accuracy of the ultrasound equipment.

3.3 Fundamental understanding of transport and sorption mechanisms: Multi-scale molecular modelling of ion sorption by C-S-H phases

During 2015 the post-doc project "A thermodynamic model for C-S-H/C-A-S-H from a bottom up approach" (L. Pegado) has been continued. This is financed for the most part by NANOCEM, the Industrial-Academic Research Network on Cement and Concrete, but also with financial contributions from the Burgundy region in France and CNRS through the program NEEDS MIPOR. The project is developed in close collaboration with the group of Dr. Christophe Labbez at the University of Bourgogne Franche-Comté, France, where L. Pegado is affiliated. Using multi-scale molecular modelling, the goal is to refine a thermodynamic model for ion adsorption by C-S-H at the level of a single C-S-H/C-A-S-H particle, which can then support and provide input to macroscopic phenomenological thermodynamic models. The microscopic, single-particle model will incorporate a description of surface charge formation, equilibrium with bulk electrolyte solutions, Si/Al substitution and silicate chain polymerization.

To extend the description of ion adsorption by C-S-H in coarse grained Grand-Canonical Monte Carlo simulations with ion specificity/solvent effects one needs effective potentials (PMF's – Potentials of Mean Force) between ions and surface groups in C-S-H. These PMF's are obtained from classical molecular dynamics (MD) simulations using a polarizable force field (FF) for ions and surface groups in C-S-H/C-A-S-H. The FF's for the surface groups are obtained on the basis of ab initio MD simulations of aqueous $\text{Si}(\text{OH})_4$ and $\text{Si}(\text{OH})_3\text{O}^-$. These FF's have to be further tested by comparing calculated

activity data for salt solutions of silicates with experimental data.

To further investigate the mechanism and thermodynamics of Al incorporation in C-S-H, the thermodynamics of Si-Al exchange reactions between Si-chains and the aqueous solution has been investigated by ab initio molecular dynamics simulations with explicit solvent. The free energy for the exchange reactions were calculated based on the thermodynamic integration technique. The obtained data were found to be in good quantitative agreement with previous static energy calculations of Al exchange in structurally different sites on the surface of C-S-H.

3.4 Benchmarking and validation of coupled codes

3.4.1 Experimental benchmarks for the verification and validation of reactive transport codes: a multi-scale investigation

A reactive transport experiment was designed to evaluate permeability-porosity changes linked to sulfate mineral dissolution-precipitation processes (PhD project J. Poonoosamy, POONOOSAMY et al., 2015a,b). The experiment involved the dissolution of a primary mineral, celestite (SrSO_4), followed by the precipitation of a secondary mineral, barite (BaSO_4), induced by infiltration of a barium chloride solution. The replacement of celestite by barite is accompanied with changes in porosity and permeability leading to non-linear changes in the flow field. The experiments were modelled with the reactive code OpenGeoSys-GEM. The description of the experiment will be published in the book on OpenGeoSys numerical benchmarks (KOLDITZ et al. 2016). Currently three teams with four different codes work on 2D test cases based on the published experiments (POONOOSAMY et al. 2016). Test cases describe 1) flow and advective-dispersive/diffusive transport in a 2D setup, 2) same as in (1) but including effects of liquid density on the transient flow field, 3) flow, transport and kinetically controlled chemical reactions that change porosity and permeability, 4) the same as (3), but including effects of liquid density on the transient flow fields.

In 2015, work was concentrated on the refinement of the post-mortem analysis and on the investigation of the dissolution/precipitation mechanisms at the pore scale. The analytical techniques which combine scanning electron microscopy (SEM) and synchrotron X-ray micro-diffraction/micro-fluorescence were performed at the XAS beamline, Swiss Light Source at PSI (SLS) in collaboration with Dr. D. Grolimund. Fig. 3.9 shows the X-ray diffraction (XRD) pattern of three distinct phases observed in the reacted porous media. The pattern in Fig. 3.9a from large celestite

crystals shows spot-like reflections characteristic for well-developed single crystals with a strong preferred orientation (e.g plane (211)). Doubled spot-like reflections as in Fig. 3.9b with identical azimuthal angle, which are consistent with pure barite and pure celestite reflections, are also visible in the XRD pattern collected at interfaces in contact with the large celestite crystals. The identical azimuthal angles imply that the barite reflections arise from crystallographic planes with the same orientation as the celestite substrate, i.e. epitaxial growth of barite on celestite. In contrast, a fine-grained phase filling the interstices is dominated by continuous diffuse Debye rings corresponding to pure barite reflections (Fig. 3.9c), a signature of randomly oriented nanometric barite particles. The small celestite grain fraction dissolved rapidly to form nano-crystalline barite filling the pore space, while large celestite grains were passivated with a thin rim of epitaxial micro-crystalline barite. It is also observed that the formation of a nano-crystalline barite precedes the growth of epitaxial barite on celestite crystals. Classical nucleation theory, using well-established parameters describing barite precipitation, was applied to explain the mineralogical changes occurring in our system.

In cooperation with National Research Nuclear University MEPhI in Moscow, Department of Radiation Physics and Safety of Nuclear Technologies and with the LES diffusion group (L. Van Loon) a master thesis was conducted by Ekaterina Zapolnova on the effect of supersaturation on the precipitation of barite in porous media. Columns filled with celestite particles were flushed with barium chloride solution. The experiment was repeated with different barium chloride concentrations, most of them considerably lower than in the experiments from POONOOSAMY et al. (2015b).

In contrast to the previous experiments the column experiments conducted by E. Zapolnova showed that barite precipitated only as a rim on small celestite crystals and in some cases resulted even in the complete consumption of the crystals as shown by the SEM image in Fig. 3.10. The experimental data will be used for further calibration of kinetic models both in continuum scale and in pore scale.

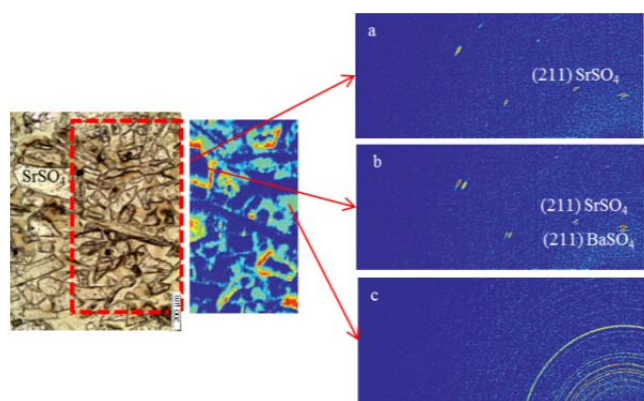


Fig. 3.9: Microscopic view of the celestite region after reaction (left) showing original celestite crystals and a fine grained phase filling the pore space. XRD diffraction intensity map for $d = 3.1 \text{ \AA}$ (right), correlated with 3 different XRD patterns from the indicated map locations (a) interior of a large celestite crystal, (b) micro-crystalline epitaxial barite at the surface of large celestite crystal and (c) nano crystalline phase filling the interstices). Intensities increase in the sequence blue < cyan < green < yellow < red.

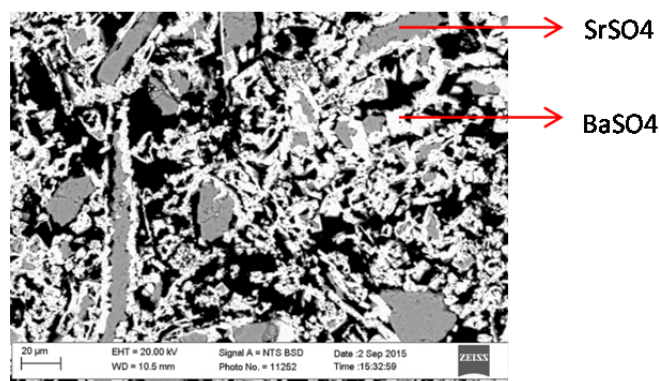


Fig. 3.10: Microscopic view of cross sectional area of the strontium sulfate region stemming from the new column experiments. (Scanning electron microscope, back scattered electron image).

3.4.2 Lattice Boltzmann pore-level modelling of dissolution-precipitation processes (epitaxial growth and rim formation mechanism)

The porosity and mineralogical evolution of the technical barriers and their respective interfaces, plays a key role in the performance assessment of a radioactive waste repository. The porosity alterations, due to geochemical reactions, directly affect important processes such as re-saturation times, corrosion rates, or the gas pressure build up within the barriers. At the same time, local transport properties at mineralogical interfaces can be altered, which in turn can affect the intermediate and longer time evolution of the entire barriers. Typical locations of interest are for example

the cement-clay interfaces, and the Engineered Gas Transport System (EGTS) which is a backfill and sealing system that allows the controlled discharge of gases produced due to metal corrosion and the degradation of organics in L/ILW waste repositories.

In order to assess, model and simulate the effect of dissolution-precipitation processes on porosity evolution the laboratory experiment described in POONOOSAMY et al. (2015b) has been performed. This reactive transport experiment considered a barite-celestite system in a porous environment mainly because on one hand the involved reactions are relatively fast, and on the other hand because there is a large amount of literature that provides a fundamental understanding of the involved processes. Dissolution and precipitation reactions indeed altered the pore space in a non-linear way. The macroscopic modelling of the experiment showed that it is impossible to reproduce the experimental results without feedback from the actual experiment. The microscopic structure examination highlighted the need for better understanding of the processes at the microscale level. At least two mechanisms have been identified: a) homogeneous nucleation which results in nanocrystalline barite, and b) heterogeneous nucleation, which results in barite epitaxial rim formation. The latter certainly has an effect on the available celestite reactive surface area, a mechanism that cannot be incorporated in purely macroscopic modelling.

As a first step towards better understanding of the processes a Lattice Boltzmann mixture model was built based on the surface reaction multicomponent model of KANG et al. (2014). The purpose was to reproduce one of the main observed mechanisms of barite precipitation, namely the barite epitaxial rim formation mechanism that passivates the celestite crystals. In Fig. 3.11, a typical microscopic image of samples originating from the reactive zone of the in-house experiment of POONOOSAMY et al. (2015b) is shown. The part of the image that was used as input geometry for the computations has been colored-enhanced to provide better understanding as follows: large celestite crystals are colored blue, and the barite layer that is formed after heterogeneous precipitation is colored green. Black color corresponds to open pore space where aqueous solution existed by the end of the reactive transport experiment. Simulations were conducted in this exact microscopic 2D geometry. The initial conditions, described an aqueous solution supersaturated in terms of Ba^{+2} and SO_4^{-2} , that surrounds the celestite crystals. Formation of barite precipitates was favored on the surface of the large celestite crystals. Barite precipitation kinetics were modelled after LIU et al. (1975).

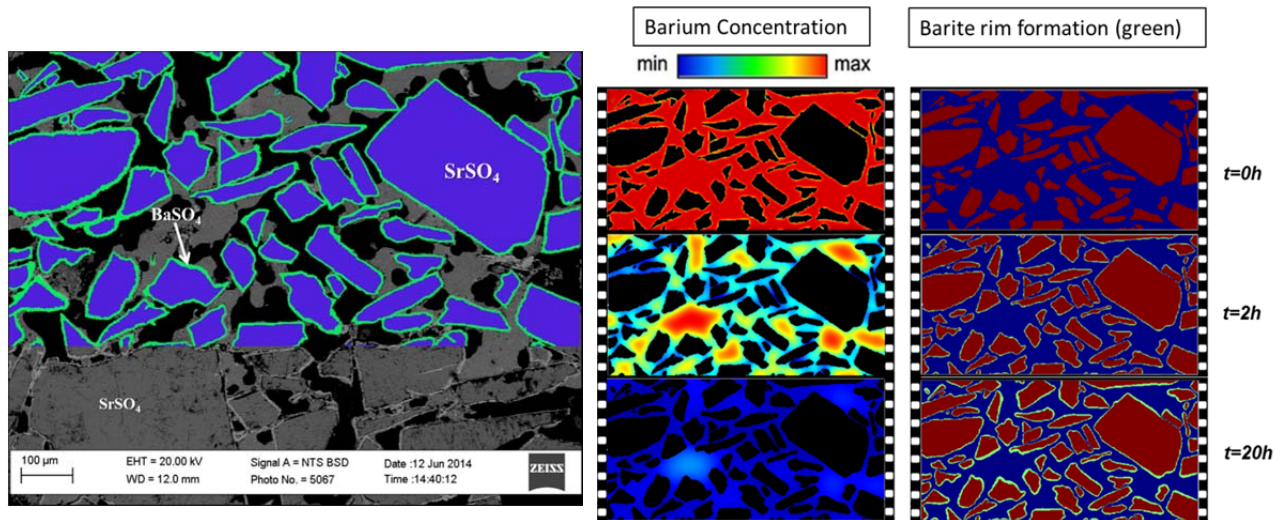


Fig. 3.11: Left: Scanning Electron Microscopy, Back Scattering method. Large celestite crystals (blue color) are passivated by the formation of barite rims (green color). Nano-crystalline barite is in between. Black is open pore space where aqueous solution existed by the end of the reactive transport simulation. Original setup contained pure celestite phases. Right: Lattice Boltzmann numerical simulation of the rim-formation mechanism and the precipitation evolution. Barium concentration drops from initial values (red) to equilibrium values (blue). Barite layer is colored green at the rightmost set of plots.

The barite growth reaction (precipitation) proceeds at a rate that is proportional to the square of the relative supersaturation. The result of the simulation was that barium precipitated on the celestite crystals in form of barite (epitaxial growth) until it reached its final equilibrium concentration. On the right side of Fig. 3.11, the evolution of the reactive simulation is presented from top to bottom for a total reaction time of 20 hours.

The barite layer formation (green), changes the pore space in a way that affects the permeability and the effective diffusivity of the domain of interest (PRASIANAKIS et al. 2015)

The investigation of the involved physical mechanisms can improve the modelling and predictive capability of macroscopic codes through the inclusion of microscopic physics. Moreover, it can pave the way for multi-scale simulations by bridging the atomistic and macroscopic scales.

3.4.3 OpenGeoSys-GEM: benchmarking and applications

In 2015, OpenGeoSys-GEM was used within the SeS-benchmarking initiative (STEEFEL et al. 2015) to investigate the porosity changes due to chemical reactions and the feedback of these changes on fluid flow and mass transport. An example is shown in Fig. 3.12, which compares the solution obtained with OpenGeoSys-GEM with the reference solution obtained with MIN3P from XIE et al. (2015). The benchmark calculates the position of a kinetically controlled dissolution front (causing the porosity

change) when a fluid is injected into a 1D column under constant pressure difference. Permeability and porosity are connected via the Kozeny-Carman relation, which causes the dissolution front to accelerate, since the average permeability in the column decreases due to the porosity change.

A. Mon, an exchange PhD student from A Coruña University (Spain) conducted part of her research for three months in the transport modelling group of LES. She contributed to the investigation of the influence of a temperature pulse on the evolution of mineralogy and porosity in the near field of a high-level radioactive waste repository in form of a code comparison study.

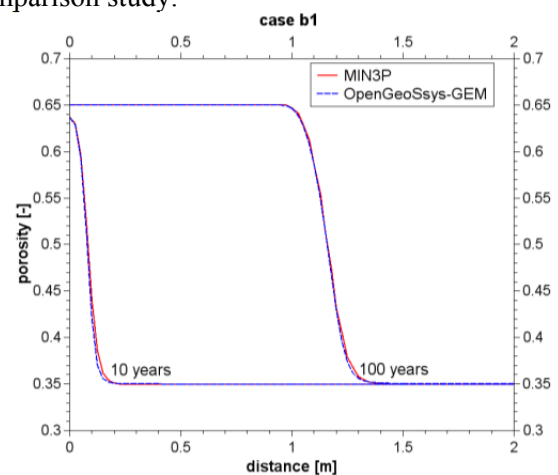


Fig. 3.12: Comparison of porosity profiles for OpenGeoSys-Gem and MIN3P (from U. Mayer, University of British Columbia, Canada) based on a 1D benchmark case (B1) taken from XIE et al. (2015).

She set up a simplified 1D benchmark for the bentonite-shotcrete-Opalinus Clay material interfaces for the THMC-code CORE2D developed by the group of J. Samper at A Coruña University and compared it to the OpenGeoSys-GEM code from LES.

3.5 Advances in computational methods for geochemical and reactive transport modelling

In the framework of the postdoc project of Dr. Allan Leal and in collaboration with the Thermodynamics group (D. Kulik) a novel numerical method for multiphase chemical equilibrium calculations based on a Gibbs energy minimization (GEM) approach was developed. The method can accurately and efficiently determine the stable phase assemblage at equilibrium independently of the type of phases and species that constitute the chemical system.

This method (implemented as "IPNewton" algorithm in the Reaktoro framework for modelling chemically reactive systems) was successfully applied in reactive transport simulations to demonstrate its effective use in computationally intensive applications. The problem consisted in modelling a dolomitization process in which MgCl_2 is injected in a porous rock initially composed of quartz and calcite (see Fig. 3.13). As the injected fluid migrates inwards due to advection and diffusion mechanisms, calcite is dissolved and dolomite is precipitated. The FEniCS algorithm has been selected to solve the governing partial differential equations of mass transport in porous media using finite element methods in unstructured meshes. The equilibrium calculations were benchmarked with GEMS3K, the numerical kernel of the geochemical modelling software GEMS. This allowed to benchmark the new GEM method with a well-established IPM-3 GEM algorithm (KULIK et al. 2013), as well as their performance on every mesh node, at every time step of the transport simulation. In Fig. 3.14 a comparison of the number of iterations required at each node of the mesh using the new GEM method and the one in GEMS3K is presented. The benchmark shows that the newly developed chemical equilibrium algorithm is accurate, robust and efficient for reactive transport applications, and it shows some improvements over the algorithm used in GEMS3K.

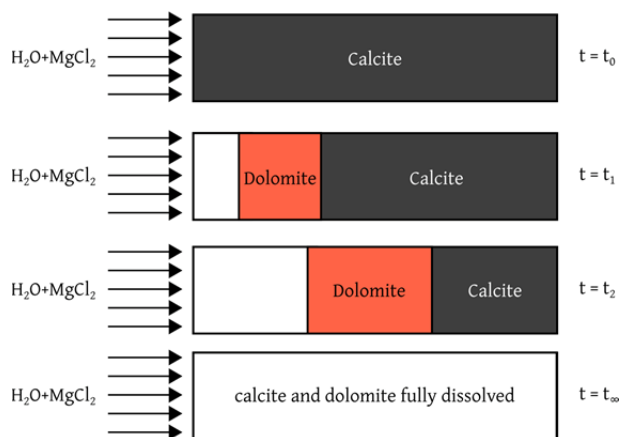


Fig. 3.13: Illustration of the dolomitization problem that has been chosen to test the chemical equilibrium method.

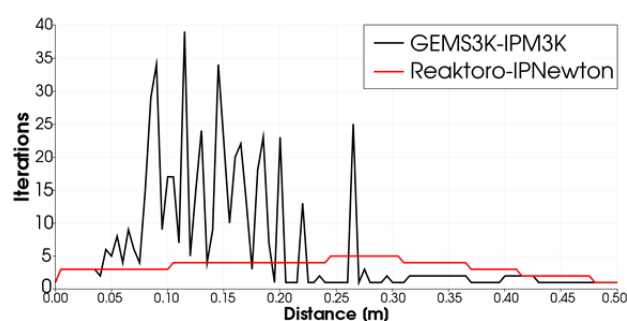


Fig. 3.14: Distribution of number of iterations in the chemical equilibrium calculations for every degree of freedom along the rock at time 10^4 s. Comparison of the reactive transport simulation using the new GEM equilibrium algorithm (red line) with GEMS3K (black line).

In addition to the new GEM method, a revised law of mass-action (LMA) approach for multiphase equilibrium calculations was developed and applied in the context of reactive transport modelling. This revised LMA formulation differs from the conventional LMA methods in that (i) it is directly derived from the Gibbs energy minimization (GEM) problem (i.e., the fundamental problem that describes the state of equilibrium of a chemical system under constant temperature and pressure); and (ii) it contains an additional term which facilitates the determination of all stable phases without presuming the types of phases and species. The proposed method (implemented as "IPAction" algorithm in the Reaktoro framework) has been successfully applied to reactive transport modelling problems using PHREEQC and GEMS as back-ends for the calculation of thermodynamic properties.

3.6 References

- KANG J., PRASIANAKIS N.I., J. MANTZARAS (2014) Thermal multicomponent Lattice Boltzmann model for catalytic reactive flows. *Phys. Rev. E* 89, 063310.
- KOLDITZ O. et al. (2016) Thermo-Hydro-Mechanical Chemical Processes in Fractured Porous Media; Modelling and Benchmarking, Springer.
- KULIK D.A., WAGNER T., DMYTRIEVA S.V., KOSAKOWSKI G., HINGERL F.F., CHUDNENKO K.V., BERNER U. (2013) GEM-Selektor geochemical modelling package: revised algorithm and GEMS3K numerical kernel for coupled simulation codes. *Computat. Geosci.* 17, 1-24.
- LEAL A.M.M., KULIK D.A., KOSAKOWSKI G. (2015) Computational methods for reactive transport modeling: A Gibbs energy minimization approach for multiphase equilibrium calculations. *Adv. Water Res.* (accepted).
- LIU S.T., NANCOLLAS G.H. (1975) The crystal growth and dissolution of barium sulfate in the presence of additives. *J. Colloid Interface Sci.* 52 582.
- PERKO J., MAYER K.U., KOSAKOWSKI G., DE WINDT L., GOVAERTS J., JACQUES D., MEEUSSEN J.C.L., (2015). Decalcification of cracked cement structures. *Comput. Geosci.*, 19(3), 673–693, doi:10.1007/s10596-014-9467-2.
- PFINGSTEN W. (1996) Efficient modeling of reactive transport phenomena by a multispecies random walk coupled to chemical equilibrium. *Nucl. Technol.* 116(2): 208-221.
- PFINGSTEN W. (2002) Experimental and modeling indications for self-sealing of a cementitious L&ILW repository by calcite precipitation. *Nucl. Technol.* 140(1): 63-82.
- PFINGSTEN W., BRADBURY M.H., BAEYENS B. (2011) The influence of Fe(II) competition on the sorption and migration of Ni(II) in MX-80 bentonite. *Appl. Geochem.* 26(8): 1414-1422.
- POONOOSAMY J., CURTI E., KOSAKOWSKI G., VAN LOON L.R., GROLIMUND D., MÄDER U.K. (2015a) Barite precipitation following celestite dissolution in porous media: a SEM/BSE and micro XRF/XRD study. *Geochim. Cosmochim. Acta* (submitted).
- POONOOSAMY J., KOSAKOWSKI G., VAN LOON L.R., MÄDER U.K. (2015b) Dissolution-Precipitation Processes in Tank Experiments for Testing Numerical Models for Reactive Transport Calculations: Experiments and Modelling. *J. Contamin. Hydrol.* 177-178, 1–17, doi:10.1016/j.jconhyd.2015.02.007.
- POONOOSAMY J., KOSAKOWSKI G., VAN LOON L.R., MÄDER U.K. (2016) Reactive transport benchmark (Book chapter), Thermo-Hydro-Mechanical-Chemical Processes in porous media, Benchmark Book, Berlin, Springer (in press).
- PRASIANAKIS N.I., POONOOSAMY J., GIMMI T., KOSAKOWSKI G., CHURAKOV S., (2015) Microscopic modelling of dissolution and surface precipitation of sulphates in granular media: effect on the permeability and effective diffusivity. 6th International Conference on "Clays in Natural and Engineered Barriers for Radioactive Waste Confinement, Brussels, Belgium, March 23-26, 2015.
- SHAFIZADEH A., GIMMI T., VAN LOON L.R., KAESTNER A., LEHMANN E., MÄDER U.K., CHURAKOV S.V. (2015) Quantification of water content across a cement-clay interface using high resolution neutron radiography. *Phys. Proc.* 69, 516–523.
- SOLTERMANN D., FERNANDES M.M., BAEYENS B., DAEHN R., JOSCHI A.P., SCHEINOST A.C., GORSKI C.A. (2014) Fe(II) uptake on natural montmorillonites. I. Macroscopic and spectroscopic characterization. *Environ. Sci. Technol.* 48(15), 8688-8697.
- STEEFEL C.I., YABUSAKI S.B., MAYER K.U. (2015) Reactive transport benchmarks for subsurface environmental simulation. *Comput. Geosci.* 439–443. doi:10.1007/s10596-015-9499-2.
- XIE M., MAYER K.U., CLARET F., ALT-EPPING P., JACQUES D., STEEFEL C., SIMUNEK J. (2015) Implementation and evaluation of permeability-porosity and tortuosity-porosity relationships linked to mineral dissolution-precipitation. *Comput. Geosci.* 19(3), 655–671. doi:10.1007/s10596-014-9458-3.

4 CLAY SORPTION MECHANISMS

B. Baeyens, R. Dähn, M. Marques Fernandes, A. Schaible, E. Eltayeb, A. Kéri (PhD student)

4.1 Introduction

In the framework of the Sectoral Plan (SGT-E2) the sorption data bases (SDB) and sorption measurements on host rocks were published in NTB 12-04 and NTB 12-05, respectively, and are currently assessed by the regulators.

The development of a thermodynamic sorption database (TD-SDB) for clay minerals based on the 2SPNE SC/CE sorption model (including non-adjustable parameters such as site types, site capacities, selectivity coefficients, surface complexation constants) is in progress. The aim is to calculate sorption values for the safety analysis under relevant geochemical conditions. The use of the 2SPNE SC/CE model enables to evaluate the influence of competitive sorption. Reports on these topics are in preparation and it is foreseen that they will be published in 2016.

The main focus in the current year was devoted to the mechanistic sorption studies on clay minerals which is a continuously on-going activity. The main topics are briefly summarised below:

- A study on the effect of temperature on the sorption behaviour of Cs^I, Ni^{II}, Eu^{III} and Th^{IV} on montmorillonite and bentonites at 25 °C and 90 °C has been completed.
- Ion exchange equilibrium experiments on montmorillonite and illite have been performed with the goal to evaluate the transferability of sorption measurements and sorption models obtained on dispersed systems to diffusion measurements in compacted systems. The results of the Zn²⁺-Na⁺ equilibrium on illite are given as an example.
- The sorption of uranyl on montmorillonite under reducing conditions has been addressed by wet chemistry and XAS.
- In the framework of two Talisman projects (PSI-ROBL-KIT and PSI-ROBL-BRGM) the influence of ferrous iron on the sorption behaviour of Tc^{VII} and Np^V on montmorillonite has been investigated.
- Spectroscopic and quantum mechanical based atomistic studies of Fe uptake by montmorillonite have started this year in the framework of the PhD project of A. Kéri.

An SNF funded PhD proposal entitled "*Sorption of thallium to illite and birnessite and its impact on the solubility of thallium in soils*" is a collaboration project between Eawag (Molecular Environmental Geochemistry Group) and LES (Clay Sorption Mechanisms Group). Thallium (Tl) is a highly toxic but poorly understood trace metal. The overarching goal of this project is to obtain a quantitative and mechanistic understanding of Tl uptake by illite and birnessite-type Mn-oxides as a basis for the quantitative assessment of the speciation and solubility of Tl in contaminated soils. This project starts on 1st February 2016.

The Swiss-Hungarian cooperation project RaWaDi finished on 14 September, 2014. A major paper on the application of the bottom up approach to the Hungarian Boda Clay and the Swiss Opalinus Clay has been published (MARQUES FERNANDES et al. 2015). A spectroscopic paper, related to this project, on the interaction of Zn with illite, Boda and Opalinus Clay, is in preparation.

4.2 Mechanistic sorption studies

4.2.1 Sorption of Cs^I, Ni^{II}, Eu^{III} and Th^{IV} on montmorillonite, native and altered MX-80 bentonite at 25 °C and 90 °C

Sorption experiments of Cs^I, Ni^{II}, Eu^{III} and Th^{IV} were performed at 25 °C and 90 °C on a reference montmorillonite (Milos), on an "undisturbed" MX-80 and on MX-80 bentonite material originating from the ABM (Alternative Buffer Material) experiment. The ABM MX-80 sample was exposed to temperatures up to 140 °C for 2 years in the Aspo URL. Experiments were carried out to verify whether the exposure to higher temperature had an influence on the sorption properties of the bentonite and to make a direct comparison of the sorption behaviour of the above-mentioned radionuclides at different temperatures.

The ABM MX-80 material used for the sorption experiments was obtained from ABM Package 1 block 18, see Fig. 4.1. The clay was taken by scraping off the bentonite block in the range from 5 to 15 mm from the boundary of the heater, which had been mounted at the center of the block. The section adjacent to the heater was removed to avoid contamination of the sample by the iron corrosion products from the heater. For the sorption experiments, the ABM MX-80 material was converted into homo-ionic Na form.



Fig. 4.1: Photograph of ABM Package 1 block 18. The sample was taken in the range from 5 to 15 mm from the boundary of the heater.

The sorption experiments with Ni^{II}, Eu^{III} and Th^{IV} were performed in an N₂ atmosphere glove box to avoid contamination with atmospheric CO₂. All experiments were carried out in triplicate. The experimental conditions are summarized in Table 4.1.

The bentonite was dispersed in 0.3 M NaClO₄ solution at a given sorbent concentration (*S*) in polyethylene bottles for the experiments at 25 °C and in Teflon bottles for the experiments at 90 °C. The bottles for the Ni^{II}, Eu^{III} and Th^{IV} experiments were transferred into the glove box and the radioactive tracer of each element was added to the bentonite suspensions. The Teflon bottles were placed in an oven at 90 °C after labeling with tracer.

Small volumes of supernatants were taken and the pH values were measured, within certain time intervals. The R_d values were determined from the radiochemical assays of the supernatants. Fig. 4.2 summarizes the results of the sorption measurements of the four radionuclides in the 3 clay systems at 25 °C and 90 °C.

Table 4.1: Overview of the experimental conditions of the sorption experiments on Milos, MX-80 reference and altered bentonite material (ABM). All experiments were carried out at 25 °C and 90 °C for time periods between 7 and 90 days.

	NaClO ₄ (M)	pH	<i>S</i> (g L ⁻¹)
Cs ^I	0.1	7	5.0
Ni ^{II}	0.3	9	0.5
Eu ^{III}	0.3	9	1.0
Th ^{IV}	0.3	7	0.5

The major features of the sorption behaviour can be summarized as follows:

- There are no pronounced kinetic effects between 7 and 90 days for all of the four radionuclides on the three different systems studied at 25 °C and 90 °C.
- For Cs^I, Ni^{II}, Eu^{III} and Th^{IV} the uptake behaviour on the ABM MX-80 sample is similar to the reference MX-80 sample. The treatment of MX-80 bentonite for 2 years at 140 °C does not influence the sorption behaviour of these radionuclides on the altered MX-80 material.
- In the case of Cs temperature has a clear effect. At 90 °C the sorption is reduced by ~0.6 log units compared to 25 °C.
- The sorption of Ni at 90 °C is in all cases slightly higher compared to 25 °C. This behaviour is in line with previous studies on the sorption properties of clays at elevated temperature (e.g. TERTRE et al. 2005).
- After 6 weeks equilibration the sorption of Eu at 90 °C is lower compared to 25 °C. However, the pH of the supernatant at 90 °C was also lower. The pH for the experiments at room temperature was 8.8 ± 0.1 whereas the pH for the samples at 90 °C was 8.4 ± 0.1.
- Within experimental error the sorption of Th is independent on temperature.

The main conclusion from this study is that a two years heat treatment up to 140 °C of MX-80 does not affect its sorption properties towards Cs^I, Ni^{II}, Eu^{III} and Th^{IV}. For those nuclides sorbing by surface complexation there is almost no effect on the R_d values neither at room temperature nor at 90 °C. For Cs which is sorbing by cation exchange the effect is well known (GAINES & THOMAS 1955) and the influence of temperature can be quantified by means of the van 't Hoff equation.

4.2.2 Zn-Na ion equilibrium on illite

The selectivity coefficients of the cation exchange component in the 2SPNE SC/CE sorption model are generally extracted from sorption edges at trace concentrations and low pH (BRADBURY & BAEYENS 1997, 2009). The aim of this study was to investigate the exchange equilibrium between Zn²⁺ and Na⁺ on illite du Puy (IdP) at Zn loadings covering 10 to 90 % of the total CEC (N_{Zn} ranging from ~0.1 to 0.9). The uptake of Zn in a bi-ionic system was studied at a low fixed total (Zn²⁺ + Na⁺) concentration of 0.011 N and at a fixed pH of 6.1. Fig. 4.3a shows the sorption isotherm of Zn on Na-IdP and clearly illustrate that for Zn equilibrium concentrations from 4·10⁻⁶ M to 3·10⁻³ M an almost ideal Langmuir isotherm behaviour is observed.

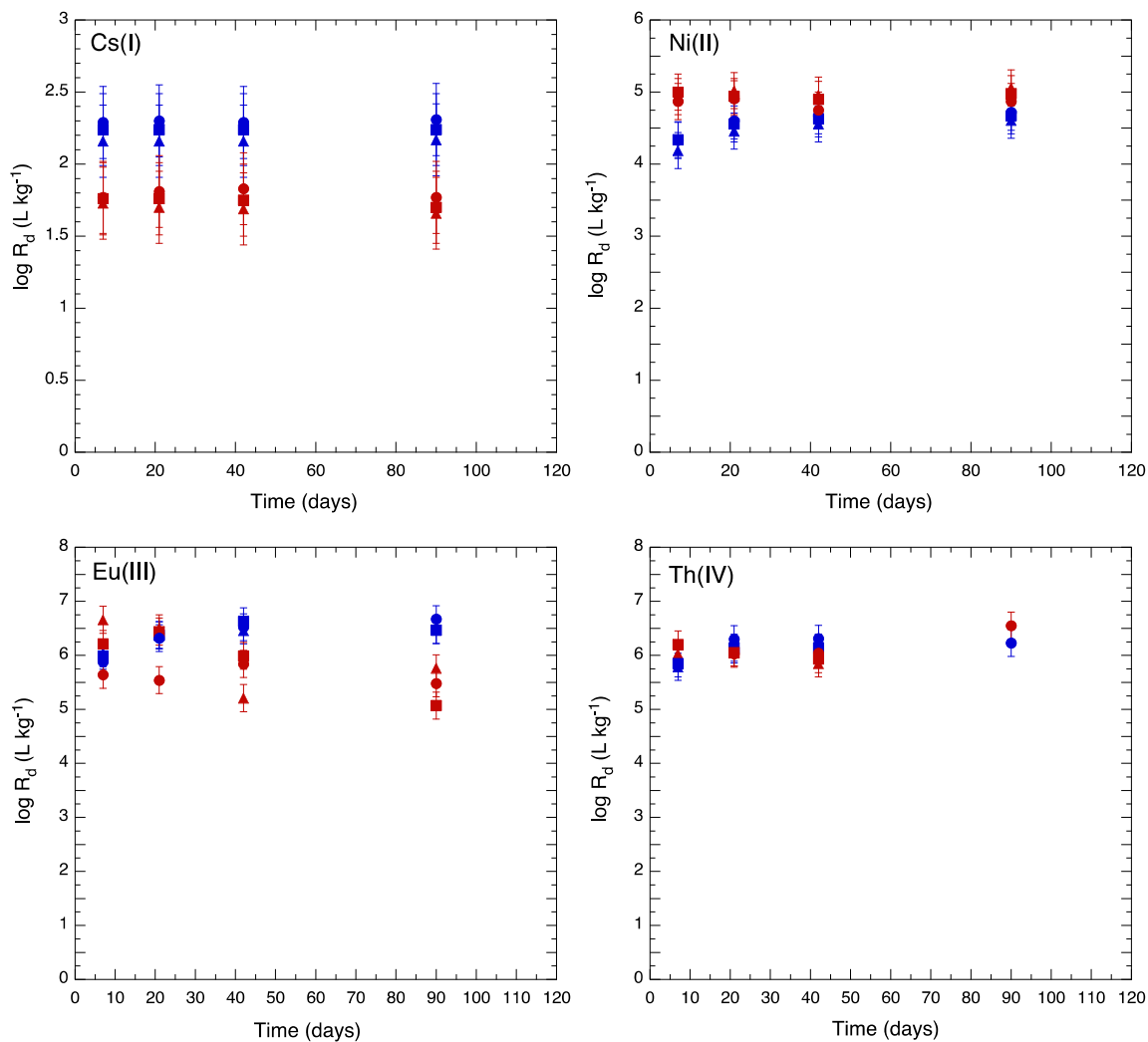


Fig. 4.2: Cs^I , Ni^{II} , Eu^{III} and Th^{IV} sorption kinetics at 25 °C and 90 °C on Milos at 25 °C (\blacktriangle) and 90 °C (\blacktriangle), on MX-80 reference at 25 °C (\blacksquare) and 90 °C (\blacksquare) and ABM MX-80 at 25 °C (\bullet) and 90 °C (\bullet).

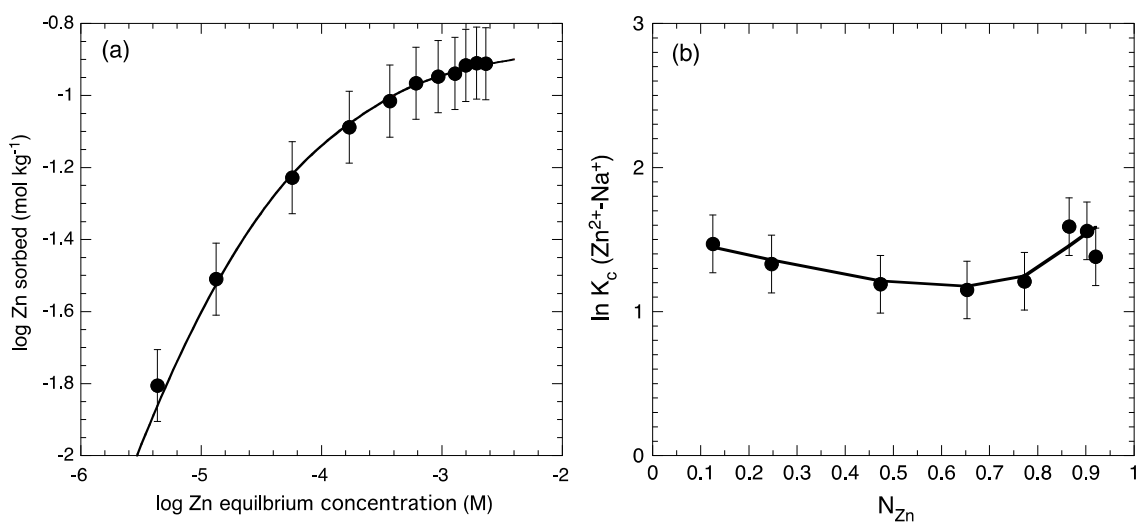


Fig. 4.3: (a) Zn sorption isotherm on Na-IdP. $pH = 6.1$, $S = 11.7 \text{ g L}^{-1}$. Total $Zn^{2+} + Na^+$ concentration is 0.011 N and (b) selectivity coefficient in the Zn-Na IdP as a function of surface composition. (CEC of Zn-IdP is taken to be 260 meq kg^{-1} .)

Zn reaches saturation at $\sim 0.12 \text{ mol kg}^{-1}$. Fig. 4.3b shows the selectivity coefficient ($\ln K_c$) as function of the Zn surface composition (fractional occupancy, N_{Zn}). This plot shows that for Zn loadings between 0.1 and 0.9 the selectivity coefficient is nearly constant with an average value of $\ln K_c = 1.4$ ($K_c^{Zn} = 4$), indicated by the solid line. Using this selectivity coefficient, the sorption isotherm given in Fig. 4.3a can be very well reproduced (solid line). This selectivity coefficient is in good agreement with K_c^{Zn} data found in the open literature for montmorillonite (MAES et al. 1976).

These above measurements are related to the transferability of sorption measurements and models developed on dispersed systems to diffusion measurements on compacted systems. If Zn diffusion experiments are set up under similar conditions as these sorption measurements in diluted systems, the uptake mechanism on the compacted clays is supposed to be solely governed by cation exchange on the planar sites (see also Chapter 7).

4.2.3 Sorption of uranyl on montmorillonite under reducing condition

The mobility of redox sensitive actinides and fission products such as U, Np, Tc highly depends on their oxidation state. In their most oxidized form *i.e.* UO_2^{2+} , NpO_2^+ , TcO_4^- these radionuclide are highly mobile whereas their transport is strongly decreased (higher sorption and lower solubility) when reduced to the oxidation state +4. The majority of sorption, modelling and spectroscopic studies so far have focused on the oxidized states. In safety analyses Th^{IV} is generally taken as a chemical analogue for tetravalent actinides but so far there is no experimental evidence for this assumption.

The sorption of UO_2^{2+} on montmorillonite (STx-2) was studied in a bulk electrolysis cell composed of a three electrode system (i) a glassy carbon working electrode, (ii) an Ag/AgCl reference electrode, and (iii) a coiled platinum wire auxiliary electrode, under reducing conditions ($E_h = -170 \text{ mV vs SHE}$). First, UO_2^{2+} was pre-equilibrated with STx-2 under anoxic conditions (no imposed E_h) and after three days the electrochemical potential was set to -170 mV . Sampling at regular intervals during 28 days allowed to follow the evolution of the uranyl sorption on the clay as shown in Fig. 4.4a. Once the reducing potential was fixed to -170 mV , sorption slightly decreased whereas after 12 days, sorption was constantly increasing and reaching a $\log R_d$ of $\sim 4.2 \text{ L}\cdot\text{kg}^{-1}$ after 28 days. The reason for the initial decrease of sorption after setting the reducing potential is unclear. The distinctive increase of sorption after 12 days suggests the reduction of U^{VI} to U^{IV} which was further investigated by extended X-ray absorption fine structure (EXAFS) spectroscopy. Clay samples with U equilibrated for 3 days (anoxic conditions) and 32 days (reducing conditions) were analysed at the U L_{III} edge in fluorescence mode at the ROBL beamline (ESRF, Grenoble). The EXAFS spectra clearly show that under reducing conditions initially sorbed U^{VI} becomes reduced to U^{IV} *i.e.* U^{IV} has an intense white line compared to U^{VI} , Fig. 4.4b. The X-ray absorption near edge structure (XANES) spectrum of U also exhibits a shoulder on the high energy side of its white line, originating from the multiple scattering (MS) from the linear $\text{O}=\text{U}=\text{O}$ moiety and which is absent in the spectra of the U sample prepared under reducing conditions. The Fourier transform (FT) of the reduced sample also shows a considerable larger U-O distance, typical for U^{IV} . The precipitation of an U^{IV} solid phase was not observed.

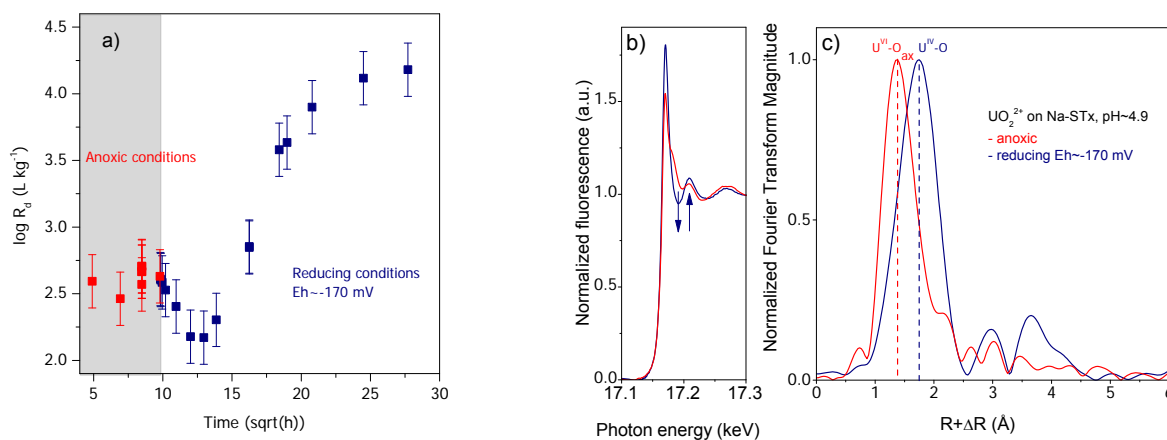


Fig. 4.4: a) Evolution of the sorption of uranium on Na-STx at pH 4.9 in 0.1 NaClO_4 under anoxic and reducing conditions (-170 mV vs SHE). U- L_{III} edge XAFS spectra of U sorbed to STx under anoxic and reducing conditions: b) XANES spectra and c) Fourier transforms (FTs).

4.2.4 Influence of ferrous iron on the retention of Np and Tc on montmorillonite

$\text{Fe}^{\text{II}}/\text{Fe}^{\text{III}}$ is, among others, a redox couple that is involved in many environmental geochemical processes and has a widespread occurrence in anaerobic conditions. In a high level radioactive waste repository the corrosion process of the stainless steel canisters will release large amounts of Fe^{II} into the engineered barrier system (bentonite). With respect to reduction reactions of inorganic and organic compounds, Fe^{II} bound to oxide/clay minerals has been observed to be much more reactive than dissolved Fe^{II} . Not only the kinetics of reaction are faster but also the redox potential of the clay/oxide associated $\text{Fe}^{\text{II}}/\text{Fe}^{\text{III}}$ redox couple is lower than the one of solute iron. Depending on the Fe location (sorbed on the clay as a surface complex, by cation exchange or incorporated in the clay structure), its reactivity can change by orders of magnitude. Iron on clay minerals may oxidize or reduce radionuclides at their surface (by acting either as an electron donor or acceptor) thus reducing their mobility and/or (bio) availability. The overall goal of this study is to unravel the influence of Fe^{II} associated to clay minerals on the reduction of Np^{V} and Tc^{VII} . This work is conducted in collaboration with ROBL/HZDR & INE/KIT (Np) and ROBL/HZDR & BRGM (Tc).

The same experimental and spectroscopic approach was used for Np^{V} and Tc^{VII} to investigate the uptake in the absence and presence of sorbed Fe^{II} . The experiments were carried out on an iron free montmorillonite (IFM) under strictly anoxic conditions inside a glove box ($< 0.1 \text{ ppm O}_2$). IFM was used to avoid any oxidation of Fe^{II} by structural Fe^{III} (SOLTERMANN et al. 2014).

The sorption experiments in the absence of Fe^{II} are shown in Figs. 4.5a and 4.5b for Np and Tc, respectively. In the case of NpO_2^+ sorption is low and independent of pH whereas for the anionic TcO_4^- there is no measurable sorption in the pH range 1 to 10 ($\log R_d < 0 \text{ L}\cdot\text{kg}^{-1}$, data not shown).

The experiments in the presence of Fe^{II} were conducted as follows. In a first step, IFM was equilibrated with an Fe^{II} solution to achieve the desired Fe^{II} loadings. After three days of pre-equilibration, NpO_2^+ or TcO_4^- was added. For the former element only trace sorption was measured whereas for the latter an isotherm was determined at pH 6.3. The sorption results for Np and Tc are shown in Figs. 2a and 2b, respectively. Clearly, for both nuclides the sorption is enhanced if ferrous iron is sorbed on the clay surface.

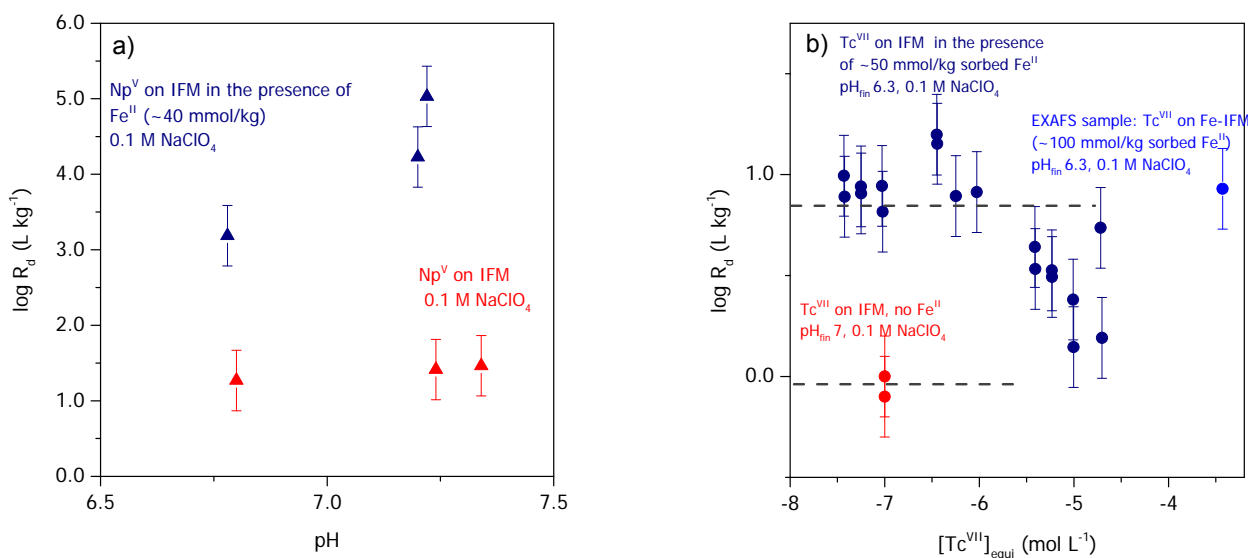


Fig. 4.5: a) Sorption of NpO_2^+ on Na-IFM at $\sim\text{pH}$ 6.8 and ~ 7.3 in 0.1 M NaClO_4 in the absence (red symbols) and presence of $\sim 40 \text{ mmol}\cdot\text{kg}^{-1}$ sorbed Fe^{II} (blue symbols), respectively. b) Sorption isotherm of TcO_4^- on Na-IFM at $\sim\text{pH}$ 6.3 in 0.1 M NaClO_4 in the presence of ~ 50 and $100 \text{ mmol}\cdot\text{kg}^{-1}$ sorbed Fe^{II} (blue symbols).

The oxidation state of Np and Tc retained at the clay surface was further investigated by EXAFS. The spectroscopic measurements were carried out on Np-IFM and Tc-IFM samples prepared in the absence and presence of sorbed Fe^{II} (see Figs. 4.6 and 4.7) at the Np L_{III} edge and Tc K edge in fluorescence mode under cryogenic conditions at 15 K using a closed-cycle He-cryostat to avoid O₂ diffusion into the samples.

Np XANES and FTs spectra are shown in Fig. 4.6a and b. The Np IFM samples prepared in the absence of Fe^{II} at pH 8 and in the presence of Fe^{II} (10 and 20 mmol·kg⁻¹, initial pH 8 drifted to values ~7) show the same XANES and FTs spectra, which are typical for NpO₂⁺ suggesting no reduction below ≤ 20 mmol kg⁻¹ Fe^{II} loading. With increasing Fe^{II} loadings from 40 to 100 mmol·kg⁻¹, increased reduction is observed (XANES: intense white line and vanishing of the features originating from the O=Np=O moiety; FT: decreasing contribution of the Np-O_{eq}, increasing Np-O distances). No Np^{IV} solid was formed. These preliminary results are in good agreement with the macroscopic sorption data.

EXAFS spectra for Tc-IFM in the absence of Fe could not be measured because Tc is not sorbing. Instead a Tc-K edge EXAFS spectrum of aqueous TcO₄⁻ as a reference for Tc^{VII} was taken from SAEKI et al. (2012). Neither was it possible to obtain EXAFS spectra of Tc on the samples prepared under the same experimental conditions as the macroscopic sorption experiments (*i.e.* with ~50 mmol·kg⁻¹). The sorption isotherm shows that the Tc loading at this condition is not sufficient for EXAFS measurements. To reach Tc loadings necessary for EXAFS measurement, the Fe^{II} was increased up to 100 mmol·kg⁻¹ leading to an increase in sorption (log R_d ~0.9 L·kg⁻¹) (see Fig. 4.5b). Under these conditions, however, a large amount of dissolved Fe^{II} remains in the equilibrium solution (~10⁻⁴ M), which might interfere with the reaction mechanism.

The EXAFS spectra of the Tc systems in the absence and presence of sorbed Fe clearly differ and suggest the complete reduction of Tc^{VII} to Tc^{IV} in the presence of sorbed/dissolved Fe^{II} (e.g. shifted E₀ and different shape of the XANES) (Fig. 4.7a). The FTs in Fig. 4.7b clearly show an elongated Tc-O distance compared to the aqueous TcO₄⁻. The Fourier back transform of the intense backscatter peak ~2.25 Å (R+ΔR), suggests that this contribution might be due to Tc-Tc bonding in the second shell. The determination of the exact nature of the complex formed and of the potential reduction mechanisms by sorbed or/and dissolved Fe^{II} is in progress.

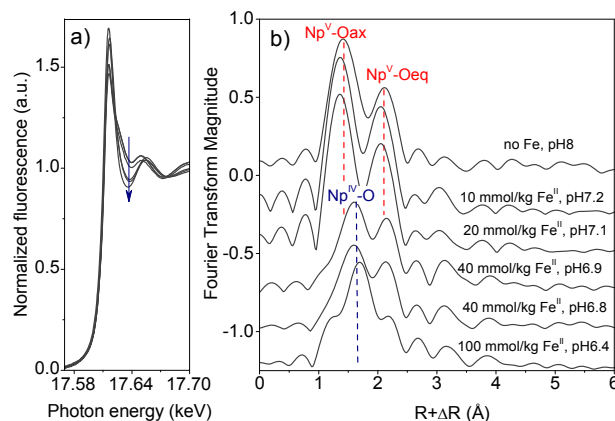


Fig. 4.6: Np-L_{III} edge XAFS spectra of Np sorbed to Na-IFM in the absence of Fe^{II} at pH 8 and in the presence of increasing amounts of sorbed Fe^{II} at pH between 7.2 and 6.4. a) XANES spectra and b) FTs.

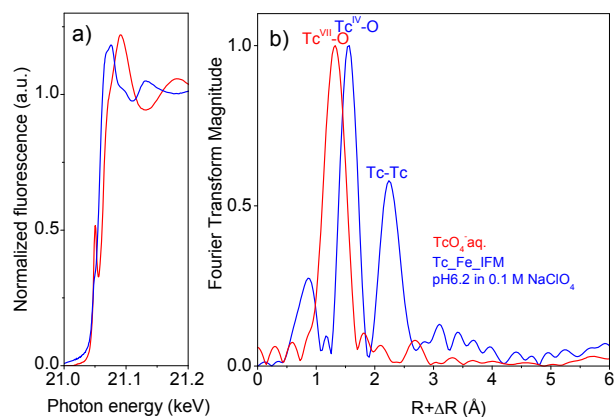


Fig. 4.7: Tc-K edge XAFS spectra of aqueous TcO₄⁻ (red) taken from SAEKI et al. (2012) and Tc on Na-IFM in the presence of ~100 mol·kg sorbed Fe^{II} at pH 6.4. a) XANES spectra and b) FTs.

4.3 XAS related activities

4.3.1 EXAFS investigations of structural Fe in clay minerals

Recent studies (SCHAEFER et al. 2011, SOLTERMANN et al. 2014) have shown that structural iron in clay minerals plays an important role in the oxidative sorption of redox sensitive elements. To explain and understand the mechanism of this process the structural environment of iron in clay minerals needs to be known. Location and distribution of iron in different natural Fe-containing clay minerals bulk were investigated by EXAFS spectroscopy at the beamline 11-2 of the Stanford Synchrotron Radiation Laboratory. The clay minerals investigated have a

well-known structure with different $\text{Fe}^{\text{II/III}}$ contents: illite (IdP) with the chemical composition $(\text{Al}_{1.17}\text{Fe}^{\text{III}}_{0.49}\text{Mg}_{0.33})[(\text{Si}_{3.52}\text{Al}_{0.48})]$ (POINSSOT 1999) is a pure Fe^{III} clay, Milos is a predominant Fe^{III} montmorillonite $(\text{Al}_{1.5}\text{Fe}^{\text{II}}_{0.01}\text{Fe}^{\text{III}}_{0.22}\text{Mg}_{0.27})[(\text{Si}_{3.88}\text{Al}_{0.12})]$ and SWa-1 is a ferruginous montmorillonite $(\text{Al}_{0.51}\text{Fe}^{\text{III}}_{1.35}\text{Mg}_{0.14})[(\text{Si}_{3.71}\text{Al}_{0.29})]$ (VANTELON 2003). The bulk X-ray spectroscopic data of the three clays show distinct features in k -space (Fig. 4.8). The oscillation at $\sim 4 \text{ \AA}^{-1}$ is influenced by the octahedral composition, *e.g.* by the Fe-Al/Mg/Fe backscattering pairs. The spectral features at higher k -values, especially the split of oscillation at $\sim 8 \text{ \AA}^{-1}$, result mainly from Fe-Fe backscattering pairs. The structural differences of Fe in the three clays are also reflected in the corresponding Fourier Transforms, in particular in the second coordination shell. The data indicate clearly that in IdP and SWa-1 clustering of Fe atoms occurs, whereas in Milos the Fe contribution is randomly distributed in the octahedral layers. The data for Milos and SWa are in a good agreement with the findings of VANTELON *et al.* (2003). Data analysis including molecular modelling calculations are described in the next section and are on-going.

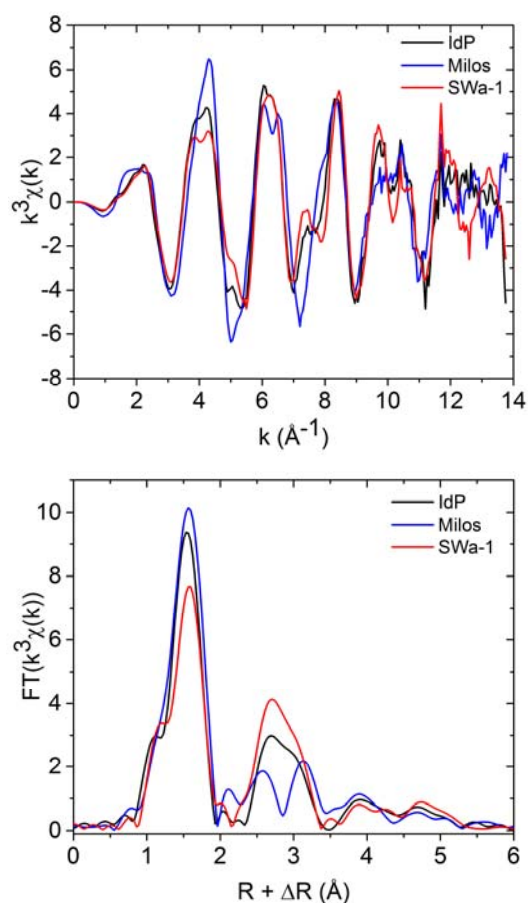


Fig. 4.8: *Fe K-edge bulk EXAFS and Fourier Transform data of IdP (blue), Milos (red) and SWa-1 (green).*

4.3.2 Molecular modelling of structural iron in clay minerals

In the SNF funded PhD project "*Detailed understanding of metal adsorption on clay minerals obtained by combining atomistic simulations and X-ray absorption spectroscopy*" quantum mechanical atomistic simulations were performed to investigate the structural environment of Fe in montmorillonite. The final aim of these calculations is to identify preferential sorption sites for Fe^{II} and Fe^{III} on the surface and the oxidation energy for structural and surface bound iron in montmorillonite.

In the first stage of the project the stability and structural environment of Fe^{II} and Fe^{III} in *cis*- and *trans*-sites of *cis*-vacant montmorillonite was investigated. The simulations are based on the density functional theory (DFT) using the QUICKSTEP module of the CP2K code [www.cp2k.org]. Since conventional DFT fails to describe localized 3d states of Fe accurately, the so-called DFT+U method was applied. The importance of the DFT+U correction is demonstrated in Fig. 4.9. The conventional DFT (U-J=0.0 eV) predicts the band gap to be as low as 2.54 eV whereas experimentally measured value is 4.0 eV using the DFT+U, the correct band gap value (4.32 eV) could be obtained (Fig. 4.9).

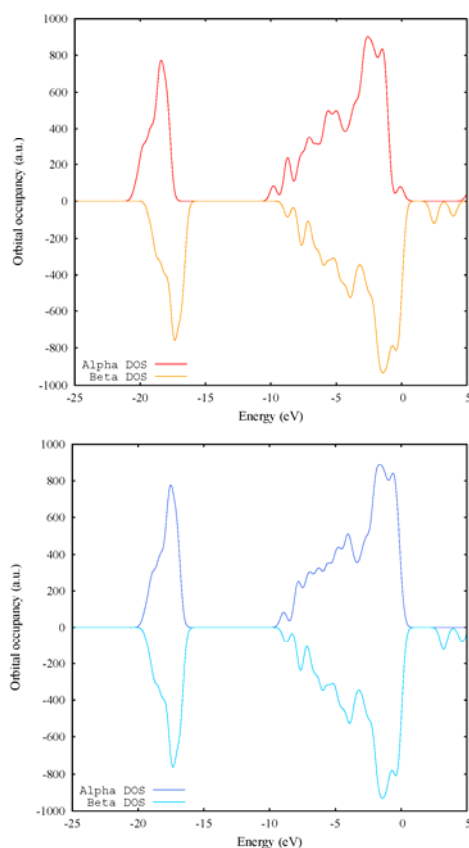


Fig. 4.9: *Density of states for α and β electrons of iron as a function of energy shifted with the Fermi level.*

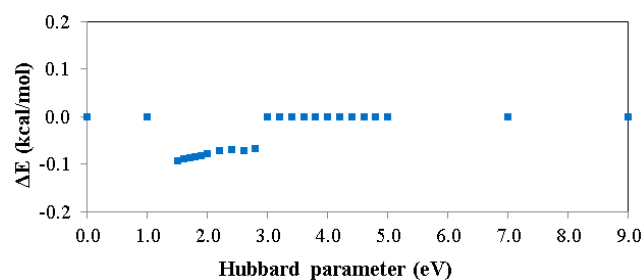


Fig. 4.10: Energy difference between systems containing Fe^{III} in *cis* or *trans* octahedral sites as a function of the Hubbard parameter.

The energies for the Fe^{III} transfer between *cis* and *trans* sites of bulk montmorillonite are shown in Fig. 4.10. The results suggested that the energy does not depend on the value of $U-J$ and that Fe^{III} is equally distributed between *cis* and *trans* sites.

The EXAFS spectra for Fe^{II} and Fe^{III} in *cis* and *trans* sites were calculated based on the geometries optimized by the DFT+ U method and were compared with the measured EXAFS spectra of structural Fe in STx-1 montmorillonite (SOLTERMANN et al. 2014). The results indicate significant differences between the spectra of Fe^{II} and Fe^{III} whereas the influence of the *cis* and *trans* symmetry of the polyhedral coordination was found to be small (see Fig. 4.11). The calculated EXAFS spectra for Fe^{III} in both *cis* and *trans* positions agree well with the experimental observations. The slight asymmetry of the EXAFS oscillation at 4 \AA^{-1} could be explained by small amounts of Fe^{II} present in the clay structure $((Si_{7.76}Al_{0.24})(Al_3Mg_{0.54}Fe^{II}_{0.02}Fe^{III}_{0.44})Na_{0.79})$ (VANTELON 2003).

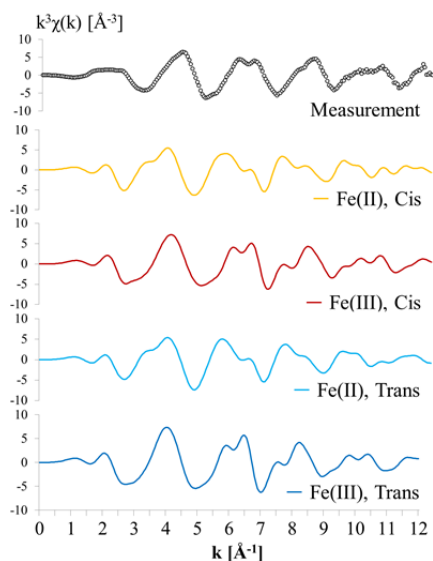


Fig. 4.11: Calculated EXAFS spectra of Fe^{II} and Fe^{III} in *cis* and *trans* octahedral sites and experimentally measured Fe-K EXAFS spectrum for STx-1 montmorillonite. (taken from SOLTERMANN et al. 2014).

4.4 References

- BRADBURY M.H., BAEYENS B. (1997)
A mechanistic description of Ni and Zn sorption on Na-montmorillonite. 2. Modelling, J. Contam. Hydrol. 27, 3-4, 223-248.
- BRADBURY M.H., BAEYENS B. (2009)
Sorption modelling on illite. Part I: Titration measurements and the sorption of Ni, Co, Eu and Sn. Geochim. Cosmochim. Acta 73, 990-1003.
- GAINES G.I., THOMAS H.C. (1955)
Adsorption studies on clay minerals. V. Montmorillonite-cesium-strontium at several temperatures. J. Chem. Phys. 23, 2322-2326.
- MAES A., PEIGNEUR P., CREMERS A. (1976)
Thermodynamics of transition metal ion exchange in montmorillonite. Proc. Int. Clay Conf. New Mexico, 1975, 319-329.
- MARQUES FERNANDES M., VER N., BAEYENS B. (2015)
Predicting the uptake of Cs, Co, Ni, Eu, Th and U on argillaceous rocks using sorption models for illite. Appl. Geochem. 59, 189-199.
- POINSSOT C., BAEYENS B., BRADBURY M.H. (1999)
Experimental and modelling studies of caesium sorption on illite. Geochim. Cosmochim. Acta 63, 3217-3227.
- SAEKI M., SASAKI Y., NAKAI A., OHASHI A., BANERJEE D., SCHEINOST A.C., FOERSTENDORF H. (2012)
Structural study on complex of MIDOA with M(VII)O₄⁻ (M = Re and Tc) by 1H-NMR, EXFAS and IR spectroscopy. Inorg. Chem. 51, 5814.
- SCHAEFER M.V., GORSKI C.A., SCHERER M.M. (2011)
Spectroscopic evidence for interfacial Fe(II)-Fe(III) electron transfer in a clay mineral. Environ. Sci. Technol. 45, 540-545.
- SOLTERMANN D., MARQUES FERNANDES M., BAEYENS B., DÄHN D., JOSH P.A., SCHEINOST A.C., GORSKI C.A. (2014)
Fe(II) uptake on natural montmorillonite under anoxic conditions. I. Macroscopic and spectroscopic characterization. Environ. Sci. Technol. 48, 8698-8705.
- VANTELON D., MONTARGES-PELLETIER E., MICHOT L.J., PELLETIER M., THOMAS F., BRIOIS V. (2003)
Iron distribution in the octahedral sheet of dioctahedral smectites. An Fe K-edge X-ray absorption spectroscopy study. Phys. Chem. Min. 30, 44-53.

5 CEMENT SYSTEMS

E. Wieland, J. Tits, A. Laube, D. Kunz, B. Z. Cvetković (post doc), H. Rojo Sanz (guest scientist)

5.1 Overview

The group "Cement Systems" carries out research on the long-term behaviour of important waste components and on radionuclide-cement interactions in the near field of the deep geological repositories for low-level and short-lived intermediate-level waste (L/ILW) and long-lived intermediate-level waste (ILW) in Switzerland.

In 2015 the main activities focussed on i) further assessing the chemical processes in waste packages in conjunction with the evolution of the heterogeneity in the cementitious near field, ii) the determination of the low molecular weight (LMW) organics produced during the anoxic corrosion of steel, iii) the development of compound-specific ^{14}C AMS (accelerator mass spectrometry) for the detection of ^{14}C bearing compounds at very low ^{14}C concentrations, iv) the development of a methodology suitable to investigate the chemical stability of LMW organics under conditions relevant to a cement-based near field, and v) mechanistic sorption studies with redox-sensitive, dose-determining Se(IV/-II) anions on hardened cement paste (HCP) and cement phases.

The ^{14}C project which includes studies on the LMW organic corrosion products and the development of a very sensitive ^{14}C AMS-based analytical method for the determination of ^{14}C bearing compounds is partially financed by Swissnuclear (Project title: Investigation on the chemical speciation of ^{14}C released from activated steel) and by the EU FP7 collaborative project "CAST". Specific tasks within this project have been developed in co-operation with PD Dr. S. Szidat and Dr. G. Salazar (Department of Chemistry and Biochemistry at the University of Bern, Switzerland), and Brechbühler AG (Schlieren, Switzerland), the commercial partner in this project.

The German collaborative project (Verbundprojekt) "IMMORAD" (Grundlegende Untersuchungen zur Immobilisierung langlebiger Radionuklide durch die Wechselwirkung mit endlagerrelevanten Sekundärphasen; Coordinator: Prof. Dr. Th. Schäfer (KIT-INE)), which was financed by the German Federal Ministry of Education and Research, was finished on July 31st, 2015. The focus of the LES contribution to this project was to explore the uptake of Se by cementitious materials under reducing conditions. The project was carried out in collaboration with Dr. A. Scheinost (Rossendorf (ROBL) beamline at the ESRF). The project will continue in 2016 in the framework of a PhD study financed by the EU

HORIZON 2020 collaborative project "CEBAMA" (Cement-based materials, properties, evolution, barrier functions).

5.2 Activities in support of the Sectoral Plan: Report on the evolution of heterogeneities in the cementitious near field

A multi-barrier concept is foreseen to ensure the safe disposal of L/ILW in cement-based deep geological repositories (NAGRA 2002). The barrier is composed of the waste matrix, the waste-containing steel drums, the emplacement containers for the steel drums, the backfill material used to fill vaults within and between the emplacement containers, liners and eventually the host rock. A report was prepared with the aim of assessing the barrier function of the waste-containing steel drums by considering the reactivity of the waste materials inside waste packages. The chemical processes determining the reactivity of the waste packages are: i) metal corrosion, ii) degradation of organic waste materials present in the waste and/or used as embedding matrix (e.g. bitumen), and iii) dissolution of sand and gravel used to make the waste-solidifying concrete. The kinetics of these processes were elaborated and preliminary mass balance calculations were carried out to assess the effect of water accessible in the waste packages on the reactivity as all the aforementioned processes consume water. The first draft of the report was reviewed by Nagra. The follow-up discussion showed that the calculations should be repeated using the new inventories published in MIRAM 2014 (NAGRA 2014) and further, considering waste packages containing decommissioning waste in addition to the selected waste packages with operational waste (a resin-containing bituminized waste package, a cemented waste package, and resin-containing waste embedded in polystyrene). The additional waste forms have been specified and preparation of the modified version of the report is ongoing (WIELAND et al. 2015a).

5.3 Speciation and fate of organic compounds in the cementitious near field

5.3.1 ^{14}C project

^{14}C , possibly carried by small organic compounds resulting from steel corrosion under reducing conditions in a cementitious near field, is a potentially major contributor to the long-term activity release rate (mSv per year) from the cement-based repositories into the far field. Previous work confirmed that small

organic molecules form in the course of the anoxic corrosion of activated (or irradiated) steel (WIELAND & HUMMEL 2015). Although the ^{14}C inventory associated with activated steel is well known, the chemical form of the ^{14}C bearing compounds produced during the anoxic corrosion of activated steel is only poorly known. The ^{14}C project aims at filling this gap in our knowledge. In 2015, the series of batch-type corrosion experiments with non-irradiated steel powders in hyper-alkaline solution were finalized, the activities related to the development of an experimental set-up for the corrosion experiment with activated steel and the development of the compound-specific ^{14}C AMS method required to detect ^{14}C containing compounds at very low concentrations were continued.

5.3.1.1 Installation of the new GC-MS and development of analytical methods

At the end of 2014 a gas chromatograph with mass spectrometry detection (GC-MS) was acquired and installed in the Hot Laboratory of PSI (Fig. 5.1). In 2015 analytical methods previously developed in collaboration with the Institute for Chemistry and Bioanalytics at the University of Applied Sciences Northwestern Switzerland (ICB/FHNW) were adapted and optimized for measurements on the new equipment, such as headspace analysis of hydrocarbons and dissolved volatiles as well as analysis of hydrocarbons in the gas phase. These methods are described in detail elsewhere (WIELAND & CVETKOVIĆ 2015).

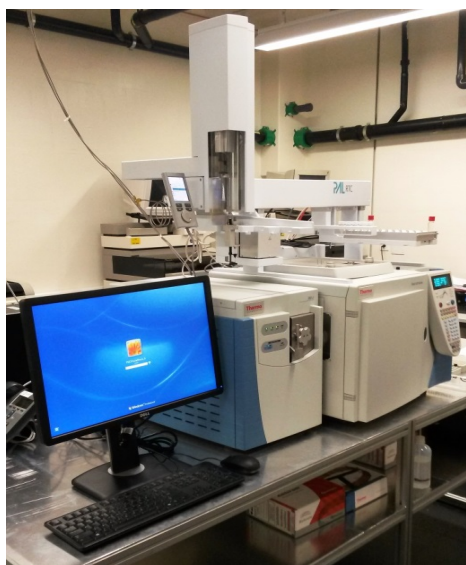


Fig. 5.1: Photography of the new GC-MS installed in the PSI Hot Laboratory.

5.3.1.2 Identification and quantification of organics released during iron corrosion

In previous studies with non-irradiated iron powders we were able to identify a total of 15 small molecules that are formed during anoxic corrosion in alkaline solution (LES progress report 2014). In 2015 we carried out an additional series of corrosion studies using the same iron powders with the aim of checking the reproducibility of the previous results with the improved analytical set-up at PSI. The instrumental set-up that had been used to determine carboxylic acids with high performance ion exclusion chromatography and mass spectrometry detection (HPIEC-MS) in the previous experiments was modified after an extensive service of the MS. As a consequence, the sensitivity of the MS substantially improved and allowed additional carboxylates, in particular lactate, propanoate and butanoate, to be detected at very low concentrations (Table 5.1). These compounds will be monitored in future corrosion experiments although the concentrations were found to be only slightly above the detection limit. Note, however, that up to date, we have not been able to detect butylene and pentene.

5.3.1.3 Coupling separation techniques with accelerator mass spectrometry (AMS) for compound-specific carbon-14 analysis

The concentrations of the ^{14}C bearing organic compounds in the planned corrosion experiments with the available activated steel sample are expected to be extremely low for several reasons: Only a small steel sample with a low surface area can be used due the high dose rate of the activated steel nut, the corrosion rate is very low in hyper-alkaline solution and eventually the ^{14}C content of activated steel is low (SCHUMANN et al. 2014; WIELAND & CVETKOVIĆ 2015).

Therefore, analysis of ^{14}C bearing single compounds requires an extremely sensitive method for the detection of ^{14}C . To this end, compound-specific ^{14}C AMS is currently being developed, which is based on the coupling of standard separation techniques (GC, HPIEC) with ^{14}C detection by AMS.

Determination of the ^{14}C background in samples: Sample contamination was checked in the last year as ^{14}C is also a naturally occurring radionuclide in the form of $^{14}\text{CO}_2$ (activity of 1 m^3 air ~ 0.044 Bq). In particular, alkaline solutions are sinks for CO_2 and therefore $^{14}\text{CO}_2$. To this end, the ^{14}C background caused by sample preparation, HPIEC separation and in the course of AMS measurements was determined.

Table 5.1: Carbon species expected to form as a result of steel corrosion as reported in literature (all table entries except lactate) and subsequently identified in this study (highlighted in bold and bold italic).

Alkane/alkene	Alcohols/aldehydes	Carboxylate ions	Carbonate
Methane (CH₄)	Methanol (CH₃OH)	Formate (HCOO⁻)	CO ₂
Ethane (C₂H₆)	Ethanol (C₂H₅OH)	Acetate (CH₃COO⁻)	CO ₃ ²⁻
Ethene (C₂H₄)	Formaldehyde (CH₂O)	Propanoate (C₂H₅COO⁻)	(CO)
Propane (C₃H₈)	Acetaldehyde (C₂H₄O)	Butanoate (C₃H₇COO⁻)	
Propene (C₃H₆)	Propionaldehyde (C₃H₆O)	Malonate (CH₂(COO⁻)₂)	
Butane (C₄H₁₀)		Oxalate (C₂O₄²⁻)	
Butylene (C ₄ H ₈)		<i>Lactate (CH₃CHOHCOO⁻)</i>	
Pentene (C ₅ H ₁₀)			

The following effects were assessed stepwise: procedures used to clean the vials, type of vials (plastic vs. glass), and use of water of different purity degrees (e.g., ultrapure water, untreated, boiled and degassed Milli-Q water) (Table 5.2).

An optimized cleaning procedure for the vials was developed to minimize the background, which was determined to be ~0.06 F¹⁴C (fraction modern carbon or fm, respectively). All the other aspects outlined above were found to have insignificant effects on the ¹⁴C background. However, a significant increase in the fraction modern carbon was observed for a Ca(OH)₂ solution with pH 12.5 (0.89 F¹⁴C) which is caused by the ingress of atmospheric ¹⁴CO₂ during sample preparation, transportation to the AMS and during the AMS measurement. As a consequence, all samples are immediately neutralized after sampling to minimize/avoid the uptake of ¹⁴CO₂. Furthermore, the ¹⁴C background did not change during HPIEC separation of the target compounds (i.e. acetic acid (AA), formic acid (FA), malonic acid (MA) and oxalic acid (OA)) although several materials (e.g. analytical column, eluent etc.) interact with the samples during separation and fractionation (Table 5.2). The above tests revealed that the analytical method under development for the AMS based detection of very low ¹⁴C concentrations of ¹⁴C bearing compounds is not subject to major ¹⁴C contamination.

Dynamic range of the AMS system and recovery tests with ¹⁴C radiotracer: Additional measurements were carried out to determine the dynamic range of the AMS system and the recovery of a tracer separated by HPIEC. ¹⁴C bearing acetic acid was used from the list of target carboxylic acids. Solutions with different ¹⁴C activities, which corresponded to 10 - 2500 F¹⁴C (in a matrix of 20 µg ¹²C), were prepared and injected into the ion chromatography (IC) system.

Table 5.2: Comparison of ¹⁴C background (BG) measurements (in F¹⁴C)¹.

Vial [F ¹⁴ C]		Solvent [F ¹⁴ C]		IC-fraction ² BG [F ¹⁴ C]	
Plastic	0.06	BG-Milli-Q	0.06	AA	0.02
Glass	0.07	BG-ultrapure water	0.07	FA	0.04
		BG-degassed-Milli-Q	0.10	MA	0.06
		BG-alkaline (pH 12.5)	0.89	OA	0.02

$$^1 1 F^{14}C (= 1 fm) = \frac{^{14}C}{(^{12}C \times 1.18 \cdot 10^{-12})}$$

² AA = acetic acid; FA = formic acid; MA = malonic acid; OA = oxalic acid

The fraction corresponding to acetic acid was collected, transferred to the AMS facility at the University of Bern and analyzed. The fraction of modern carbon in the fractionated sample (acetic acid fraction) should correspond to 0.2 - 50 F¹⁴C (in the matrix of 20 µg ¹²C) due to a 1:50 dilution during IC separation. In Fig. 5.2 the experimental scheme (left) and the results of the separation process (right) are shown. The table shows the expected fraction modern (calculated from the ¹⁴C activity of the starting solution and taking into account dilution during IC separation), the fraction modern measured with AMS as well as the recovery obtained from the ratio of the two values (in %). A rather poor recovery was observed for the lowest fraction modern (0.21) while the average recovery determined from the samples with 0.47 - 49.12 F¹⁴C is close to 100 % (93 ± 17 %). It appears that for most samples the measured recovery is systematically lower than the expected value, which could be caused by an incorrect window

setting during fraction collection. Additional tests are ongoing to check and optimize the recovery.

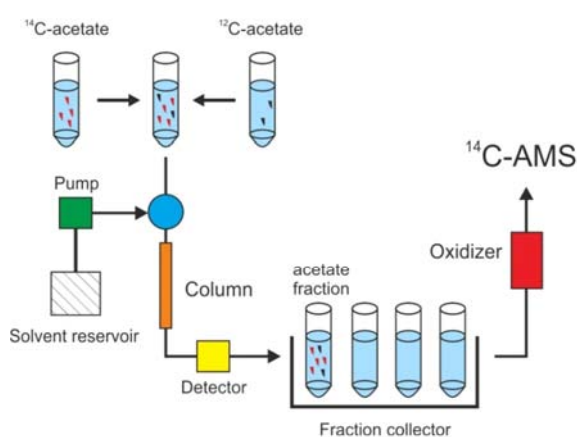
The test with ^{14}C labelled acetic acid further allowed the dynamic range and possible cross contamination between IC samples to be explored. Even the highest activities gave reproducible results in the AMS measurements, suggesting that cross contamination is not a major problem. The dynamic (linear) range of the AMS was found to extend over three orders of a magnitude, i.e. from 0.06 to 50 F^{14}C . This wide range opens up sufficient flexibility for sample dilution with the aim of preparing samples with ^{14}C concentrations in the dynamic range of the AMS.

5.3.1.4 Development of a reactor for the corrosion experiment with activated steel

An experimental set-up for the long-term corrosion experiment with the activated steel nut from the Gösgen nuclear power plant was developed. The set-up consists of a custom-made gas-tight overpressure reactor placed within a 10 cm lead shielding (Fig. 5.3). The reactor is equipped with a digital pressure transmitter as well as a dissolved oxygen sensor (Visiferm DO Arc, Hamilton, USA). The Visiferm DO Arc is an optical oxygen sensor without electrolyte, thus eliminating the risk of contamination of the aqueous phase, and an oxygen detection limit as low as 4 ppb. The overpressure reactor is designed in such a way that all manipulations necessary for regular sampling can be carried out outside the lead shielding to minimize exposure of the experimentalist to radiation. Transfer of the activated steel nut into or

out of the reactor takes place via a door in the lead shielding (Fig. 5.3a).

In 2015, the construction of the reactor was completed and "cold" experiments, i.e. without activated material, were carried out to check the tightness of the reactor, to test the proper functioning of the different sensors (dissolved O_2 , pressure) and their response to O_2 contaminations, and to evaluate the extent of O_2 contamination during a sampling procedure (Fig. 5.3b). Furthermore, the entire sampling procedure was tested several times, which includes a gas phase sampling step (50 mL gas), a liquid phase sampling step (7 mL liquid) followed by a re-adjustment of the liquid volume with 7 mL O_2 -free solution and a re-adjustment of the N_2 overpressure. For these tests, the reactor was filled with 300 mL artificial cement porewater ($\text{ACW}_{\text{eq-II}}$), a piece of iron wire (length: 1 m, $\text{Ø}=0.5\text{mm}$, Fe content $>99.9\%$) was submerged and a N_2 overpressure of 4 bar was applied. A typical record of pressure and dissolved oxygen during one of these test experiments is shown in Fig. 5.3b. The samplings are clearly visible as short pressure drops. During initial filling of the reactor, a small amount of O_2 could enter the reactor. This amount of O_2 is consumed by oxidation of the Fe wire. Subsequent samplings do not result in significant O_2 accumulation. The tests show that the reactor is gas-tight and that O_2 concentration, temperature and pressure can be monitored accurately during an experiment in the reactor. Presently, the ^{14}C background in the reactor is determined.



Expected [F^{14}C]	Measured [F^{14}C]	SD [%]	Recovery [%]
0.21	(0.13)	(2.2)	(64)
0.47	0.59	-	125
0.95	0.91	1.2	96
2.67	2.47	-	93
4.39	(1.80)	-	(41)
11.16	8.50	0.5	76
24.61	17.79	0.5	72
49.12	46.37	1.4	94
			Average: $93 \pm 17\%$

Fig. 5.2: Recovery test for IC separation using ^{14}C labelled acetic acid. Left: scheme of the experimental setup; Right: results obtained from IC separation. Note that 0.2 F^{14}C corresponds to a ^{14}C concentration in the initial solution (before IC separation) of $2 \cdot 10^{-12} \text{ mol L}^{-1}$.

5.3.2 Chemical stability of organic compounds under hyper-alkaline conditions

^{14}C containing LMW organic molecules released during the corrosion of activated steel may not be chemically stable under the hyper-alkaline, reducing conditions of a cement-based repository. Thermodynamic calculations revealed that in case of complete thermodynamic equilibrium, the predominant species are $\text{CO}_2(\text{aq})$, HCO_3^- , CO_3^{2-} and $\text{CH}_4(\text{aq})$ (WIELAND & HUMMEL 2015). However, complete thermodynamic equilibrium is rarely achieved in the C-H-O system at moderate temperatures. It is still unclear what kind of organic compounds will predominate in the repository, if partial thermodynamic equilibria prevail (e.g. if CH_4 formation is kinetically hindered).

The chemical stability of acetic acid under hyper-alkaline anoxic conditions is currently being studied with the aim of checking the possibility for partial and complete thermodynamic equilibrium, respectively, under conditions relevant to a cement-based repository. To this end, O_2 -free, portlandite saturated solution ($\text{pH} = 12.5$) containing 0.3 mM Na-acetate and a pure, O_2 -free, portlandite-saturated solution (blank), were aged under anoxic conditions, i.e. an inert N_2 atmosphere at an overpressure of 4 bar. Both the liquid and gas phases were regularly sampled and analyzed over the ageing period using HPIEC-MS and in-house GC-MS and determining total organic carbon (TOC). The presence of propane, propene, butane and ethane in the gas phase reported earlier could not be confirmed (LES progress report 2014). Hence, the significant concentrations of these compounds observed in the earlier experiment are attributed to an

analytical artefact. These earlier gas phase measurements were carried out at ICB/FHNW.

The stability tests show that Na-acetate is stable under hyper-alkaline anoxic conditions, i.e. an inert N_2 atmosphere at an overpressure of 4 bar, over a period up to 120 days. This indicates that the decomposition of LMW organics into CH_4 and CO_2 predicted by thermodynamic equilibrium calculations is kinetically hindered. The experiment will be repeated in the presence of iron and at elevated temperature.

5.3.3 Sorption/diffusion of LMW organic compounds

^{14}C containing LMW organic molecules may further interact with cementitious materials thus being retarded in the near field. In the past years sorption and diffusion studies with LMW organics, in particular methanol, ethanol, formaldehyde, acetaldehyde, acetic and formic acids, were carried out on HCP (LES progress reports 2010, 2013). The sorption studies were carried out on intact cement samples, i.e. hydrating cement, as the distribution ratio (R_d value) for these compounds was expected to be very low (Fig. 5.4a).

In 2015 sorption and desorption studies with formic acid were carried out on the most important cement phases, that is monocarbonate (AFm- CO_3), hemi-carbonate (AFm-OH- CO_3), monosulfate (AFm- SO_4), ettringite (AFt- SO_4) and C-S-H phases with Ca/Si (C/S) ratios = 0.8 and 1.65, with the aim of checking the reversibility of the uptake process.

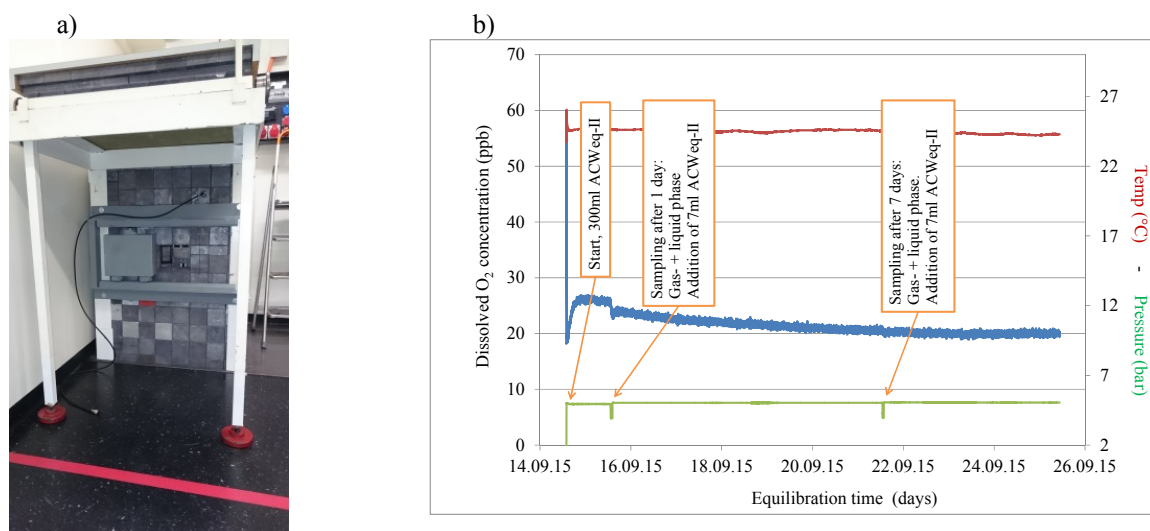


Fig. 5.3: Pressure reactor designed for use in corrosion studies with activated steel samples. a) Picture of the lead shielding and lead door for sample loading, b) Record keeping of temperature, pressure and dissolved O_2 .

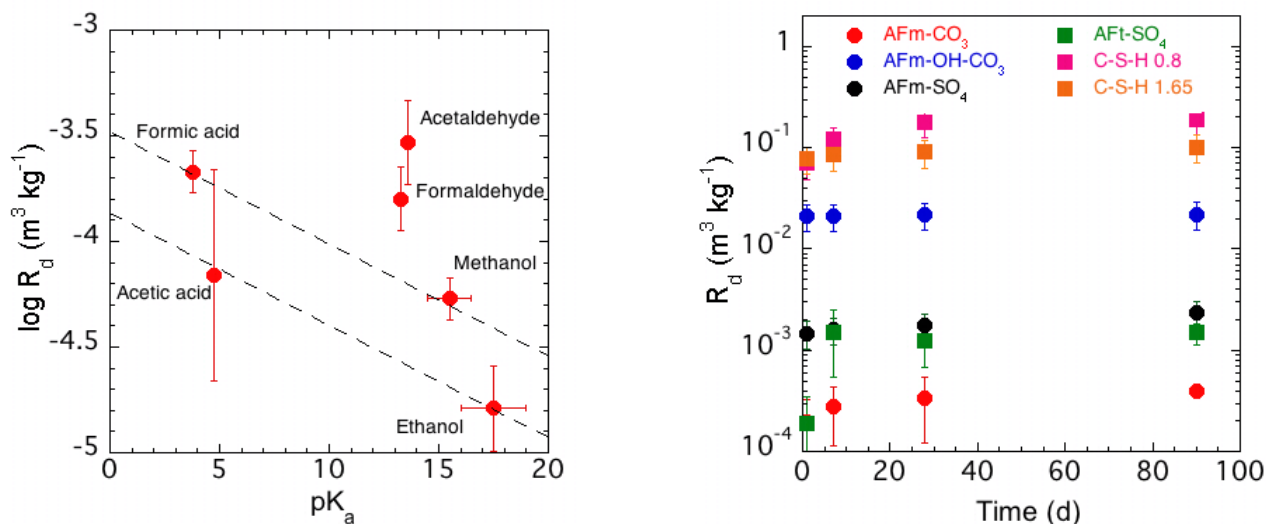


Fig. 5.4: Sorption studies with ethanol, methanol, formaldehyde, acetaldehyde, formic and acetic acids. a) R_d values on HCP as function of the pK_a of the compounds. Note that the relatively strong uptake of formaldehyde and acetaldehyde could be attributed to experimental artefacts caused by the high volatility of these compounds; b) Kinetics of the uptake by the most important cement phases. AFm-CO₃: monocarbonate; AFm-OH-CO₃: hemiacarbonate; AFm-SO₄: monosulfate; AFt-SO₄: ettringite; C-S-H 0.8: C-S-H phase with C/S = 0.8; C-S-H 1.65: C-S-H phase with C/S = 1.65.

Sorption measurements with the other organic compounds besides formic acid were not possible due to their very weak interaction with the cement phases. Uptake of formate by all cement phases was found to be fast (Fig. 5.4b). The strongest uptake was observed on hemiacarbonate and the C-S-H phases. The uptake process was found to be reversible on all phases with the exception of ettringite where the R_d values determined from desorption were about an order of magnitude larger than those determined from sorption (WIELAND et al. 2015b). This finding is consistent with observations made earlier during the out-diffusion of formate from HCP where a small portion of strongly bound formate caused a continuous release in the out-diffusion experiment over more than 100 days (WIELAND et al. 2015b). The studies show that the selected LMW organics are only weakly and largely reversibly bound to HCP and cement phases, except formic acid.

5.4 Retention of selenium by cementitious materials under reducing conditions

⁷⁹Se (half-life $3.27 \cdot 10^5$ years) is an important redox-sensitive, dose-determining radionuclide in an L/ILW repository (NAGRA 2002). The selenium speciation under oxidizing conditions is dominated by SeO₄²⁻ and SeO₃²⁻ (HUMMEL et al. 2002; OLIN et al. 2005) while in alkaline, reducing conditions, i.e. $10.0 < \text{pH} < 13.5$ and $-750 \text{ mV} < E_h < -230 \text{ mV}$, Se(0), HSe⁻ and polyselenide species exist. Robust sorption data and, in particular, a sufficiently detailed mechanistic understanding of Se(-II) retention in a cementitious

environment are lacking. Closing this gap was the main objective of a postdoc project carried out between May 2012 and July 2015 in the framework of the German collaborative project "IMMORAD".

Sorption studies on various cement phases (C-S-H phases, AFm phases, AFt) showed that R_d values for SeO₃²⁻ and HSe⁻ on C-S-H phases are lower than those on AFm phases, although the latter phases have a much lower surface area (BAUR et al. 2004). In the case of the AFm phases, the R_d values strongly depended on the interlayer distance (d-spacing) and the type of anion originally present in the interlayer. These observations suggest that interlayer sorption could be important for the SeO₃²⁻ and HSe⁻ uptake by AFm phases.

In 2015, SeO₃²⁻ and HSe⁻ sorption isotherms were determined on AFm-OH-CO₃ and AFm-CO₃ (Fig. 5.5). Note that in the case of the experiments with HSe⁻, redox potentials measured in the supernatant solutions ($-560 \text{ mV} < E_h < -360 \text{ mV}$) confirmed that Se(-II) still was the dominant redox species in most experimental systems although in some cases, there was a minor contribution of polyselenide species to the aqueous Se speciation. This indicates that oxidation of Se(-II) was negligible in the course of the experiments.

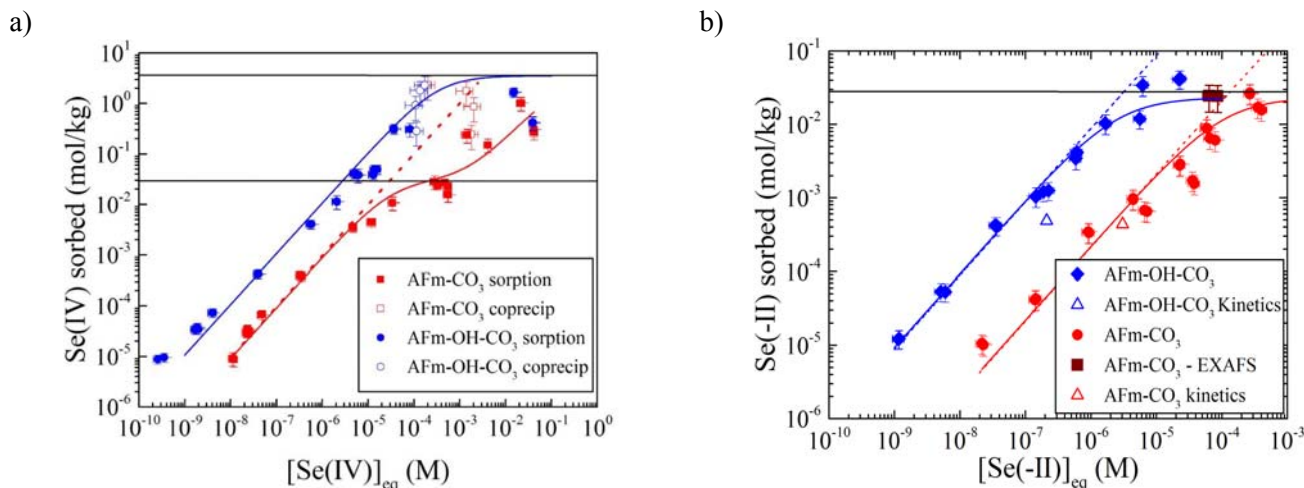


Fig. 5.5: SeO_3^{2-} (a) and HSe^- (b) sorption isotherms and co-precipitation data with AFm-CO₃ (pH = 11.6) and AFm-OH-CO₃ (pH = 12.2). Dotted lines: fit assuming linear sorption, (interlayer) site capacity = $3.52 \text{ mol}\cdot\text{kg}^{-1}$. Solid line: fit assuming non-linear sorption with 2 sites: surface site capacity, $S_1 = 2.9 \cdot 10^2 \text{ mol}\cdot\text{kg}^{-1}$, interlayer site capacity, $S_2 = 3.52 \text{ mol}\cdot\text{kg}^{-1}$.

The R_d values determined from both SeO_3^{2-} and HSe^- isotherms were found to be similar. The sorption isotherms clearly confirm the observations made earlier in kinetic tests that the uptake of both SeO_3^{2-} and HSe^- by AFm-OH-CO₃ is stronger than uptake by AFm-CO₃, thus further supporting the idea that the anion present in the AFm structure (and thus the interlayer distance) has a strong effect on the uptake.

For both Se redox states, the isotherms are linear up to a loading of $\sim 3 \cdot 10^2 \text{ mol}\cdot\text{kg}^{-1}$. Above this loading, a tendency towards a non-linear behaviour was observed in the case of the SeO_3^{2-} - AFm-CO₃ system, suggesting the presence of more than one type of sorption sites. This non-linear behaviour was not observed in the co-precipitation experiments (Fig. 5.5a). The difference between sorption and co-precipitation is tentatively explained as follows: In sorption experiments on AFm-CO₃, CO_3^{2-} prevents SeO_3^{2-} from being taken up into the interlayer as CO_3^{2-} is strongly bonded in the interlayer. In the co-precipitation experiments, however, there is no competition between CO_3^{2-} and SeO_3^{2-} because AFm-SeO₃ and AFm-CO₃ are precipitating simultaneously. This results in higher R_d values for SeO_3^{2-} . This finding indicates that SeO_3^{2-} can be taken up into the interlayer (thermodynamically) while the uptake is kinetically hindered during sorption. In the case of HSe^- , sorption and co-precipitation experiments with AFm-CO₃ are ongoing.

In the Se(IV)-AFm-OH-CO₃ system the difference between uptake by sorption and co-precipitation was not observed (Fig. 5.5a). This suggests that uptake of SeO_3^{2-} into the interlayer also occurs during sorption. The structural orientation of CO_3^{2-} in the interlayer of AFm-OH-CO₃ is different from that in AFm-CO₃,

which results in weaker bonding in the interlayer of AFm-OH-CO₃ and hence reduces competition with SeO_3^{2-} . The sorption behavior of HSe^- on AFm-OH-CO₃ is similar to that on AFm-CO₃ while co-precipitation is currently being studied.

X-ray absorption near edge (XANES) and extended X-ray absorption fine structure (EXAFS) spectra of AFm-CO₃ and AFm-OH-CO₃ samples loaded with SeO_3^{2-} or HSe^- , respectively, were recorded at the ROBL beamline at the ESRF (Grenoble, France). To avoid oxidation of Se, the samples were stored in a Dewar vessel filled with liquid N₂ during transport to the beamline and the X-ray absorption fine structure (XAFS) measurements were carried out at $\sim 15 \text{ K}$. XANES spectra of AFm-CO₃ and AFm-OH-CO₃ loaded with 1500 ppm HSe^- (Fig. 5.6a: MC1500 and HC1500) confirm that the dominant Se redox species sorbed is Se(-II).

XAFS spectra of HSe^- sorbed onto both AFm phases (Figs. 5.6b and c) were modelled assuming a local coordination of HSe^- similar to that of Cl^- in Friedel's salt (AFm-Cl₂). In the case of AFm-OH-CO₃ the Se-Ca and Se-Al coordination numbers are high as it is expected for HSe^- bound to both double hydroxide layers in the AFm interlayer environment (Table 5.3 and Fig. 5.7). Analysis of the XAFS spectra of HSe^- sorbed onto AFm-CO₃ (Fig. 5.6b and c), however, revealed slightly shorter distances for the shells as well as lower Ca and Al coordination numbers compared to HSe^- sorbed onto AFm-OH-CO₃ (Table 5.3). These trends suggest that a substantial portion of HSe^- is bound to sites on the outer surface of AFm-CO₃, forming a complex similar to that in the interlayer space of AFm-OH-CO₃, but with bonding solely to one double hydroxide layer.

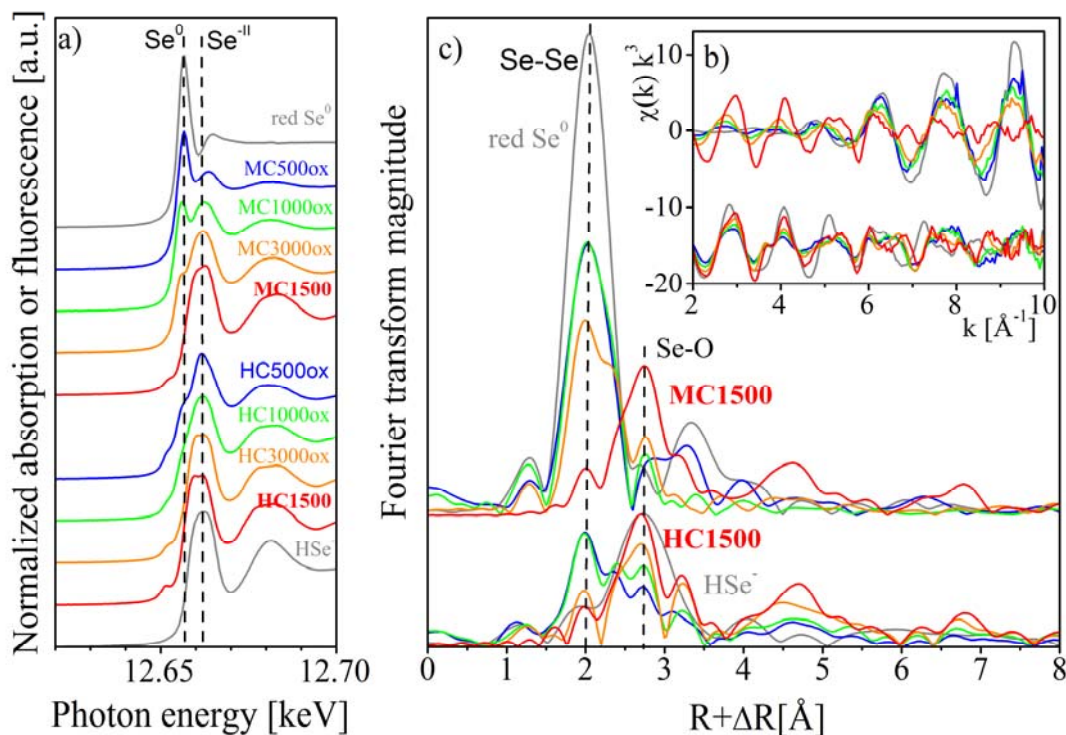


Fig. 5.6: Se K-edge XAFS data of the Se-loaded AFm- CO_3 (MC, red top) and AFm-OH- CO_3 (HC, red bottom) samples along with their respective oxidation series (orange \rightarrow green \rightarrow blue). XANES (a), radial structure function (c) and k^3 -weighted EXAFS spectra (b). The spectra of red Se^0 and of HSe^- are shown in grey.

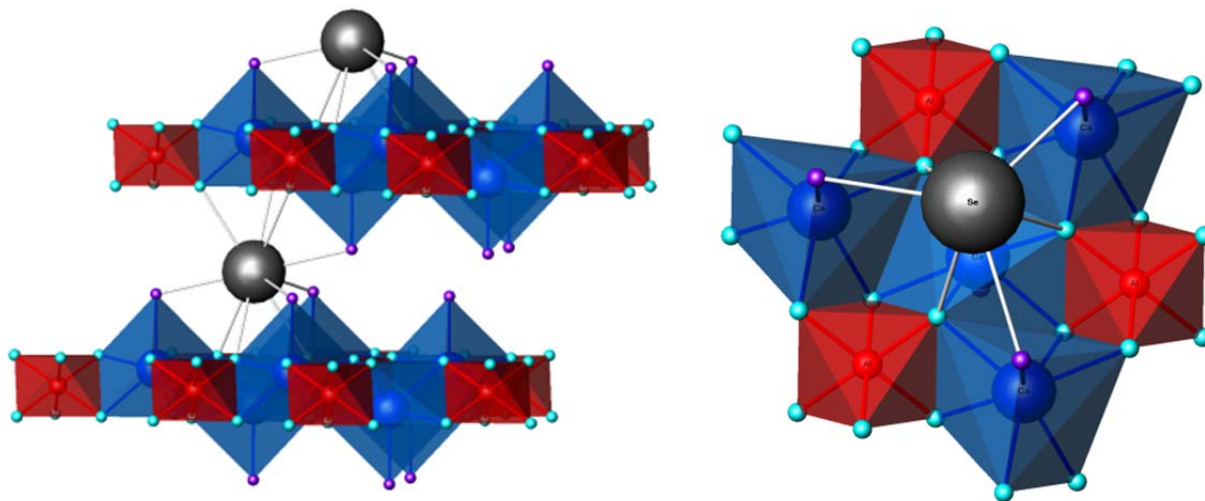


Fig. 5.7: Friedel's salt-based structural model of the EXAFS-derived positions of Se (gray spheres) in MC and HC (left: side view, right: top view). HSe^- attaches to the surface of Ca/Al double hydroxide layers through three OH-oxygen atoms (light blue spheres) and three H_2O -oxygen atoms (purple spheres), forming edge-sharing complexes with four $\text{Ca}(\text{OH})_7$ polyhedra (blue) and corner sharing complexes with 3 $\text{Al}(\text{OH})_6$ octahedra (red). In the interlayer space, this coordination geometry is doubled since HSe^- is able to bind to the two adjacent layers in the same way (center left).

Table 5.3: Se K-edge energies and EXAFS fit results of Se(-II) doped AFm samples and selected references. Crystallographic values of Friedel's salt as reference for HSe⁻ in HC1500 (ROUSSELOT et al. 2002), of Na₂Se·9H₂O as reference for the HSe⁻ aquo complex (BEDLIVY & PREISINGER 1965) and of red Se⁰ (CHERIN & UNGER 1972) are given between brackets.

Sample	E ₀ [eV]	First shell			Further shells			ΔE ₀ [eV]	χ ² _{res} [%]
		CN	R [Å]	σ ² [Å ²]	CN	R [Å]	σ ² [Å ²]		
HC1500	12650.3	6 ^f O	3.28 (3.41)	0.0047	2.0 Ca (2)	4.41 (4.51)	0.0121	4.1	19.0
		6 ^f O	3.49 (3.45)	0.0062	6.8 ^c Ca (6)	4.65 (4.70)	0.0150		
					6.8 ^c Al (6)	5.27 (5.13)	0.0070		
MC1500	12650.4	6 ^f O	3.25	0.0052	0.6 Ca	4.38	0.0120	3.5	18.1
		6 ^f O	3.43	0.0065	4.8 ^c Ca	4.60	0.0128		
					4.8 ^c Al	5.21	0.0059		
HSe ⁻ (aq)	12650.5	12.4 O (12)	3.36 (3.31-3.56)	0.0106				3.1	11.7
red Se ⁰	12655.6	2 Se	2.36 (2.33)	0.0026	4.9 Se (5)	3.73 (3.66-3.82)	0.0076	13.5	17.7
					4.1 Se (4)	3.92 (3.83-3.99)	0.0100		

CN: coordination number with error ± 25 %, R: Radial distance with error ± 0.01 Å, σ²: Debye-Waller factor with error ± 0.0005 Å², ΔE₀: inner potential correction, χ²_{res}: relative residual in percent, f: values fixed during fit, c: values correlated during fit.

Further support for the proposed HSe⁻ sorption mechanisms onto AFm-CO₃ and AFm-OH-CO₃ results from XANES measurements on HSe⁻ sorption samples in which HSe⁻ sorbed on both AFm phases was exposed to small quantities of O₂ (Fig. 5.6a: MC500ox, MC1000ox, MC3000ox, HC500ox, HC1000ox, HC3000ox). The spectra of HSe⁻ sorbed onto AFm-CO₃ show that substantial amounts of sorbed HSe⁻ are oxidized to Se(0) after exposure to O₂, while oxidation after exposure to O₂ is almost negligible in the case of HSe⁻ sorbed onto AFm-OH-CO₃. These observations support the idea that HSe⁻ is sorbed in the interlayer of AFm-OH-CO₃ while HSe⁻ sorption on AFm-CO₃ occurs at surface sites. HSe⁻ sorbed in the interlayer of AFm phases is expected to be much better protected against oxidation.

5.5 References

BAUR I., KELLER, P., MAVROCORDATOS D., WEHRLI B., JOHNSON C.A. (2004)
Dissolution-precipitation behaviour of ettringite, monosulfate, and calcium silicate hydrate. Cement Concr. Res. 34, 341-348.

BEDLIVY D., PREISINGER A. (1965)
Die Struktur von Na₂S·9H₂O und Na₂Se·9H₂O. Z. Kristallogr. 121, 114-130.

CHERIN P., UNGER P. (1972)
Refinement of the crystal structure of alpha-monoclinic Se. Acta Crystallogr., B 28, 313-317.

HUMMEL W., BERNER U.R., CURTI E., PEARSON F.J., THOENEN T. (2002)
Nagra-PSI chemical thermodynamic database, version 01/01. Nagra Technical Report NTB 02-16. Nagra, Wettingen, Switzerland, and Universal Publishers / uPublish.com, Parkland, Florida, USA.

NAGRA (2002)
Project Opalinus Clay: Safety report. Demonstration of disposal feasibility for spent fuel, vitrified high-level waste and long-lived intermediate-level waste (Entsorgungsnachweis). Nagra Technical Report NTB 02-05. Nagra, Wettingen, Switzerland.

NAGRA (2014)
Modellhaftes Inventar für radioaktive Materialien MIRAM 14. Nagra Technical Report NTB 14-04. Nagra, Wettingen, Switzerland.

OLIN Å., NOLÅNG B., OSADCHII E.G., ÖHMAN L.-O., ROSÉN E. (2005)
Chemical thermodynamics of Selenium. Elsevier, Amsterdam.

ROUSSELOT I., TAVIOT-GUEHO C., LEROUX F., LEONE P., PALVADEAU P., BESSE J.P. (2002)

Insights on the structural chemistry of hydrocalumite and hydrotalcite-like materials: Investigation of the series $\text{Ca}_2\text{M}^{3+}(\text{OH})_6\text{Cl}\cdot 2\text{H}_2\text{O}$ (M^{3+} : Al^{3+} , Ga^{3+} , Fe^{3+} , and Sc^{3+}) by X-ray powder diffraction. *J. Solid State Chem.* 167, 137-144.

SCHUMANN D., STOWASSER T., VOLMERT B., GÜNTHER-LEOPOLD I., LINDER H.-P., WIELAND E. (2014)

Determination of the ^{14}C content in activated steel components from a neutron spallation source and a nuclear power plant. *Anal. Chem.* 86, 5448-5454.

WIELAND E., HUMMEL W. (2015)

Formation and stability of carbon-14 containing organic compounds in alkaline iron-water-systems: Preliminary assessment based on a literature survey and thermodynamic modelling. *Mineral. Mag.* 79, 1275-1286.

WIELAND E., CVETKOVIĆ B.Z. (2015)

Development of a compound-specific C-14 AMS technique for the detection of C-14 labelled organic compounds. EU Project "CAST" report D 2.3 (submitted).

WIELAND E., KOSAKOWSKI G., BERNER U. (2015a)

Preliminary assessment of the temporal evolution of waste packages in the near field of an L/ILW repository. Nagra Working Report NAB (in prep.).

WIELAND E., JAKOB A., TITS J., LOTHENBACH B., KUNZ D. (2015b)

Sorption and diffusion studies with low molecular weight organic compounds in cementitious systems. *Appl. Geochem.* (submitted).

6 COLLOID CHEMISTRY

C. Degueldre, S. Frick

6.1 Overview

The goal of the colloid sub-program is to study the role of colloids in the migration of radionuclides in the geosphere. Colloid properties such as their concentration, size distribution and nature dictate their behavior in subsurface ground water. The main activities over the past years were within the framework of the Grimsel colloid project: "Colloid Formation and Migration" (CFM) and were focused on measuring colloid size distributions in batch and in quasi-stagnant conditions using single particle counting (SPC). This year, the samples from long-term in-situ test (LIT) were successfully analyzed at PSI and the project was completed. The knowledge and understanding gained over the last decade allows well founded estimates for colloid assisted migration of radionuclides in the argillaceous rock to be made.

6.2 Activities in the CFM project

The CFM project is conducted at the Grimsel Test Site (GTS), Switzerland in the framework of Phase VI of the research program, which runs from 2004 to originally 2013 and was extended up to 2016. The program is dedicated to repository-relevant (i.e. large-scale, long-term) in-situ experiments. After installation of the clay source, see Fig. 6.1, nine samples were taken from August 12 to September 9, 2014.

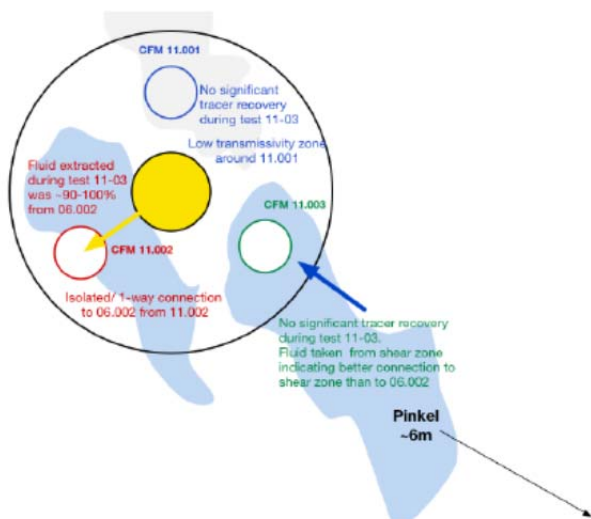


Fig. 6.1: Shema of the CFM system as suggested from tracer tests during LIT.

The collected samples were kept below 15 °C, under anaerobic conditions. The samples were analysed at PSI in spring 2015.

The results may be discussed as follows. At the GTS, the deep Na-Ca-HCO₃F groundwater has been collected at depth of 450 m below surface since 1988 (DEGUELDRE et al. 1989). The water chemistry has been found constant over the last 30 years (DEGUELDRE & BENEDICTO 2012).

After installation of the CFM clay source, the concentration of AGA tracer decreased significantly after 5 days. The turbidity decreased as expected for large colloids after a transient (see DEGUELDRE & BENEDICTO 2012). The conductivity increased from 75 to 150 during the early phase then reached a plateau and seems to recover very slowly. This corresponds to an increase of salt concentration in the ground water due to the dissolution of the clay pore water in the Grimsel ground water. The pH and Eh has been rather constant. The value of pH did not decrease below 9.0. The normalized concentration $\delta N_i \cdot \delta d_i^{-1}$ was reported as $\delta N_i \cdot \delta d_i^{-1} = 1013.32 \text{ d}^{-4.17}$ where N_i is given in ml^{-1} and d_i in nm (DEGUELDRE et al. 1990). This corresponds to a normalized concentration of $\sim 105 \text{ ml}^{-1} \text{ nm}^{-1}$ for 100 nm size and $\sim 1 \text{ ml}^{-1} \text{ nm}^{-1}$ for 1000 nm. These values are similar to that recorded for the LIT ground water samples (see Fig. 6.2).

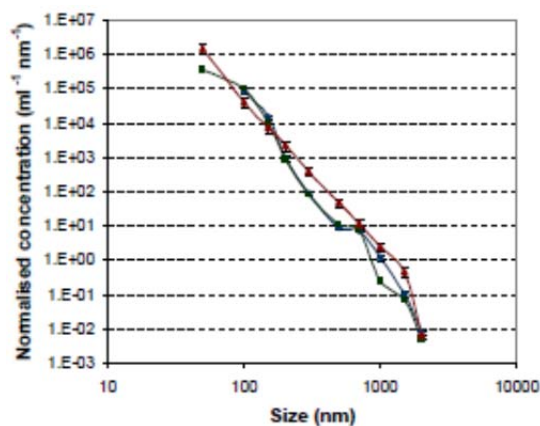


Fig. 6.2: Comparison of the Grimsel colloid size distributions recorded in DEGUELDRE & BENEDICTO (2012) study (◆, ■) as well as in earlier studies (DEGUELDRE et al. 1989) (▲).

Actually, the colloid concentration could have been somewhat slightly lower than in Grimsel ground water if a higher salinity (conductivity) and slightly lower pH would have been still observed (see Fig. 2 for early LIT period). However the LIT water chemistry and colloid concentrations should today (sampling date) be similar to that observed in the Grimsel ground water. This behavior could be estimated using the PSI colloid generation model for a clay source in contact with a given ground water and for a given batch design. This last test completes the participation of LES/NES/PSI in the CFM project at the GTS.

6.3 References

- DEGUELDRE C., BENEDICTO A. (2012)
Colloid generation during water flow transients.
Appl. Geochem. 27, 1220-1225.
- DEGUELDRE C., LONGWORTH G., MOULIN V., VILKS P. (1990)
Grimsel Test Site - Grimsel Colloid Exercise: An international intercomparison exercise on the sampling and characterisation of groundwater colloids. Nagra Technical Report NTB 90-01, Nagra, Wettingen, Switzerland.

7 DIFFUSION PROCESSES

L.R. Van Loon, M.A. Glaus, S. Frick, P. Bunic, Y. Chen (PhD student), C. Wigger (PhD student), E. Fetz (PhD student), Y. Fukatsu (visiting PhD student)

7.1 Overview

The "Diffusion Processes" group performs experimental and theoretical studies aiming at improving the understanding of diffusive transport of cations, anions and neutral species in compacted clay materials in order to better evaluate the long term migration behaviour of radionuclides in argillaceous host rocks and technical barrier systems (bentonite). To this end, different projects are currently ongoing:

- The TRAPHICCS project deals with diffusion in single phase clay minerals with different physico-chemical properties and focuses on strongly sorbing radionuclides. The main emphasis is on the surface diffusion processes of transition metals and lanthanides/actinides.
- Two PhD projects on reactive transport are ongoing in close co-operation with the Transport Mechanisms Group. A guest scientist from the Tokyo Institute of Technology studies precipitation reactions in illite and their effect on diffusive transport.
- A PhD project related to the migration behaviour of small organic molecules in compacted clay systems (ROLOC) is ongoing. The aim is to study whether ^{14}C -containing organic molecules are retarded in clays and to find a relationship between the sorption behaviour and the chemical structure of the molecules.
- A PhD project concerning the anion accessible porosity in clay rocks (ANPOR) was continued. This project aims at a better understanding of anion exclusion effects in clay rocks. To this end, clay rocks with different mineral compositions and physicochemical properties are used.
- A PhD project on properties of confined water was started in cooperation with ETHZ. By targeted modification of the interlayer space of montmorillonite and its effect on the diffusion of water, anions and cations, information on the type of water will be gained.

7.2 Transport phenomena in compacted clay systems (TRAPHICCS)

The activities of the Catclay project were continued within the scope of the Traphiccs project with the aims of (i) testing the internal consistency of sorption data and diffusion data for illite and (ii) testing the blind prediction capacities of the "EDL diffusion

model" recently published (GLAUS et al. 2015) using Eu(III) as a test cation (EDL: electrical double layer).

In-diffusion of $^{65}\text{Zn}^{2+}$ tracer in compacted illite preparations with substantial fractional loadings of stable Zn was measured at pH 5 and various concentrations of NaClO_4 as the background electrolyte. Under such conditions the majority of surface bound $^{65}\text{Zn}^{2+}$ was present in the EDL, or on the planar cation exchange sites – in a non-electrostatic view. The measured effective diffusion coefficient (D_e , $\text{m}^2 \text{s}^{-1}$) values under such conditions ranged from $10^{-10} \text{m}^2 \text{s}^{-1}$ to $10^{-8} \text{m}^2 \text{s}^{-1}$ and exhibited the characteristic correlation with R_d values that is frequently observed for the diffusion of metal cations of the alkaline and earth-alkaline series in compacted illite and montmorillonite (GLAUS et al. 2010). This was not the case in the experiments carried out at very low fractional loadings of the illite with stable Zn^{2+} . Under such conditions the majority of $^{65}\text{Zn}^{2+}$ is bound to the specific surface complexation sites ("weak or strong" binding sites). These surface species are assumed to exhibit no surface mobility and consequently do not contribute to the overall diffusive fluxes (GLAUS et al. 2015). In such cases almost no correlation was observed between D_e and R_d values.

The experiments at high fractional Zn loadings demonstrate that the diffusive behaviour of a transition metal cation can readily be "mutated" to the typical surface diffusion behaviour of cation exchange species, if it has been displaced from the specific sorption sites to non-specific planar binding sites. The results further corroborate our general conception of surface diffusion: Chemically different surface species may exhibit different surface mobilities and the assessment of cation diffusion in compacted swelling clays cannot be understood without a thorough knowledge of the chemical type of these interactions on the surface. An increased reconciling of the diffusion experiments with the investigations of sorption is therefore envisaged in the future.

A large experimental effort was dedicated to in-diffusion experiments in compacted illite with Eu(III). Fig. 7.1 shows the diffusion profile measured at pH 5 and 0.1 M NaClO_4 background electrolyte concentration after an in-diffusion time of ~30 d. At this low pH conditions cation exchange and adsorption on external basal plane of minerals are expected to be the dominant sorption mechanisms. According to the EDL diffusion model for strongly sorbing cationic species

(GLAUS et al. 2015), the effective diffusion coefficient (D_e) can be described as follows:

$$D_e = \frac{\varepsilon}{G} D_w \left(f_{free} + f_{EDL} \frac{c_{EDL}}{c} q_\eta \right) \quad (7.1)$$

where f_{free} and f_{EDL} are the volume fractions of aqueous phase water and water in the EDL in the clay porosity, c and c_D are the respective cation concentrations (mol m^{-3}) in these phases, ε is the total porosity, G the geometric factor estimated independently by HTO diffusion experiments, D_w ($\text{m}^2 \text{s}^{-1}$) the cation diffusion coefficient in bulk water and q_η a viscosity factor determining the cation mobility on the surface. Note that both the volume fractions and the ratio of cation concentrations in the diffuse layer and the aqueous phase depend characteristically on the background electrolyte concentration in the contacting solution. The EDL diffusion model was calibrated for Sr^{2+} , Co^{2+} and Zn^{2+} by adjusting q_η and assuming the thickness of the EDL being related to the 2-fold Debye length. The green line in Fig. 7.1 is a blind prediction based on the EDL diffusion model and the '2SPNE SC/CE' sorption model for Eu(III) on illite (BRADBURY & BAEYENS, 2009). The good agreement between the model curve and the experimental data shows that the EDL diffusion model correctly captures the intrinsic features of cation distribution between the EDL and the aqueous phase for cations with different charges. It is clearly superior to the pore diffusion model (shown as a red curve), which is devoid of a surface diffusion component. The pore diffusion model underestimates the D_e value for Eu(III) under the experimental conditions by a factor of ~ 50 . The trend of the experimental data and the model curves underline the fact that the latter – common – approach for assessing the diffusive properties of a species, for which no specific parameter values are available, is not conservative and may underestimate the penetration depths of cationic species in compacted swelling clays depending on the chemical composition of the pore water solution.

7.3 Porosity changes in porous media

Due to dissolution-precipitation reactions occurring at interfaces with strong chemical gradients (e.g. cement-clay), porosity changes can result in changes in the transport properties of solutes and gases. In order to achieve a better understanding of dissolution-precipitation reactions and their effect on solute transport, two projects are ongoing, one on the interface between cement and montmorillonite, another on the effect of porosity changes on transport phenomena.

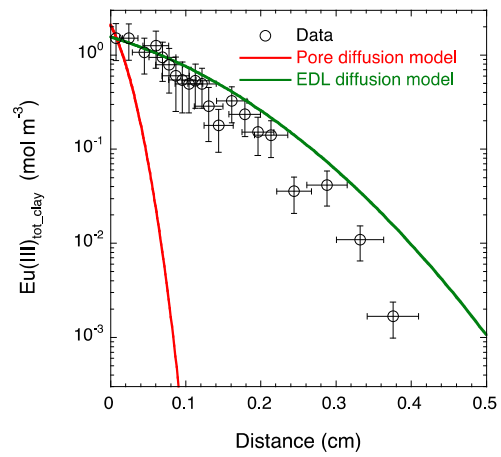


Fig. 7.1: Diffusion profile of Eu(III) in compacted illite measured at pH 5 and 0.1 M NaClO_4 as the background electrolyte. The two model curves show the conceptual difference between a model taking the mobility of double layer species (DL) into account (green) and the pore diffusion model (red) devoid of such a contribution. The EDL diffusion model is a blind prediction using model parameters of divalent cations (cf. the text).

The projects are a co-operation between the Transport Mechanisms Group, the Diffusion Processes Group and the University of Bern. More information on these projects is given in Chapter 3.

A visiting PhD student (Yuta Fukatsu) from the Tokyo Institute of Technology studied the effect of precipitation reactions on the diffusion of anions (^{36}Cl) and water (HTO) in compacted illite with the aim to better understand the diffusion pathways for charged and uncharged species in compacted clay systems. To this end an experiment described in the literature was repeated (CHAGNEAU et al., 2015): compacted illite (Illite du Puy, bulk dry density = 1700 kg m^{-3}) was contacted with 0.5 M SrCl_2 at one end and 0.5 M Na_2SO_4 at the other end. The solution containing SrCl_2 was labelled with HTO and ^{36}Cl and diffusion of both species was followed up as a function of time. After ca. 2 months, diffusion profiles of HTO, ^{36}Cl , Sr and SO_4 were determined.

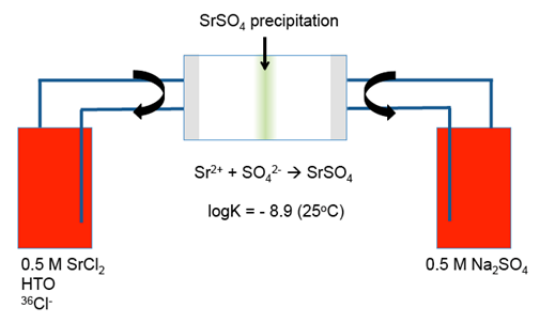


Fig. 7.2: Experimental setup for inducing precipitation reactions in compacted clay systems.

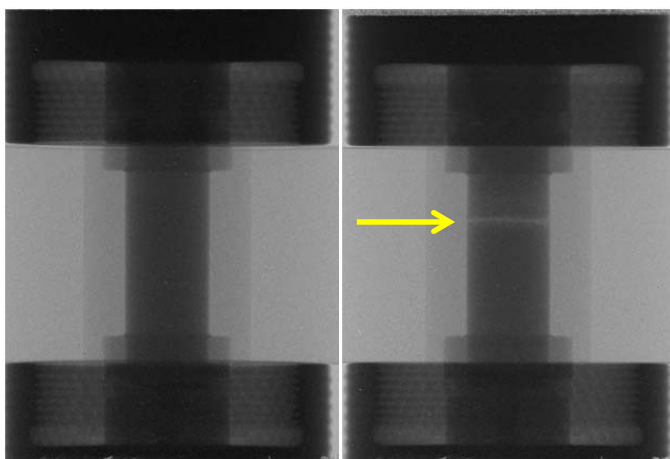


Fig. 7.3: Precipitation zone of SrSO_4 in illite (indicated by the arrow) as observed with neutron radiography (right). The left picture shows a reference system without SrSO_4 precipitation.

A clear decrease of the diffusive fluxes of HTO and $^{36}\text{Cl}^-$ could be observed. The diffusion of HTO is reduced significantly whereas the diffusion $^{36}\text{Cl}^-$ was completely hindered. Neutron radiography measurements clearly show a narrow (ca. 0.3 mm) precipitation zone with a reduced porosity and thus less water content. More details on the application of neutron radiography to porosity measurements can be found in Chapter 3.

7.4 Transport of small organic molecules in dense clay systems

Carbon-14 is an important contributor to the annual radioactive dose predicted in performance assessment of a low- and intermediate-level radioactive waste repository in Switzerland. ^{14}C is assumed to be mainly released to the biosphere as organic compounds, yielding from the anoxic corrosion of activated steel (NAGRA 2008). Current performance assessment studies are based on the assumption that the transport of organic compounds is unretarded. However, if a weak retardation can be robustly demonstrated, this would lead to a larger decay of ^{14}C within the barriers and to a significant reduction of its maximum dose at the surface. Possible interactions of the organic model compounds with clay are still poorly known, they are presumed rather weak. The main tasks of this project are: (i) to investigate the transport behaviour of organic model compounds with different structure in argillaceous media, and (ii) to derive the quantitative relationships (SCHWARZENBACH et al. 2006) between the sorption properties and structural elements of organic compounds.

The sorption behaviour of selected organic molecules in illite, kaolinite and Opalinus Clay was investigated using an infiltration technique. In the infiltration experiments, a constant advective flow through a

column of compacted clay sample was generated by pressurised helium. Focus in 2015 was on the behaviour of stereoisomers (D- and L-lactate enantiomers) in illite and on the transport behaviour of selected organic molecules in Opalinus Clay. Due to the very low flow rates in Opalinus Clay, infiltration experiments on this material are very time consuming, i.e. the experiments lasts for up to 20 weeks.

The resolution of the infiltration technique was improved by using a longer column. It could clearly be shown that D- and L-lactate have a different retention behaviour in illite (Fig. 7.4). From this behaviour it could be concluded that the hydroxy group in the α -position is involved in the sorption reaction. First results on Opalinus Clay also indicate a clear retention of α -hydroxycarboxylic acids.

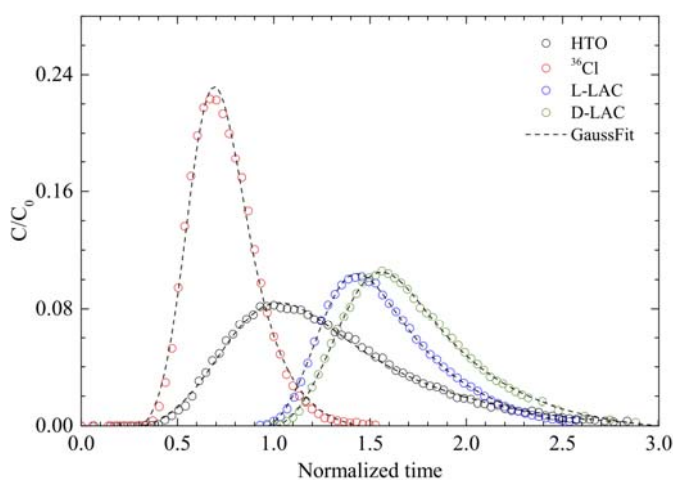


Fig. 7.4: Breakthrough curves for D- and L-lactate in compacted illite.

7.5 Anion exclusion phenomena in low porosity clay rocks (ANPOR)

Argillaceous rocks consist to a large part of clay particles composed by TOT-layers. They are negatively charged and these negative charges are compensated by cations in the pore solution such that a diffuse double layer forms. Anions are repulsed by the negative charges of the clay minerals and are excluded from the diffuse double layer. The latter process is well known as anion exclusion and has been observed in soils, clay rocks and compacted bentonite. For neutral and positively charged chemical species, the whole porosity of a clay rock (ϵ_{tot}) is available for transport. Anions, however, are partially excluded and the corresponding transport porosity, i.e. the anion accessible porosity (ϵ_{an}), is smaller than the total porosity. Earlier studies on compacted bentonite showed that both the mechanical compaction of bentonite and the composition of the pore water had an effect on the diffusion accessible porosity of anions (VAN LOON et al. 2007). Compaction of bentonite

resulted in a decreased anion accessible porosity. Increasing ionic strength of the pore water led to an increase in the anion accessible porosity. A similar dependence was expected for clay rocks such as Opalinus Clay, due to a similar structure. Recent measurements, however, did not confirm this (VAN LOON 2014). Anion exclusion can thus be explained qualitatively but not quantitatively in the case of clay rocks. A project aiming at shedding more light on anion exclusion/diffusion in clay rocks is currently ongoing. The effect of the ionic composition ($0.01\text{M} < C_{\text{NaCl}} < 5\text{M}$) of the pore water on the diffusion of $^{36}\text{Cl}^-$ in Opalinus Clay and Helvetic Marl was studied.

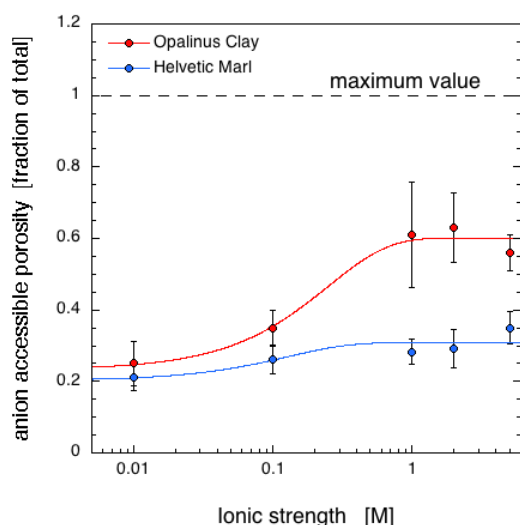


Fig. 7.5: Anion accessible porosity in Opalinus Clay (OPA Schlattingen borehole) and Helvetic Marl as a function of the ionic strength of the pore solution. The accessible porosity is given as a fraction of the total porosity as measured with tritiated water (HTO).

It could be shown that the anion diffusion behaviour in the two rocks is significantly different.

In the case of Opalinus Clay, 60 % of total porosity became accessible to anions at an ionic strength larger than 1 M, whereas in the case of Helvetic Marl only 35 % is accessible. This can qualitatively be explained by the higher fraction of charged clay minerals in Helvetic Marl. This results in a larger anion exclusion effect.

Identical experiments with CaCl_2 and CsCl instead of NaCl are currently ongoing. Also two Canadian samples (Blue Mountain and Queenston) are being prepared for starting similar diffusion experiments.

7.6 Water properties in confinement

Water confined in narrow pore spaces is known to have properties different from that of bulk water. Despite of that, it is common practice in geochemistry to treat confined water as bulk water. As an example, speciation calculations for radionuclides dissolved in clay pore water are performed assuming that thermodynamic properties in the confined water are the same as in bulk water.

Studying the properties of confined water is very challenging. A direct observation is in most cases not possible and therefore indirect measurements to become insight in the properties of confined water are necessary. It is known that differently charged species have different mobility in differently confined media. Diffusion thus can be used to probe the different types of water confinement in clay. Moreover, targeted modification of clay minerals might help to explore the water properties in clay. A joint PSI-ETHZ PhD project was recently submitted to SNF. The aim of the study is to use differently modified montmorillonites and to study the effect of modification on the diffusion behaviour of water, cations and anions. The modification of the interlayer pores can be done by enlargement and blocking of the interlayer pores (Fig. 7.6). Enlargement can be achieved by pillaring (SCHOONHEYDT et al. 1999). Here the pillaring agents prop apart the interlayer pore space. With the enlarged interlayer even anions are potentially able to diffuse through the interlayer. The blocking of the interlayer can be achieved with an agent that strongly adsorbs in the interlayer leaving no space for other molecules or by collapsing the interlayer by alternate wetting and drying of K^+ -montmorillonite (MAES et al. 1985). With blocking, even water might be forced to diffuse through the interparticle pore spaces only. By modifying the interlayer pores the role of the different pores can be explored. Also the water present in the different pore spaces can be analysed and a possible interplay of the water present and the types of pores can be illuminated.

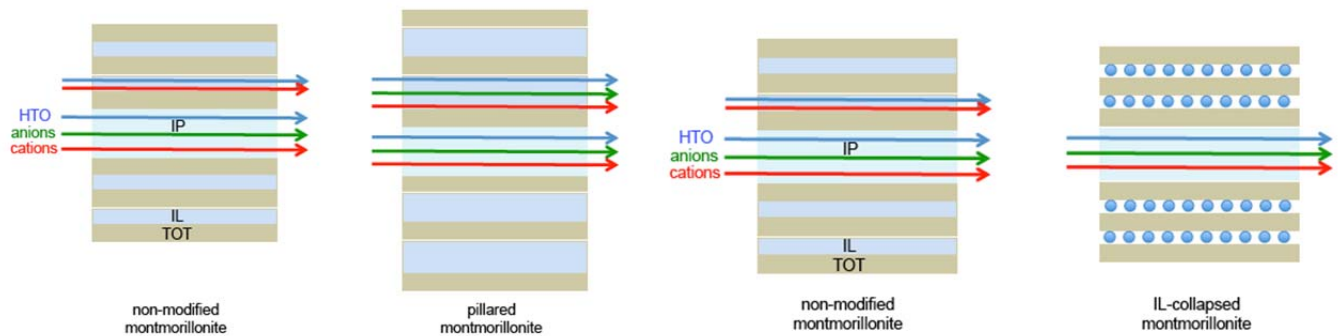


Fig. 7.6: Effect of pillaring (left) and collapsing (right) on the diffusion of HTO, anions and cations in montmorillonite (IP: interparticle pore space; IL: interlayer pore space; TOT: Si-tetrahedral Al-octahedral Si-tetrahedral layer).

7.7 References

- BRADBURY M.H., BAEYENS B. (2009)
Sorption modelling on illite Part I: Titration measurements and the sorption of Ni, Co, Eu and Sn. *Geochim. Cosmochim. Acta* 73, 990–1003.
- CHAGNEAU A., TOURNASSAT C., STEEFEL C., BOURG I.C., GABOREAU S., ESTEVE I., KUPCIK T., CLARET F., SCHÄFER T. (2015).
Complete restriction of $^{36}\text{Cl}^-$ diffusion by celestite precipitation in densely compacted illite. *Environ. Sci. Technol.* 2, 139-143.
- GLAUS M.A., FRICK S., ROSSÉ R., VAN LOON L.R. (2010)
Comparative study of tracer diffusion of HTO, $^{22}\text{Na}^+$ and $^{36}\text{Cl}^-$ in compacted kaolinite, illite and montmorillonite. *Geochim. Cosmochim. Acta* 74, 1999-2010.
- GLAUS M.A., AERTSENS M., APPELO C.A.J., KUPCIK T., MAES N., VAN LAER L., VAN LOON L.R. (2015)
Enhanced mass transfer rates for Sr^{2+} , Co^{2+} and Zn^{2+} in compacted illite caused by cation diffusion in the electrical double layer. *Radiochim. Acta* 102, 723-730.
- MAES A., VERHEYDEN D., CREMERS A. (1985)
Formation of highly selective cesium-exchange sites in montmorillonites. *Clays Clay Miner.* 33, 251-257.
- NAGRA (2008)
Begründung der Abfallzuteilung, der Barrierensysteme und der Anforderungen an die Geologie: Bericht zur Sicherheit und Machbarkeit. Nagra Technischer Bericht. NTB 08-05. Nagra, Wettingen.
- SCHOONHEYDT R.A., PINNAVAIA T., LAGALY, G., GANGAS N. (1999)
Pillared clays and pillared layered solids. *Pure Appl. Chem.* 71, 2367-2371.
- SCHWARZENBACH R.P., ESCHER B.I., FENNER K., HOFSTETTER T.B., JOHNSON C.A., VON GUNTEN U., WEHRLI B. (2006)
The challenge of micropollutants in aquatic systems. *Science* 313, 1072-1077.
- VAN LOON L.R., GLAUS M.A., MÜLLER W. (2007)
Anion exclusion effects in compacted bentonites: Towards a better understanding of anion diffusion. *Appl. Geochem.* 22, 2536-2552.
- VAN LOON L.R. (2014)
Effective diffusion coefficients and porosity values for argillaceous rocks and bentonite: measured and estimated values for the provisional safety analyses for SGT-E2. Nagra Technical Report NTB 12-03, Nagra, Wettingen, Switzerland.

8 PUBLICATIONS

8.1 Peer reviewed journals

Brandt F.¹, Curti E., Klinkenberg M.¹, Rozov K.¹, Bosbach D.¹ (2015)

Replacement of barite by a (Ba,Ra)SO₄ solid solution at close-to-equilibrium conditions: A combined experimental and theoretical study. *Geochim. Cosmochim. Acta* 155, 1-15.

¹ Research Centre Jülich, Jülich, Germany

Breitner D.¹, Osán J.¹, Fábíán M.¹, Zagyvai P.¹, Szabó C.², Dähn R., Marques Fernandes M., Sajó I.E.¹, Máthé Z.¹, Török S.¹ (2015)

Characteristics of uranium uptake of Boda Claystone Formation as the candidate host rock of high level radioactive waste repository in Hungary. *Env. Earth Sci.* 73, 209-219.

¹ Hungarian Academy of Sciences, Budapest, Hungary

² University Pázmány, Budapest, Hungary

Curti E., Puranen A.¹, Grolimund D., Jädernas D.², Sheptyakov D., Mesbah A.² (2015)

Characterization of selenium in UO₂ spent nuclear fuel by micro X-ray absorption spectroscopy and its thermodynamic stability. *Env. Sci-Processes & Impacts* 17, 1760-1768.

¹ Studsvik Nuclear AB, Nyköping, Sweden

² Northwestern University, Evanston, USA

³ CEA, Bagnols-sur-Cèze, France

Faux D.A.¹, Cachia S.-H.P.¹, McDonald P.J.¹, Bhatt J.S.¹, Howlett N.C.¹, Churakov S.V. (2015)

Model for the interpretation of nuclear magnetic resonance relaxometry of hydrated porous silicate materials. *Phys. Rev. E* 91, 032311.

¹ University of Surrey, Guildford, United Kingdom

Glaus M.A., Aertsens M.¹, Appelo C.A.J.², Kupcik T.³, Maes N.¹, Van Laer L.¹, Van Loon L.R. (2015)

Cation diffusion in the electrical double layer enhances the mass transfer rates for Sr²⁺, Co²⁺ and Zn²⁺ in compacted illite. *Geochim. Cosmochim. Acta* 165, 376-388.

¹ SCK-CEN, Mol, Belgium

² Hydrochemical Consultant, Amsterdam, The Netherlands

³ KIT-INE, Karlsruhe, Germany

Glaus M.A., Aertsens M.¹, Maes N.¹, Van Laer L.¹, Van Loon L.R. (2015)

Treatment of boundary conditions in through-diffusion: A case study of ⁸⁵Sr²⁺ diffusion in compacted illite. *J. Contam. Hydrol.* 177, 239-248.

¹ SCK-CEN, Mol, Belgium

Lützenkirchen J.¹, Marsac R.¹, Kulik D.A., Payne T.E.², Xue Z.³, Orsetti S.³, Haderlein S.B.³ (2015)

Treatment of multi-dentate surface complexes and diffuse layer implementation in various speciation codes. *Appl. Geochem.* 55, 128-137.

¹ KIT-INE, Karlsruhe, Germany

² Nuclear Science and Technology Organisation, Kirrawee DC, Australia

³ Universität Tübingen, Tübingen, Germany

Marques Fernandes M., Ver N.¹, Baeyens B. (2015)

Predicting the uptake of Cs, Co, Ni, Eu, Th and U on argillaceous rocks using sorption models for illite. *Appl. Geochem.* 59, 189-199.

¹ Hungarian Academy of Sciences, Budapest, Hungary

Meier D.B.¹, Waber H.N.¹, Gimmi T., Eichinger F.², Diamond L.W.² (2015)

Reconstruction of in-situ porosity and porewater compositions of low-permeability crystalline rocks: Magnitude of artefacts induced by drilling and sample recovery. *J. Contam. Hydrol.* 183, 55-71.

¹ University of Bern, Bern, Switzerland

² Hydroisotop GmbH, Schweitenkirchen, Germany

Miron G.D.¹, Kulik D.A., Dmytrieva S.V.², Wagner T.³ (2015)

GEMSFITS: Code package for optimization of geochemical model parameters and inverse modeling. *Appl. Geochem.* 55, 28-45.

¹ ETH Zürich, Zürich, Switzerland

² Institute of Environmental Geochemistry, Palladina, Kyiv, Ukraine

³ University of Helsinki, Helsinki, Finland

Perko J.¹, Mayer K.U.², Kosakowski G., De Windt L.³, Govaerts J.¹, Jacques D.¹, Meeussen J.C.L.⁴, Su D.² (2015)

Decalcification of cracked cement structures. *Comp. Geosci.* 19, 673-693.

¹ SCK-CEN, Mol, Belgium

² University of British Columbia, Vancouver, BC, Canada

³ MINES ParisTech, Fontainebleau, France

⁴ Nuclear Research and Consultancy Group, Petten, The Netherlands

Poonosamy J., Kosakowski G., Van Loon L.R., Mäder U.K.¹ (2015)

Dissolution-precipitation processes in tank experiments for testing numerical models for reactive transport calculations: Experiments and Modelling. *J. Contam. Hydrol.* 177-178, 1-17.

¹ University of Bern, Bern, Switzerland

Shafizadeh A., Gimmi T., Van Loon L.R., Kaestner A., Lehmann E., Mäder U.K.¹, Churakov S.V. (2015)

Quantification of water content across a cement-clay interface using high resolution neutron radiography. *Phys. Procedia* 69, 516-523.

¹ University of Bern, Bern, Switzerland

Thien B.M.J., Kosakowski G., Kulik D.A. (2015) Differential alteration of basaltic lava flows and hyaloclastites in Icelandic hydrothermal systems. *Geothermal Energy* 3:11.

Tits J., Walther C.¹, Stumpf T.¹, Macé N., Wieland E. (2015)

A luminescence line-narrowing spectroscopic study of the uranium(VI) interaction with cementitious materials and titanium dioxide. *Dalton Trans.* 44, 966–976.

¹ KIT-INE, Karlsruhe, Germany

Van Loon L.R., Mibus J.¹ (2015)

A modified version of Archie's law to estimate effective diffusion coefficients of radionuclides in argillaceous rocks and its application in safety analyses. *Appl. Geochem.* 59, 85-94.

¹ Nagra, Wettingen, Switzerland

Vespa M.¹, Wieland E., Dähn R., Lothenbach B.², (2015)

Identification of the thermo-dynamically stable Fe-containing phase in aged cement pastes. *J. Am. Ceram. Society* 98, 2286-2294.

¹ KIT-INE, Karlsruhe, Germany

² EMPA, Dübendorf, Switzerland

Wieland E., Hummel W. (2015)

Formation and stability of carbon-14 containing organic compounds in alkaline iron-water-systems: Preliminary assessment based on a literature survey and thermodynamic modelling. *Mineral. Mag.* 79, 1275-1286.

8.2 Conferences/workshops/presentations

Baeyens B., Marques Fernandes M., Bradbury M.H. Sorption values derived for argillaceous rocks in sorption data bases for safety analysis compared with measured values. 6th International Conference on "Clays in Natural and Engineered Barriers for Radioactive Waste Confinement", Brussels, Belgium, March 23-26, 2015.

Berner U.

Setting up a thermodynamic solid solution model for illites. 6th International Conference on "Clays in Natural and Engineered Barriers for Radioactive Waste Confinement", Brussels, Belgium, March 23-26, 2015.

Chen Y., Glaus M.A., Jakob A., Van Loon L.R., Mäder U.K.

Retardation of low-molecular weight organic compounds in clays. 6th International Conference on "Clays in Natural and Engineered Barriers for Radioactive Waste Confinement", Brussels, Belgium, March 23-26, 2015.

Chen Y., Glaus M.A., Van Loon L.R., Mäder U.K. Migration of small organic molecules in dense clay systems. Goldschmidt 2015, Prague, Czech Republic, August 16-21, 2015.

Churakov S.V., Gimmi T., Van Loon L.R., Juranyi F. Nature of water diffusion in montmorillonite at different scales: Combination of experimental and modelling approaches. 6th International Conference on "Clays in Natural and Engineered Barriers for Radioactive Waste Confinement", Brussels, Belgium, March 23-26, 2015.

Curti E., Puranen A., Jädnäs D., Froideval-Zumbiehl A., Grolimund D.

X-ray spectroscopy of selenium in high-burnup UO₂ spent nuclear fuel. 16th International Conference on "X-ray Absorption Fine Structure (XAFS 16)", Karlsruhe, Germany, August 23-28, 2015.

Cvetković B.Z., Kunz D., Wieland E.

Development of a ¹⁴C AMS based compound-specific analytical technique for aqueous species. Analytical Workshop of the EU FP7 Project "CAST" (Carbon Source Term), Villigen PSI, Switzerland, May 29, 2015.

Cvetković B.Z., Wieland E., Kunz D., Salazar G., Szidat, S.

Development of analytical techniques for the identification of organic carbon-14 species released during anoxic corrosion of activated steel in a cementitious repository for radioactive waste. Migration 2015, Santa Fe, USA, September 13-18, 2015.

Dähn R.

XAS and XRD investigations of argillaceous rock formations and cement-clay interfaces relevant to the Swiss radioactive waste disposal program. "SNBL – Planning for the next decade" Swiss-Norwegian Workshop, Grenoble, France, May 28-29, 2015.

Dähn R., Osan J., Marques Fernandes M., Baeyens B., Torok S.

X-ray microspectroscopic investigations of heavy metal uptake by argillaceous rocks. 16th International Conference on "X-ray Absorption Fine Structure (XAFS 16)", Karlsruhe, Germany, August 23-28, 2015.

Dähn R., Osan J., Pattison P., Wieland E. The challenge of analyzing micro-diffraction patterns: From argillaceous rock formations to cement-clay interfaces. 6th International Conference on "Clays in Natural and Engineered Barriers for Radioactive Waste Confinement", Brussels, Belgium, March 23-26, 2015.

Gimmi T., Leupin O.X., Soler J.M., Van Loon L.R., Eikenberg J., Glaus M.A., Waber H.N., Pfingsten W., Xie M., Mayer K.U., Appelo C.A.J., Steefel C.I. Perturbing a field diffusion experiment: The DR-A test at the Mont Terri Underground Rock Laboratory (Switzerland). 6th International Conference on "Clays in Natural and Engineered Barriers for Radioactive Waste Confinement", Brussels, Belgium, March 23-26, 2015.

Glaus M.A., Aertsens M., Appelo C.A.J., Kupcik T., Maes N., Van Laer L., Van Loon L.R.

Surface diffusion effects for transition metals in compacted illite. 6th International Conference on "Clays in Natural and Engineered Barriers for Radioactive Waste Confinement", Brussels, Belgium, March 23-26, 2015.

Glaus M.A., Baeyens B., Marques Fernandes M., Van Loon L.R.

The importance of cation exchange species for the diffusive behaviour of moderately and strongly sorbing radioelements in compacted. Migration 2015, Santa Fe, USA, September 13-18, 2015.

Kosakowski G.

Continuum scale reactive transport calculations on porosity changes at material interfaces in a repository for low- and intermediate-level radioactive waste. Interpore 2015, Padova, Italy, May 18-21, 2015.

Kosakowski G., Kulik D.A., Leal A., Shao H., Wang W., Kolditz O.

OpenGeoSys-GEM: A coupled thermo-hydro-chemical (-mechanical) code THC(M) for geoscientific and engineering applications. PASC 15 Conference, Zürich, June 1-3, 2015.

Best Poster Award in Engineering.

Kulik D.A., Klinkenberg M., Brandt F., Weber J., Vinograd V.L., Rozov K., Winkler B., Bosbach D. Experimental and simulation study of phase equilibrium in the system (Ba,Sr,Ra)SO₄ + H₂O. Migration 2015, Santa Fe, USA, September 13-18, 2015.

Kulik D.A., Grambow B., Suzuki T., Bosbach D., Spahiu K., Duro L.

Impact of slow processes close to equilibrium on radionuclide migration. Migration 2015, Santa Fe, USA, September 13-18, 2015.

Kulik D.A., Miron G.D., Wagner T., Heinrich C.A. Internally consistent thermodynamic data for aqueous species in the Na-K-Al-Si-O-H-Cl system. Goldschmidt 2015, Prague, Czech Republic, August 16-21, 2015.

Kulik D.A., Vinograd V.L., Brandt F., Klinkenberg M., Weber J., Rozov K., Winkler B., Bosbach D. Phase equilibria in the system (Ba,Sr,Ra)SO₄ + H₂O. Goldschmidt 2015, Prague, Czech Republic, August 16-21, 2015.

Kulik D.A., Yapparova A., Gabellone T., Whitaker F., Matthai S.K.

A new CSMP++GEM reactive transport code. Goldschmidt 2015, Prague, Czech Republic, August 16-21, 2015.

Kupcik T., Glaus M.A., Van Loon L.R., Baeyens B., Schaefer T., Geckeis H.

Multitracer (HTO, ³⁶Cl, ⁸⁵Sr) diffusion in compacted Cu(en)₂²⁺-illite and -montmorillonite. 6th International Conference on "Clays in Natural and Engineered Barriers for Radioactive Waste Confinement", Brussels, Belgium, March 23-26, 2015.

Meng S., Pfingsten W.

Multispecies random walk simulations in radial symmetry – model concept, benchmark and application to HTO, ²²Na & ³⁶Cl diffusion in clay. 6th International Conference on "Clays in Natural and Engineered Barriers for Radioactive Waste Confinement", Brussels, Belgium, March 23-26, 2015.

Montoya V., Kupcik T., Van Laer L., Bruggeman C., Glaus M.A., Baeyens B., Maes N., Schaefer T., Geckeis H.

Zn and Co sorption onto Na-illite – batch sorption study and modelling. 6th International Conference on "Clays in Natural and Engineered Barriers for Radioactive Waste Confinement", Brussels, Belgium, March 23-26, 2015.

Pegado L., Labbez C., Churakov S.V.

An approach to adsorption isotherms in liquid media from multi-scale molecular modelling: application to Calcium-Silicate-Hydrate. 4th Meeting of the French Association for Adsorption, Chimie Paris Tech, Paris, France, February 5-6, 2015.

Poonosamy J., Kosakowski G., Prasianakis N.I. Multi-scale investigation of porosity change due to mineral dissolution and precipitation. 7th International Conference on "Porous Media", Padova, Italy, May 18-21, 2015.

Poonosamy J., Kosakowski G., Prasianakis N.I., Van Loon L.R., Mäder U.K.

A numerical and experimental reactive transport benchmark investigation of the coupling between density driven flow, solute transport and chemical reactions. 13th Swiss Geoscience Meeting, Basel, November 21, 2015.

Poonoosamy J, Kosakowski G, Van Loon L.R., Mäder U.K.

Experimental benchmark for testing reactive transport codes. Goldschmidt 2015, Prague, Czech Republic, August 16-21, 2015.

Poonoosamy J., Kosakowski G., Van Loon L.R. Experimental and numerical benchmark of a 2D reactive transport system. Goldschmidt 2015, Prague, Czech Republic, August 16-21, 2015.

Prasianakis N.I., Sui R., Mantzaras J., Buechi F.N. Microscopic modeling of evaporative heat and mass transfer in porous media with application to fuel cell systems. Interpore 2015, Padova, Italy, May 18-21, 2015.

Prasianakis N.I., Poonoosamy J., Gimmi T., Kosakowski G., Churakov S.V.

Microscopic modelling of dissolution and surface precipitation of sulphates in granular media: effect on the permeability and effective diffusivity. 6th International Conference on "Clays in Natural and Engineered Barriers for Radioactive Waste Confinement", Brussels, Belgium, March 23-26, 2015.

Rojo H., Tits J., Lothenbach B., Scheinost A.C., Wieland E.

The uptake of selenium by cementitious materials under oxidizing and reducing conditions, Swiss Cemnet Meeting, Bern, March 16, 2015.

Rojo H., Tits J., Scheinost A.C., Lothenbach B., Wieland E.

The retention of Se under oxidizing and reducing conditions in the cementitious near-field of a repository for radioactive waste. Immorad Workshop, Paul Scherrer Institut, Switzerland, April 23-24, 2015.

Shafizadeh A., Gimmi T., Van Loon L.R., Kaestner A., Lehmann E., Mäder U.K., Churakov S.V.

Neutron imaging study of heavy water transport across a cement-clay interface. 6th International Conference on "Clays in Natural and Engineered Barriers for Radioactive Waste Confinement", Brussels, Belgium, March 23-26, 2015.

Soler J., Steefel C., Leupin O., Gimmi T. Modeling the DR-A in situ diffusion experiment (Opalinus Clay): Ionic strength effects on solute transport. Goldschmidt 2015, Prague, Czech Republic, August 16-21, 2015.

Soltermann D., Marques Fernandes M., Dähn R., Gorski C., Baeyens B.

Fe(II) uptake on montmorillonites: surface complexation and oxidation. 6th International Conference on "Clays in Natural and Engineered Barriers for Radioactive Waste Confinement", Brussels, Belgium, March 23-26, 2015.

Soltermann D., Marques Fernandes M., Dähn R., Gorski C., Baeyens B., Scheinost A.C.

Iron & montmorillonite: Surface complexation and redox processes. Goldschmidt 2015, Prague, Czech Republic, August 16-21, 2015.

Sui R., Prasianakis N.I., Theile J., Mantzaras J. Hydrogen combustion in catalytic microreactors, 12th International Conference on "Energy for a Clean Environment", Lisboa, Portugal, July 5-9, 2015.

Thien B., Kosakowski G., Kulik D.A.

Fluid-rock interactions in Icelandic hydrothermal systems. COTHERM SP2, SCCER-SoE, Swiss Geoscience Meeting, Basel, Switzerland, November 20-21, 2015

Thien B., Weremeichik J.M., Sadekov A., Gabitov R.I.

The effect of growth rate on uranium partitioning between calcite and fluid. AGU Joint Assembly, Montreal, Canada, May 3-7, 2015.

Altmaier M., Gaona X., Endrizzi F., Brendler V., Steudtner R., Franzen C., Tsushima S., Panak P.J., Skerencak-Frech A., Hagemann S., Brandt F., Kruger S., Colàs M., Grivé M., Thoenen T., Kulik D.A.

THERMAC – A joint project on aquatic actinide chemistry and thermodynamics at elevated temperature conditions. Migration 2015, Santa Fe, USA, September 13-18, 2015.

Tits J., Rojo H. Scheinost A.C., Lothenbach B., Wieland E.

Selenium uptake by cementitious materials: effect of the redox state. Migration 2015, Santa Fe, USA, September 13-18, 2015.

Van Loon L.R., Pflingsten W.

On the role of "surface diffusion" and competing cations for diffusion of transition metal ions in Opalinus Clay. 6th International Conference on "Clays in Natural and Engineered Barriers for Radioactive Waste Confinement", Brussels, Belgium, March 23-26, 2015.

Wersin P., Mazurek M., Waber H.N., Mäder U.K., Gimmi T., Rufer D., Lerouge C., Oyama T., Traber D. Constraining porewater chemistry in a clay-rich rock sequence. 6th International Conference on "Clays in Natural and Engineered Barriers for Radioactive Waste Confinement", Brussels, Belgium, March 23-26, 2015.

Wieland E., Cvetković B.Z., Kunz D.

Development of a ¹⁴C AMS based compound-specific analytical technique for gaseous species: Status. Analytical Workshop of the EU FP7 Project "CAST" (Carbon Source Term), Villigen PSI, Switzerland, May 29, 2015.

Wieland E., Rojo H., Scheinost A.C., Lothenbach B., Tits J.

Redox transformations and the disposal of radioactive waste: Influence on the Se immobilization, Goldschmidt 2015, Prague, Czech Republic, August 16-21, 2015.

Wigger C., Van Loon L.R., Gimmi T.

Anion diffusion in low porosity argillaceous rocks. 6th International Conference on "Clays in Natural and Engineered Barriers for Radioactive Waste Confinement", Brussels, Belgium, March 23-26, 2015.

Wigger C., Van Loon L.R., Gimmi T.

Pore size distribution measurements on low porosity argillaceous rocks. Goldschmidt 2015, Prague, Czech Republic, August 16-21, 2015.

8.3 Invited talks

Curti E.

Geochemical long-term perspective for nuclear waste, Materials Science & Technology 2015, Columbus OH, USA, October 4-8, 2015.

8.4 Teaching

Alt-Epping P., Gimmi T.

Lecture "Ausbreitung von Schadstoffen in Böden und Grundwasser: Von der Realität zum Modell – und zurück", Weiterbildungskurs Altlasten, University of Bern, June 18–19, 2015.

Churakov S.V.

Bachelor Course: Crystallography I, Institute for Geological Sciences, University of Bern.

Curti E.

Lecturer for master course "Geological Disposal of Radioactive Waste", Institut für Geologie, Universität Bern.

Gimmi T., Alt-Epping P.

Lecture and examinations "Geochemical Modelling II: Reactive Transport", University of Bern, Master Course in Environmental and Resource Geochemistry, Spring semester 2015.

Gimmi T.

Habilitation, Institute for Geological Sciences, University of Bern.

Hummel W.

Lecturer for master courses on "Geochemistry of radioactive waste management", ETH Zürich.

Kosakowski G.

Lecture and examinations "Geostatistics 2015" at University of Bern, April 13–17, 2015.

Kosakowski G.

Lecture "Flow and transport modeling in concrete". Course on "Cement thermodynamic modelling with GEM-Selektor" at Hiroshima University, Japan, June 9–15, 2015.

Kulik D.A.

Pre-Immorad-Workshop GEMS training, Paul Scherrer Institut, April 20-22, 2015.

Kulik D.A.

Invited GEMS3 software short course, Dept. Geology and Geography, University Helsinki, October 5-11, 2015.

Pfingsten W.

Modelling of Processes in Soils and Aquifers (701-1334-00L). Department for Environmental Sciences, ETH Zürich, Spring Semester 2015.

8.5 Other

Churakov S.V.

Examinations of PhD Thesis Florian Dolder, Institute for Geological Sciences, University of Bern.

Churakov S.V.

Examinations of Habilitation Thesis of Dr. Cécile Ferry, Ecole nationale supérieure de chimie de Paris/Chimie Paris Tech, France.

Gimmi T.

Associate Editor of Applied Geochemistry.

Kosakowski G.

Examineur at the PhD defense of Ikram Fatnassi at University Montpellier, December 17, 2015.

Kulik D.A.

Member of ISSP-16 International Scientific Advisory Committee.

Kulik D.A.

Executive Guest Editor, Special Issue on geochemical speciation codes and databases. Applied Geochemistry Vol. 55.

Kulik D.A.

Associate Editor of Applied Geochemistry.

Tits J., Gschwend B.

Organizers of the 3rd IMMORAD Workshop on "Basic research on the immobilization of long-lived radionuclides by interaction with relevant secondary repository phases". Schloss Böttstein, Switzerland, April 23-24, 2015.

Wieland E.

Organizer of the EU FP7 project "CAST" Workshop on "Analytical techniques for C-14 detection: Knowledge exchange", Villigen, Switzerland, May 29, 2015.

